The role of intracellular Ca^{2+} signaling in the exocrine pancreatic damage during acute pancreatitis

Júlia Fanczal

Ph.D. Thesis

Supervisor: József Maléth, M.D., Ph.D

Hegyi Péter, M.D., Ph.D., D.Sc

Doctoral School of Theorical Medicine

First Department of Internal Medicine

University of Szeged

Szeged, Hungary

2020

LIST OF FULL PAPERS RELATED TO THE THESIS

Articles closely related to the subject of the thesis and cited in the thesis:

I. **Fanczal J**, Pallagi P, Görög M, Diszházi G, Almássy J, Madácsy T, Varga Á, Csernay-Biró P, Katona X, Tóth E, Molnár R, Rakonczay Z Jr, Hegyi P, Maléth J. TRPM2-mediated extracellular Ca^{2+} entry promotes acinar cell necrosis in biliary acute pancreatitis.
J Physiol. 2020 Jan 9; doi: 10.1113/JP279047
[IF$_{2018}$: 4.95]

II. Molnár R, Madácsy T, Varga Á, Németh M, Katona X, Görög M, Molnár B, **Fanczal J**, Rakonczay Z Jr, Hegyi P, Pallagi P, Maléth J., Mouse pancreatic ductal organoid culture as a relevant model to study exocrine pancreatic ion secretion.
Lab Invest. 2020 Jan; doi: 10.1038/s41374-019-0300-3
[IF$_{2018}$: 3.684]

Articles not related to the subject of the thesis:

III. Tóth E, Maléth J, Závogyán N, **Fanczal** J, Grassalkovich A, Erdős R, Pallagi P, Horváth G, Tretter L, Bálint ER, Rakonczay Z Jr, Venglovecz V, Hegyi P., Novel mitochondrial transition pore inhibitor N-methyl-4-isoleucine cyclosporin is a new therapeutic option in acute pancreatitis"
J Physiol. 2019 Dec; doi: 10.1113/JP278517
[IF$_{2018}$: 4.95]

IV. Szentesi A, Tóth E, Bálint E, **Fanczal** J, Madácsy T, Laczkó D, Ignáth I, Balázs A, Pallagi P, Maléth J, Rakonczay Z Jr, Kui B, Illés D, Márta K, Blaskó Á, Demcsák A, Párniczky A, Pár G, Gódi S, Mosztbacher D, Szücs Á, Halász A, Izbéki F, Farkas N, Hegyi P; Hungarian Pancreatic Study Group. Analysis of Research Activity in Gastroenterology: Pancreatitis Is in Real Danger
PLoS one. 2106 Oct 24; doi: 1.01371/jurnal.pone.0165244
[IF$_{2015}$: 3.057]

Number of full publications:	**4 (1 first author)**
Cumulative impact factor:	**16.641**

Contents

LIST OF FULL PAPERS RELATED TO THE THESIS 1
LIST OF ABBREVIATIONS 4
1. Introduction 5
1.1. Intracellular Ca^{2+} signaling in pancreatic acinar cells 5
1.2. Acute pancreatitis 6
1.3. Bile acid induced acute pancreatitis 8
1.4. Reactive oxygen species role in Ca^{2+} signaling 9
1.5. Transient Receptor Potential Melastatin 2 11
1.6. 3D organoids as models of epithelial physiology 12
2. Aim of the Study 14
3. Materials and Methods 15
3.1 Animals and Ethics 15
3.2. Isolation of pancreatic exocrine cells 16
3.2.1. Isolation of pancreatic acinar cells 16
3.2.2. Isolation of mouse ductal pancreatic ductal fragments and establishment of pancreatic organoid culture 16
3.3. Gene expression analysis 18
3.4. Immunofluorescent labeling 18
3.5. Electrophysiology 18
3.6. Measurement of intracellular Ca^{2+} concentration in acinar cells, ductal fragments and organoids 19
3.7. Mitochondrial membrane potential measurements 20
3.8. Investigation of acinar cell fate 20
3.9. In vivo acute pancreatitis models 21
3.10. Statistics 22
4. Results 23
4.1. TRPM2 channel is expressed in the exocrine pancreas 23
4.2. Functional TRPM2 channels are present in pancreatic acinar 23
4.3. TRPM2 contributes to bile-acid-induced extracellular Ca^{2+} influx in pancreatic acinar cells 25
4.4. Lack of TRPM2 decreases acinar cell necrosis during bile acid exposure 26

4.5. Lack of TRPM2 does not prevent mitochondrial damage during bile acid exposure 28
4.6. Lack of TRPM2 decreases the severity of experimental biliary pancreatitis 30
4.7. Intracellular Ca^{2+} signaling in pancreatic organoids 32
5. Discussion.....35
5.1. TRPM2-mediated extracellular Ca^{2+} entry promotes acinar cell necrosis in biliary acute pancreatitis 35
5.2. Intracellular Ca^{2+} signaling in pancreatic organoids.....39
6. Summary 40
New observations.....42
7. Acknowledgement 43
8. References 45

LIST OF ABBREVIATIONS

7 TM	7-transmembrne
ACH	acetylcholine
ADPR	ADP-ribose
AMP	adenosine monophosphate
AP	acute pancreatitis
$[Ca^{2+}]_I$	intracellular Ca^{2+} concentration
CCK	cholecystokinin
CDC	chenodeoxycholic acid
CXCL2	macrophage inflammatory protein-2
CPA	cyclopiazonic acid
DAG	diacylglycerol
ER	endoplasmic reticulum*
GDP	guanosine diphosphate
GTP	guanosine-5'-triphosphate
IP3	inositol 1,4,5-triphosphate
OCs	organoid cultures
PAC	pancreatic acinar cells
PARP	poly (ADP-ribose) Polymerase
PI	phosphoinositide
PIP2	phosphatidylinositol, 4,5-bisphosfate
PKC	protein kinase C
PM	plasma membrane
PCR	polymerase chain reaction
ROS	reactive oxygen species
TBS	Trish buffered saline
TC	Na-taurocholate
TLC-S	taurolithocholate sulfate
TMRM	tertamethylrhodamine-methyl ester
TRPM2	Transient Receptor Potential Melastatin 2

1. Introduction

The exocrine pancreas plays a central role in the digestion of meal in the duodenum under physiological conditions. Whereas pathophysiological stimuli (like excessive ethanol intake, or biliary reflux) can provoke acute pancreatitis (AP), which is a frequent disorder with high mortality in severe cases. Most of the gland (~80%) consist of acinar cells, with about 4% of ductal cells, 4% of blood vessels and 8% of endocrine cells and cells of the extracellular matrix. One of the features of the exocrine pancreas is the ´tree like´ structure whereas the acinar cells located at the end of the ´branches´ organized in lobolus. The pancreatic acinar cells produce and secrete the digestive enzymes in response to meal intake. The other cell type pancreatic ductal epithelial cells secrete high amount of HCO_3^--rich alkaline fluid. The alkaline pancreatic fluid secretion washes out the digestive enzymes of the pancreatic ductal tree and neutralizes the acidic chyme entering the duodenum. Under physiological conditions the acinar cells are protected against premature and intracellular activation of zymogenes. When this protective mechanism fails pancreatic autodigestion is initiated and AP can develop. Numerous studies suggesting that extra - as well as intracellular Ca^{2+} play an important role in the initiation of pancreatic protease activation [1].

1.1. Intracellular Ca^{2+} signaling in pancreatic acinar cells

In the exocrine pancreas intracellular Ca^{2+} signaling plays a major role in the signal transduction during neural and hormonal stimulation of digestive enzyme and fluid secretion [2]. The produced digestive enzymes are packed in zymogen granules in the apical pole of the acinar cells, which is released in response to secretagogue stimuli induced intracellular Ca^{2+} elevation.

During physiological stimulation agonist binding – such as acetylcholine (Ach), cholecystokinin (CCK), or bombesine - to G protein coupled cell surface receptors activates phospholipase C β (PLCβ) in pancreatic acinar cells. PLCβ than binds to plasma membrane (PM) phosphoinositides [3] and hydrolyses phosphatidylinositol 4,5-bisphosphate (PIP_2) releasing inositol trisphosphate (IP_3) and diacylglycerol [4]. The released IP_3 binds to its receptors (IP_3 receptors - IP_3R), which are Ca^{2+} release channels in the endoplasmic reticulum (ER) membrane [5] and allow Ca^{2+} release from the ER to the cytosol. During physiological stimuli, intracellular Ca^{2+} increase is restricted to the apical, secretory region of the acinar cells and the propagation of the Ca^{2+} signals is limited by the mitochondria, which buffer the released Ca^{2+} and prevents global intracellular Ca^{2+}

elevation. The depletion of the ER Ca^{2+} store also induces Ca^{2+} influx trough the plasma membrane (PM), which contributes to the intracellular Ca^{2+} signals in response to long lasting stimulations. In a process called store operated Ca^{2+} entry (SOCE) the extracellular Ca^{2+} influx is initiated by the ER Ca^{2+} sensor Stim1, which clusters in specific ER-PM junctions (also called puncta formation) [6]. In these junctions Stim1 interacts and activates a PM Ca^{2+} channel Orai1, which mediates the extracellular Ca^{2+} influx [7]. Besides Orai1, transient receptor potential canonical 3 and 6 (TRPC) Ca^{2+} channels can also contribute to the extracellular Ca^{2+} influx in a Stim1 dependent manner [8]. Since sustained intracellular Ca^{2+} elevation and prolonged ER Ca^{2+} depletion is potentially toxic, the released Ca^{2+} has to be extruded from the cytoplasm, which is carried out by two ATP dependent mechanisms. The sarco/endoplasmic reticulum Ca^{2+}-ATPase (SERCA), and the plasma membrane Ca^{2+}-ATPase (PMCA) pumps move Ca^{2+} from the cytosol to the ER and the extracellular space, respectively, to restore basal $[Ca^{2+}]_i$. This terminates the Ca^{2+} signals and maintains the cellular integrity by avoiding sustained elevation of intracellular Ca^{2+}, which can have severe consequences (see below).

1.2. Acute pancreatitis

Acute pancreatitis (AP) is one of the leading causes of acute hospitalization among non-malignant gastrointestinal diseases and thus having a significant clinical and economic burden [9]. Major etiologic factors leading to the development of AP are impacted gallstones causing biliary AP and heavy alcohol consumption [10]. Primarily AP is a localized to and represents a sterile inflammation of the exocrine pancreas, which however can lead to local and systemic complications. Local complications include infected necrosis of the pancreatic tissue and surrounding visceral fat, whereas systemic complications are dominated by acute lung injury and renal dysfunction leading to multiorgan failure. The severity of AP can vary among mild (no multiorgan failure), moderate (multiorgan failure is only temporal, < 48 h) to severe form (multiorgan failure is only permanent, > 48 h). The average mortality rate is ~ 3%, however in severe cases it can reach to 28-30% [10, 11]. The disease incidence has been continuously increasing in the last two decades reaching 5-100/100.000 cases per year depending on the region [12].

Although the disease pathogenesis is multifactorial sustained intracellular Ca^{2+} overload caused

cell toxicity is considered as a hallmark of the disease [13]. Intracellular Ca^{2+} overload can lead to premature activation of trypsinogen [1], mitochondrial damage and cell necrosis in acinar cells [14]. In pancreatic acinar cells several PM Ca^{2+} channels were demonstrated to contribute to cell damage during AP. Gerasimenko et al. showed that the inhibition of extracellular Ca^{2+} entry via Orai1 decreases acinar cell necrosis *in vitro* [15], and others demonstrated that prevention of sustained Ca^{2+} overload by Orai1 inhibition significantly impaired pancreatic oedema, inflammation and necrosis in experimental models of AP [16]. On the other hand Kim et al found that deletion of TRPC3 markedly reduced the bile-acid-evoked Ca^{2+} signals and decreased the intracellular trypsin activation *in vitro* and the severity of cerulein-induced AP *in vivo* [17]. Mitochondria act as Ca^{2+} buffers in non-excitable cells and play crucial roles in the spatial and temporal localization of the intracellular Ca^{2+} signals [18]. However sustained mitochondrial Ca^{2+} overload can induce the opening of the mitochondrial membrane permeability pore (MPTP) across the inner and outer membranes of mitochondria, resulting in an increased permeability of the mitochondrial membranes to molecules and ions with molecular mass less than 1.5 kDa, including protons and water [19]. Another possible way to disrupt the mitochondrial membrane is following mitochondrial outer membrane permeabilization (MOMP), which is proposed to be a crucial event during apoptosis, causing the release of proapoptotic factors from the mitochondrial intermembrane space to the cytosol [20]. Due to the increased membrane permeability the $(\Delta\Psi)_m$ disappears, mitochondria become swollen and mitochondrial membranes rupture, and a consequent drop of ATP production happens [19, 21, 22]. Moreover, ATP is necessary for the activity of SERCA and PMCA Ca^{2+} pumps and therefore the drop of $[ATP]_i$ can further contribute to the maintenance of the sustained Ca^{2+} rise [23]. The sustained elevation of $[Ca^{2+}]_i$ and the resulting mitochondrial damage can lead to a vicious cycle which in turn triggers cell necrosis [24, 25]. Independently from mitochondrial damage, other Ca^{2+}-dependent toxic effects of bile acids have been described, which could also contribute to acinar cell necrosis. Bile acids were shown to activate calcineurin via the elevation of intracellular Ca^{2+} in pancreatic acinar cells, leading to intra-acinar activation of chymotrypsinogen and NF-κB activation, and acinar cell death [26]. In addition, genetic or pharmacological inhibition of calcineurin reduced the severity of TLC-S-induced AP, and pharmacologic and genetic inhibition of calcineurin abolished the translocation of protein kinase C, which is a critical upstream regulator of NF-κB activation [27].

1.3. Bile acid induced acute pancreatitis

Biliary pancreatitis is one of the most common forms of AP, although the mechanism of the disease development is still a matter of debate. One of the theories suggest that due to an impacted gallstone a 'common channel' connects the bile duct and the pancreatic duct allowing bile acids to enter the pancreatic ductal system and reach ductal and acinar cells [28]. Although the connection of bile acids and biliary pancreatitis has been described in several studies, this hypothesis is continuously questioned. The most widespread critique suggest that instead of the reflux mechanism, increased luminal pressure is the trigger of the pancreatic damage [29]. Whether or not BA reach the pancreatic exocrine cells, several observations suggest that bile acids can trigger multiple intracellular changes in pancreatic acinar and ductal cells contributing to the development of biliary acute pancreatitis. In acini bile acids provoke a sustained elevation of the intracellular Ca^{2+} [30] due to IP_3R and ryanodine receptor activation. In addition, taurolithocholicacid 3-sulfate induced mitochondrial damage in acinar cells accompanied by diminished intracellular ATP production [31] and loss of the mitochondrial membrane potential ($\Delta\Psi_m$), which was not affected by BAPTA-AM treatment [32]. On the other hand Perides et al. observed that the G-protein-coupled cell surface bile acid receptor (Gpbar1) is expressed at the apical membrane of pancreatic acinar cells and activation of the receptor by bile acids induce pathological Ca^{2+} elevation, intraacinar digestive enzyme activation, and a consequent cell damage [33]. Moreover Gpbar1 knockout mice developed less severe bile acid-induced AP, whereas the severity of caerulein-induced AP was not changed. In pancreatic ductal cells non-conjugated bile acids induced dose-dependent changes in the HCO_3^- secretion [34]. Lower concentration of chenodeoxycholate stimulated, in contrast high concentrations remarkably inhibited the ion transport activities of ductal cells. Low concentration of chenodeoxycholate from the luminal membrane triggered short oscillatory Ca^{2+} signals, which is usually associated with agonist stimulation. In contrast, bile acids in high concentrations evoked sustained Ca^{2+} elevation and severe damage of the mitochondrial morphology and function [35].

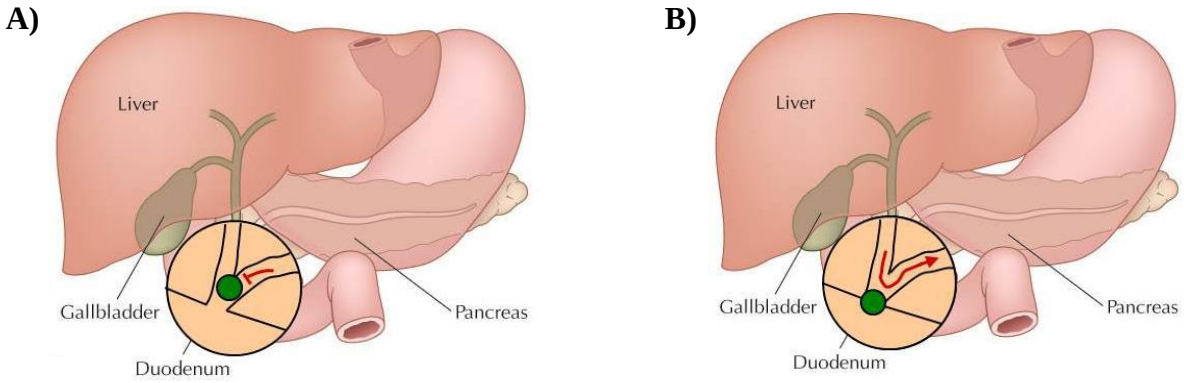

Figure 1. Opie´s two hypothesizes. A: Opie´s duct obstruction theory is the impaired secretion hypothesis, when the gallstone obstructs the pancreatic duct which impairs the outflow from the pancreas and leads to acinar and ductal cell damage. **B**: Opie´s common channel theory is the bile reflux hypothesis when the gallstone impacted at the duodenal papilla and creates the communication between the common bile duct and the pancreatic duct where bile can flow through into the pancreatic duct and triggers a series of events which initiate acute pancreatitis [36]

Markus M. Lerch, Ali Aghdassi, Gallstone-releated pathogenesis of acute pacreatitis.. Pancreapedia, 2016

1.4. Reactive oxygen species role in Ca^{2+} signaling

Reactive oxygen species (ROS) are essential component of the signal transduction in cells and their generation is balanced by oxidant and antioxidant molecules. ROS are produced during mitochondrial respiration derived from complexes I and III of the mitochondrial electron transport chain [37]. In the recent years several effects of ROS in intracellular signalling has been described [38]. As an example of this regulation of intracellular signalling Booth et al showed that the ER-mitochondrial interface hosts a nanodomain of H_2O_2, which was triggered by cytoplasmic Ca^{2+} elevations and is a positive regulator of Ca^{2+} oscillations. Such nanodomains can be considered as important elements of inter-organelle communication [39]. ROS production also have many effects on the ion channels and pumps involved in the intracellular Ca^{2+} signalling, which was reviewed by Criddle et al. [40]. In contrast, unbalanced generation of ROS has been suggested as crucial step in the pathogenesis of diseases via disruption of lipid membranes, proteins and DNA [41]. In the pathogenesis of AP ROS production was shown to determine pancreatic acinar cell fate as the ROS induced by menadione triggered apoptotic cell death [42]. Booth et al showed that bile acids induces ROS generation in pancreatic acinar cells from mice and humans [43]. They

also demonstrated that generation of ROS in response to bile acids occurred within the mitochondria and was dependent on the increase of mitochondrial Ca^{2+} [43]. In addition, during the pathogenesis of AP, ROS released by circulating neutrophils during in the inflammatory response might also contribute to the development of cell damage and local and systemic complications of AP [44].

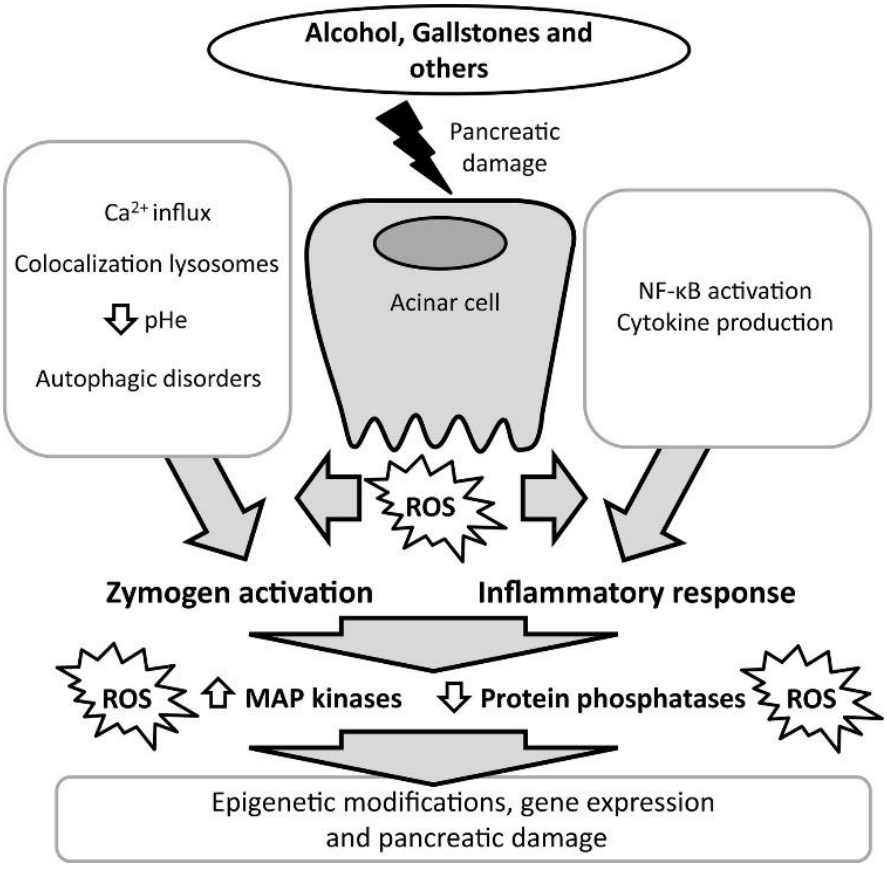

Figure 2. Mechanisms triggering acute pancreatitis in relation with oxidative stress. Illustration showing the main mechanisms triggering acute pancreatitis in relation with oxidative stress [45]. Oxidative stress is a crucial modulator of cell signaling and a key promoter of the inflammatory cascade, but it´s role is more complex and still needed to be elucidated. The pathophysiology of the disease still not fully understood especially the interaction of antioxidant and redox status with the gene expression is still needed to be clarified. Perez, S. et al., *Redox signaling in acute pancreatitis.* Redox Biol, 2015. **5**: p. 1-14.

1.5. Transient Receptor Potential Melastatin 2

TRPM2 is a member of Melastatin subfamily of the TRP channels [46], which is one of the largest cation channel family. Like most of the TRP channels are permeable to Ca^{2+} [47] TRPM2 is also a Ca^{2+} permeable cation channel [48], which is involved in different physiological and pathophysiological processes associated with redox signaling and oxidative stress [49]. The expression of TRPM2 has been demonstrated in different cell types and organs including pancreatic β cells [50] , spleen, neurons[51], bone marrow cells [51, 52], cardiomyocytes [53] and immune cells such as T lymphocytes, macrophages and neutrophils [54-56]. The channel is activated under oxidative stress by ROS and can be activated by free intracellular ADP-ribose (ADPR) in synergy with free intracellular Ca^{2+} as well. The pore opening of TRPM2 is initiated by binding of ADPR to its C-terminal cytosolic Nudix hydrolase 9 homology domain (NUDT9H) domain, which cleaves ADPR into adenosine monophosphate (AMP) and ribose-5-phosphate [57]. ADPR is produced by the enzyme Poly (ADP-ribose) Polymerase (PARP) in response to oxidative stress induced DNA damage and promotes apoptotic cell death. Another possible source of ADPR are the mitochondria, where oxidative stress could induce the production of free ADPR [41]. Indeed, reduced mitochondrial ADPR concentrations suppressed H_2O_2 -mediated TRPM2 currents [42].

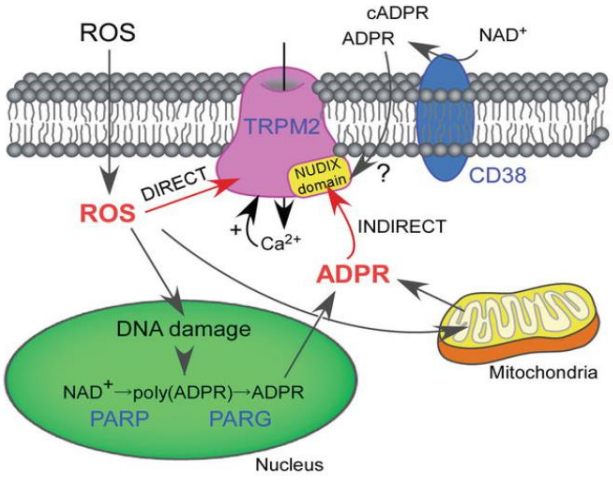

Figure 3. Activation cascade of TRPM2 by ROS. The activation of TRPM2 can be through an ADPR dependent direct and ADPR independent indirect way [58]. Kashio, M.. et al., Redox - Principles and Advanced Applications (2017)

The most prominent role of TRPM2 has been established in the development of inflammatory disorders [47]. In monocytes Ca^{2+} influx via TRPM2 was shown to increase chemokine production, leading to enhanced neutrophil infiltration in inflammatory bowel disease [55]. In addition, the role of TRPM2 has been identified in the pathogenesis of irradiation-induced xerostomia. In this study Liu *et al.* demonstrated that irradiation increased ROS production in the salivary glands and activated TRPM2, which lead to extracellular Ca^{2+} influx. The intracellular Ca^{2+} overload damaged the acinar cells and lead to the loss of acinar cell function (saliva production) in the salivary glands [59]. In a another study, the same group showed that under these conditions irradiation activated the intrinsic, mitochondrial pathway of apoptosis in a TRPM2-dependent manner that lead to caspase-3 activation and induced cleavage of stromal interaction molecule 1, which then attenuated store-operated Ca^{2+} entry [60]. In the β cells of the endocrine pancreas, TRPM2 has been suggested to play a role in diabetic stress-induced mitochondrial fragmentation. Abuarab *et al.* demonstrated that high extracellular glucose concentrations enhanced ROS production and activated TRPM2, which permeabilized the lysosomal membranes and induced Zn^{2+}-mediated mitochondrial fission [61]. These and other studies describe the expression of TRPM2 in various epithelial cells, moreover, emphasize the central role of the channel in the pathogenesis of oxidative-stress-related diseases. Although very likely, the expression or function of TRPM2 in exocrine pancreatic cells has never been investigated.

1.6. 3D organoids as models of epithelial physiology

In the last decades several studies highlighted that 2-dimensional cell cultures have several limitations (including artificial cell surface interactions, limited membrane contacts, lack of cell polarity), which limit their potential research use. On the other hand, rodent models of human diseases show major differences from the human disease phenotype and outcome inhibiting the translation of preclinical findings to clinical benefit. In then recent years, 3 dimensional organoid cultures emerged as potential preclinical tools for disease modeling and drug screening. Organoid cultures (OC) are established from isolated tissue specific Leucine-rich repeat-containing G-protein coupled receptor 5 positive (Lgr5+) adult stem cells using in vitro cell culture techniques [62, 63]. In these cultures, the activity of Wnt/β-Catenin signaling is maintained [64] which maintains the cell division and thus helps the generation of OCs long-term in 3D extracellular

matrix based scaffolds. Several reports suggest that epithelial cells in OC maintain the original cellular diversity and organization of the organ of origin [65]. Although the technique was originally described by using small intestinal Lgr5+ adult stem cells [66] OCs have now been established from a wide range of organs of the gastrointestinal tract, including the pancreas [67]. As cell-to-cell contacts dominate OCs due to the spheroid shaped architecture of the organoids, it seems to be more relevant representation of the original cell microenvironment in contrast to 2D cultures [68]. In pancreatic research currently OCs are studied as relevant human models of tissue development [69] and carcinogenesis [70]. Due to the above described advantages of the OCs, they might be a better model in exocrine pancreatic research, however we have only limited information about the functional properties (like Ca^{2+} signaling) of OCs.

2. Aim of the Study

I. TRPM2 – mediated extracellular Ca^{2+} entry promotes acinar cell necrosis in biliary acute pancreatitis

Aberrant Ca^{2+} signaling and increased ROS production can cause mitochondrial damage, intraacinar digestive enzyme activation and cell death. TRPM2 is a non-selective cation channel that plays a major role in oxidative stress induced cellular Ca^{2+} overload in different cell types, but its expression and function is not known in the exocrine pancreas.

Therefore, our aims were to:

- characterize the expression and function of TRPM2 in the exocrine pancreas;
- assess the role of TRPM2 in bile acid induced cell damage;
- investigate the role of TRPM2 in the determination of acinar cell fate;
- compare the severity of cerulean induced and biliary AP in wild type and TRPM2 knockout mice.

II. Intracellular Ca^{2+} signaling in pancreatic organoids

Organoid cultures seem to be a suitable model for in vitro tests; however we have no information how Ca^{2+} signals are developed in the epithelial cells in organoids.

Therefore, our aim was to:

- compare the Ca^{2+} signaling in primary epithelial cells and organoids.

3. Materials and Methods

3.1 Animals and Ethics

TRPM2 knockout mice were generously provided by Yasuo Mori, Kyoto, Kyoto University, Department of Synthetic Chemistry and Biological Chemistry, Graduate School of Engineering. The knockout mice were generated on C57B1/6 background as described previously [55]. TRPM2 +/+ and TRPM2-/- mice were breed from TRPM2 +/- animals and used for experiments between the age of 8-12 weeks. Genotyping was performed by polymerase chain reaction (PCR) and visualized by standard agarose gel electrophoresis. The animals were kept at a constant room temperature of 22-24°C with a 12 h light–dark cycle and were allowed in the Animal Facility of the First Department of Medicine, University of Szeged. Mice were used in adherence to the NIH guideline and the EU directive 2010/63/EU for the protection of animals used for scientific purposes. The study was approved by the National Scientific Ethical Committee on Animal Experimentation under license number: **XXI./2523/2018.**

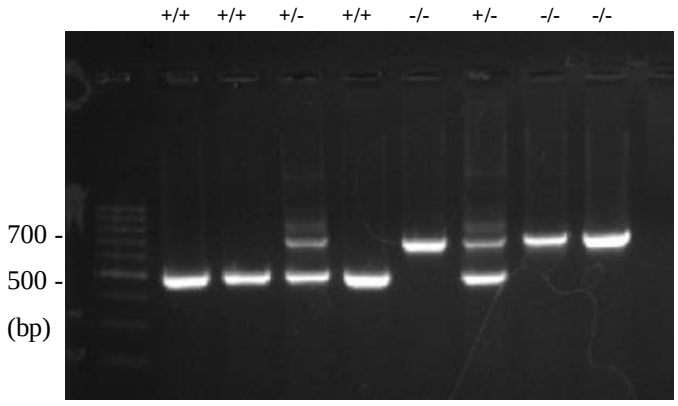

Figure 4. Agarose gel electrophoresis image of TRPM2 gene expression of +/+, +/- and -/- mice. The different bands show different genotype, the band at ~500 bp represents the homozygous TRPM2 WT (+/+), the band at ~ 700 bp represents the TRPM2 KO (-/-) and where both band seen it represents the heterozygous (+/-) mice individuals.

3.2. Isolation of pancreatic exocrine cells

3.2.1. Isolation of pancreatic acinar cells

WT and TRPM2 KO mice were sacrificed using terminal anesthesia with 250 mg/bwkg sodium pentobarbital. The sensitivity of pancreatic tissue during experimental manipulation is higher, due to the high content of glycolytic, proteolytic, and lipolytic enzymes digesting the pancreatic tissue upon removal [71]. Therefore, isolation of acinar cells requires special attention and use of trypsin inhibitor. To avoid unwanted acinar cell damage, we adopted the isolation protocol described by Gout et al [71] that extends acinar cells survival 4- 5 h after isolation allowing the functional examinations of acinar cells. During the isolation process the pancreas was placed into ice-cold HBSS (Sigma;8264 solution). Then the tissue was, cut into small pieces in a 1.5 ml Eppendorf and placed into a sterile flask with 10 ml isolation solution (10 ml HBSS (Sigma; *8264),* 200 U/ml of collagenase (*Worthington; 5273*), 10 mM Hepes (Sigma; *3375)*. The tissue was incubated for 25-30 min at 37 ºC and the flask was vigorously shaken every 5 minutes during the incubation. After digestion the pancreas was placed into a 50 ml Falcon tube with 10 ml ice-cold buffered washing solution (containing 10 ml HBSS (Sigma; *8264)*, 10 mM Hepes (Sigma; *3375),* 0.5 ml Fetal Bovine Serum) and centrifuged at 700 rpm on 4°C for 2 min. This step was repeated twice. At the end the supernatant was removed, and the pellet was resuspended in 1 ml HBSS solution. Until experimental use, the acinar cells were kept in an incubator at 37°C and with 5% CO_2. Only acinar clusters of 4-8 cells were chosen for experiment.

3.2.2. Isolation of mouse ductal pancreatic ductal fragments and establishment of pancreatic organoid culture

Mouse pancreatic organoid cultures were established using the previously published protocol by Boj et al. [20]. In the first step, mouse pancreatic ductal fragments were isolated as described earlier [72]. Briefly, after terminal anesthesia with 250 mg/bwkg sodium pentobarbital, the pancreas was surgically removed and digested for 15 min with 100 U/mL purified collagenase (Worthington, Cat. No.: LS005273), 0.1 mg/mL trypsin inhibitor (ThermoFisher Scientific, Cat. No.: 17075029) and 1 mg/mL bovine serum albumin (VWR, Cat. No.: 9048-46-8) in DMEM Nutrient Mixture F-12 Ham (Sigma, Cat. No.: D6421) at 37°C in a shaking water bath. Then small intra-/interlobular ducts were isolated by microdissection under a stereomicroscope. Isolated ductal fragments were then used for experiments or resuspended in Corning® Matrigel (VWR,

Cat. No.: 734-1100). 10 µl Matrigel domes were plated into 24-well plates and let solidify on 37°C. 3 mL prewarmed Mouse Feeding Media was added to each well (for the composition of the media please see Table 1.). Feeding media was replaced every other day and organoids were passaged weekly by gentle physical disruption and centrifugation. For the experiment's organoids were used until passage no. 5. to avoid any changes in gene expression.

Mouse Feeding Media			
Name	**Producer**	**Catalog number**	**Final concentration**
Mouse Splitting Media			
A83-01	Tocris	2939	500 nM
EGF Recombinant Mouse Protein	ThermoFisher	PMG8041	50 ng/ml
Recombinant Human FGF-10	Shenadoah Biotechnology	100-183	100 ng/ml
Gastrin I	Tocris	3006	0.01 µM
mNoggin conditioned media			100 ng/ml (0.1% V/V)
N-acetylcysteine	Sigma-Aldrich	A9165	1.25 mM
Nicotinamide	Sigma-Aldrich	72340	10 mM
recombinant R-Spondin	R&D Systems	4645RS-100	
B27 Supplement 50X serum free	ThermoFisher	17504044	1X
Y-27632 Rho-kinase inhibitor	Tocris	1254/1	10.5 µM
Prostaglandin E2	R&D Systems	2296/10	1 µM
Wnt-3A conditioned media from L Wnt-3A Cells	ATCC	CRL-2647	50% (V/V)

Table 1. Composition of solutions used for organoid culture.

3.3. Gene expression analysis

The combination of reverse-transcription (RT-PCR) and conventional PCR were used to investigate the gene expression of TRPM2. Total mRNA was isolated from 3 independent biological replicates of mouse brain and isolated pancreatic acini using NucleoSpin RNA XS kit (Machery- Nagel, Ref.:74092.50) according to the producer's protocol. The mRNA concentrations were measured with NanoDrop™ 2000 spectrophotometer (ThermoFisher Scientifics). 1 µg purified mRNA was used to synthetize cDNA using an iScript™ cDNA Synthesis kit (Bio-Rad, Cat. No.:1708890) Conventional PCR amplification was performed by DeramTaq Hot Start DNA Polymerase (ThermoFisher Scientific, Cat No.: EP1702) with cDNA specific primers (forward: ACGGGCAATATGGTGTGGAG; reverse: CACCTCCCCTTTCCTTCGTT) for 35 cycles. To validate the primers mouse brain lysate was used.

3.4. Immunofluorescent labeling

The acinar cells of WT and TRPM2 KO mice were isolated and attached to poly-l-lysine coated cover glass. Sections were fixed in 4% PFA-PBS for 15 minutes then washed in Trish buffered saline (TBS) 3 times for 5 minutes. Sodium Citrate Buffer - Tween20 was used to perform antigen retrieval (0,001 M Sodium Citrate Buffer, pH 6.0 and 0,05 % Tween 20). During this process the cells were kept between 90-96°C for 15-20 minutes. For the next step the cells were blocked with 0.01% goat serum and 5x bovine serum albumin in TBS for 1 hour. The sections were incubated with an ATTO-594 conjugated rabbit polyclonal primary antibody against TRPM2 (Anti - TRPM2 - ATTO-594; Alamone Labs; Cat. No: ACC-043-AR) in 1:50 dilution in 5xBSA-TBS overnight on 4°C. Nuclear labelling was performed with Hoechst33342 for 15 minutes. Finally, the samples were mounted in Flouromount mounting medium (Sigma-Aldrich) and visualized with a ZEISS LSM 880 confocal microscope equipped with at 40x water based immersion objective.

3.5. Electrophysiology

For electrophysiology recordings, pancreatic acinar cells were isolated from mouse pancreas as described previously [73], with slight modifications. The pancreas was removed and injected with

a F12/DMEM (ThermoFisher Scientific Cat. No.: 11320033) medium containing 100 U/mL collagenase P (Roche), 0.1 mg/mL trypsin inhibitor and 2.5 mg/mL BSA. These were then incubated in 5 mL volume of the same solution in a 37°C shaking water bath for 30 min, which was continuously gassed with carbogen. The tissue was dissociated by pipetting with a serological pipette 4–6 times before filtering through a 150 μm mesh. Cells were layered on top of 400 mg/mL BSA and washed through the medium by gentle centrifugation. The pellet was resuspended in Ca^{2+}-free, collagenase-containing Tyrode's solution before being further digested for 10 min. Following this, cell clumps were gently agitated with a 1 mL pipette tip attached to a serological pipette. The resulting cells were collected by centrifugation, resuspended in DMEM medium and kept gassed at room temperature until use in patch clamp experiments. Whole cell currents were acquired at room temperature using an Axopatch 200B amplifier and a Digidata 1322A digitizer (Axon Instruments) at a 50 kHz sampling rate and filtered online at 5 kHz using a low-pass Bessel filter. Data acquisition was performed using p Clamp 9 software package (Axon Instruments). Pipettes of ~6 MΩ resistance were used with the intracellular solution containing 130 mM Cs-glutamate, 5 mM $CaCl_2$, 10 mM EGTA (resulting in 135 nM ionized Ca^{2+}), 5 mM $MgCl_2$ and 10 mM HEPES, pH: 7.3. Pancreatic acinar cells were continuously perfused with extracellular saline solution (140 mM Na-glutamate, 4 mM CsCl, 2 mM $CaCl_2$, 2 mM $MgCl_2$, 10 mM HEPES, pH: 7.4) with or without 100 μM H_2O_2. Cation currents were recorded during 100 ms long test pulses at step potentials between −60 and +120 mV both under control conditions and during treatment.

3.6. Measurement of intracellular Ca^{2+} concentration in acinar cells, ductal fragments and organoids

Intracellular Ca^{2+} concentration ($[Ca^{2+}]_i$), was measured by loading cells with 5μM Fura-2-acetoxymethyl ester (FURA-2-AM) for 15 min in acinar cells and 30 minutes in pancreatic ductal fragments or organoids in the presence of 0.05% Pluronic F-127 [74]. Acini, pancreatic ductal cells and organoids were attached to a poly-L-lysine-coated coverslip (24 mm diameter) as the base of a perfusion chamber and were mounted on the stage of an Olympus IX71 inverted microscope and were perfused with different solutions at 37°C. Region of interests (ROIs) were determined by the Xcellence Software (Olympus) and changes of $[Ca^{2+}]_i$, was determined by exciting the cells with an Olympus MT-20 illumination system equipped with a 150 W xenon arc light source. For Fura2 the filter combination was as follows: 340/26 nm and 387/11 nm single-

band bandpass filters for excitation (Semrock; P/N: FF01-340/26- 25 and FF01-387/11-25, respectively), 409 nm edge single edge standard epi-fluorescence dichroic beam splitter (Semrock; P/N: FF409-Di03-25 × 36) and 510/84 nm single-band bandpass filters for emission (Semrock; P/N: FF01-510/84-25). The fluorescent signal was captured by a Hamamatsu ORCA-ER CCD camera through a ×20 oil immersion objective (Olympus; NA: 0.8) with a temporal resolution of 1 s. Ratio-metric image analysis was performed by Olympus excellence software.The changes of $[Ca^{2+}]_i$ were calculated from the F340/F380 fluorescence ratio.

3.7. Mitochondrial membrane potential measurements

Changes of the mitochondrial membrane potential ($\Delta\Psi_m$) were followed by using tetramethylrhodamine - methyl ester (TMRM) which accumulates in the mitochondria depending on $\Delta\Psi_m$. Pancreatic acinar cells were incubated with 100nM TMRM (ThermoFisher Scientific Cat. No.: T668) in standard HEPES solution for 20 min at 37°C on a poly-l-lysine-coated cover glass and were then perfused with solutions at 37°C. The perfusion solutions were also supplemented with 100nM TMRM to avoid dye leakage. Changes in TMRM fluorescence was monitored using a ZEISS LSM880 confocal microscope equipped with a 40x water immersion objective. The cells were exited with 543 nm and the emitted light was captured between 560nm and 650nm. ROIs were places on the mitochondria of pancreatic acinar cells. Fluorescence signals were normalized to initial fluorescence intensity (F_1/F_0) and were expressed as relative fluorescence.

3.8. Investigation of acinar cell fate

To quantify acinar cell death an apoptosis/necrosis detection kit was used according to the manufacturer´s instruction (Abcam Cat. No.: ab176750). CytoCalcein Violet 450 is sequestered in the cytoplasm of live cells. In apoptosis, phosphatidylserine (PS) is transferred to the outer leaflet of the plasma membrane, which can be detected by the PS sensor Apopxin Deep Red. During necrosis the cell membrane integrity is lost and thus the DNA Nuclear Green DCS1, a membrane-impermeable dye can label the nucleus of damaged cells. Briefly, pancreatic acinar cells from wild-type (WT) and TRPM2 KO mice were isolated as described above with modifications to improve overall cell survival (shorter tissue digestion and gentle centrifugation was applied) and incubated with 1 mM H_2O_2 or 250 µM CDC for 30 min. Cells were then centrifuged at 500 RCF for 5 min

at 4°C and washed twice with PBS. Cells were then resuspended in 200 µL of Assay Buffer and loaded with CytoCalcein 450, Nuclear Green and Apopxin Deep Red at room temperature for 30–60 min. Following this, cells were collected and centrifuged at 500 RCF for 5 min at 4°C before being placed on a Cellview cell culture slide (Greiner Bio-One cat. no.: 543979) for imaging. Images were captured using a Zeiss LSM880 confocal microscope with different channels and wavelengths according to each dye: CytoCalcein 450 (Ex/Em = 405/450 nm), Nuclear Green (Ex/Em = 490/520 nm) and Apopxin Deep Red (Ex/Em = 630/660 nm). For each condition, five images were captured, and the total number of cells was counted by two independent investigators. Cells with Nuclear Green staining were considered necrotic, with Apopxin Deep Red staining apoptotic, whereas double stained cells were considered necrotic.

3.9. In vivo acute pancreatitis models

Cerulein-induced acute pancreatitis was triggered by 10, hourly intraperitoneal injections of 50 µg/bwkg cerulein (Bachem Cat. No.: H-3220) (control groups received physiological saline) [74]. Two hours after the last injection, mice were euthanized with 85 mg/kg pentobarbital. Biliary AP was triggered by the administration of 4% Na-taurocholate (TC) (Sigma-Aldrich Cat. No.: 86339) into the common bile duct as described previously by Perides et al. [75]. Briefly, mice were anaesthetized with 125 mg/kg ketamine and 12.5 mg/kg xylazine, and median laparotomy was performed, where the papilla of Vater was cannulated by a 0.4 mm diameter needle connected to an infusion pump. Mice were administered 4% Na-taurocholate or physiological saline at a perfusion rate of 10 µL/min [TSE System GmbH-cat. no.: 540060-HP] for 5 min. After the abdominal wall and the skin were closed separately, the animals were placed on a heating pad until they regained consciousness, following which they were given buprenorphine (0.075 mg/kg) i.p. to reduce pain. Mice were sacrificed 24 h later using pentobarbital (85 mg/kg i.p.). In both cases, blood samples were collected after terminal anesthesia through the inferior vena cava, and the pancreas were removed immediately. Blood samples were placed on ice and then centrifuged at 2500 RCF for 15 min at 4°C. Serum samples were collected and stored at −20°C. Pancreas samples were placed into a 4% formaldehyde solution and stored at 4°C until histology. A colorimetric kit (A Amylase Assay) was used to measure serum amylase activity (Diagnosticum, Cat. No.: 47462). Absorbance of the samples was detected at 405 nm using a FLUOstar OPTIMA (BMG Labtech) microplate reader. Formaldehyde-fixed pancreas samples were embedded in paraffin, and 4 µm

thick sections were cut and stained with hematoxylin–eosin. Histologic parameters such as oedema, inflammatory cell infiltration and necrosis were scored (0–5 points for oedema, leukocyte infiltration and necrosis for the total histological score, or % of total area for necrosis) by three independent investigators blinded to the protocol [74]. Averages of the scores were calculated and included to the manuscript. Total histological score was calculated by adding the individual scores together.

3.10. Statistics

Statistical analysis was performed by GraphPad Prism software. All data are expressed as means ± SD. Both parametric (one-way analysis of variance) and nonparametric (Mann Whitney test, Kruskal Wallis test - for analysis of the acinar cell survival assay) tests were used based on the normality of data distribution. A p value of less than 0.05 was accepted as statistically significant.

4. Results

4.1. TRPM2 channel is expressed in the exocrine pancreas

End-point PCR analysis of isolated acini confirmed that the TRPM2 gene was expressed in the exocrine pancreatic cells (Figure 5.A.). The immunofluorescent labelling of TRPM2 was performed on isolated acinar clusters the confocal images showed that TRPM2 channels were expressed on the basolateral membrane of the pancreatic acinar cells (Figures 5.B).

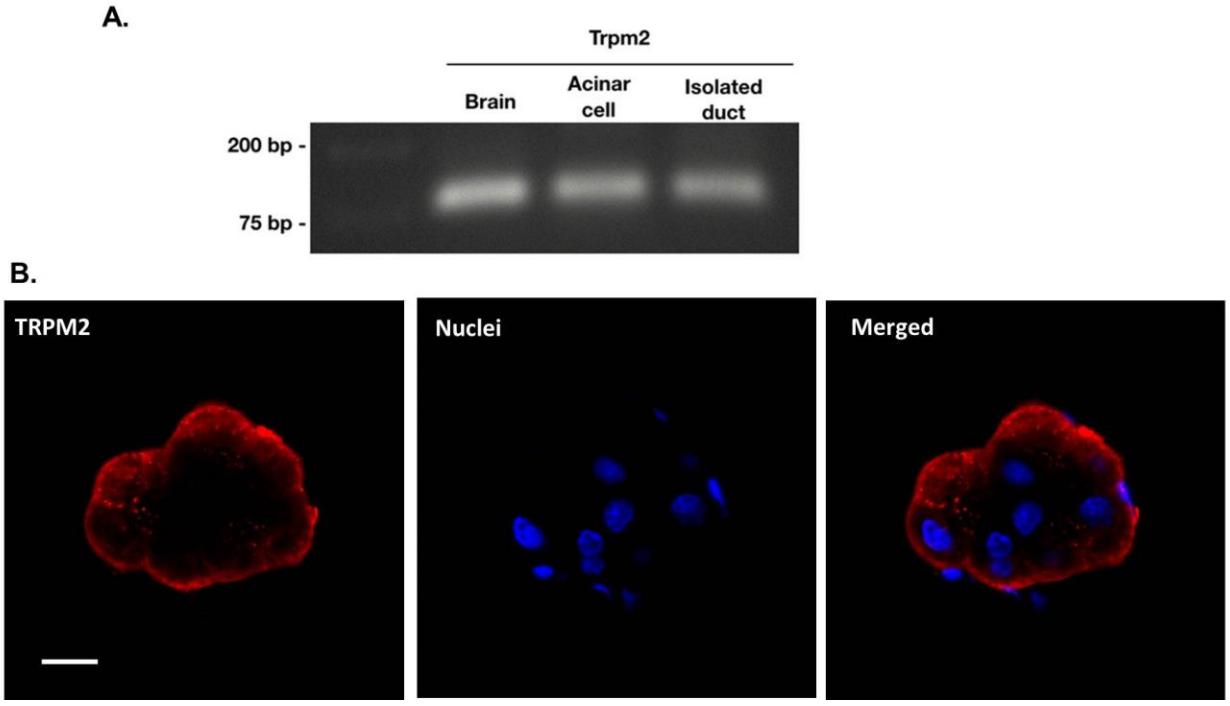

Figure 5. Expression of TRPM2 in the pancreatic acinar cells. A. Agarose gel images of cDNA samples derived from isolated acini confirmed that the TRPM2 gene is expressed in the isolated pancreatic acinar cells. **B.** Immunofluorescent labelling of TRPM2 on isolated acinar clusters. TRPM2 channels are expressed on the basolateral membrane of the pancreatic acinar cells. Scale bar: 10 μm.

4.2. Functional TRPM2 channels are present in pancreatic acinar

When isolated WT pancreatic acini were challenged with 1 mM H_2O_2 to increase ROS, a rapid and sustained increase of $[Ca^{2+}]_I$ was observed (Figure 6.A-B), which was significantly reduced in the

TRPM2 knockout (KO) acini (0.41 ± 0.09 vs 0.17 ± 0.029, respectively). In cells treated in an extracellular Ca^{2+}-free medium, Ca^{2+} elevation was found to be significantly impaired, and no difference was detected between WT and TRPM2 KO cells. This suggests that the sustained elevation of $[Ca^{2+}]_I$ in response to H_2O_2 was largely due to TRPM2-channel-mediated influx of extracellular Ca^{2+}. In addition, H_2O_2 activated a reversible cationic membrane current, with a relative linear I–V relationship as was reported previously for TRPM2 [59] (Figure 7.A-B)

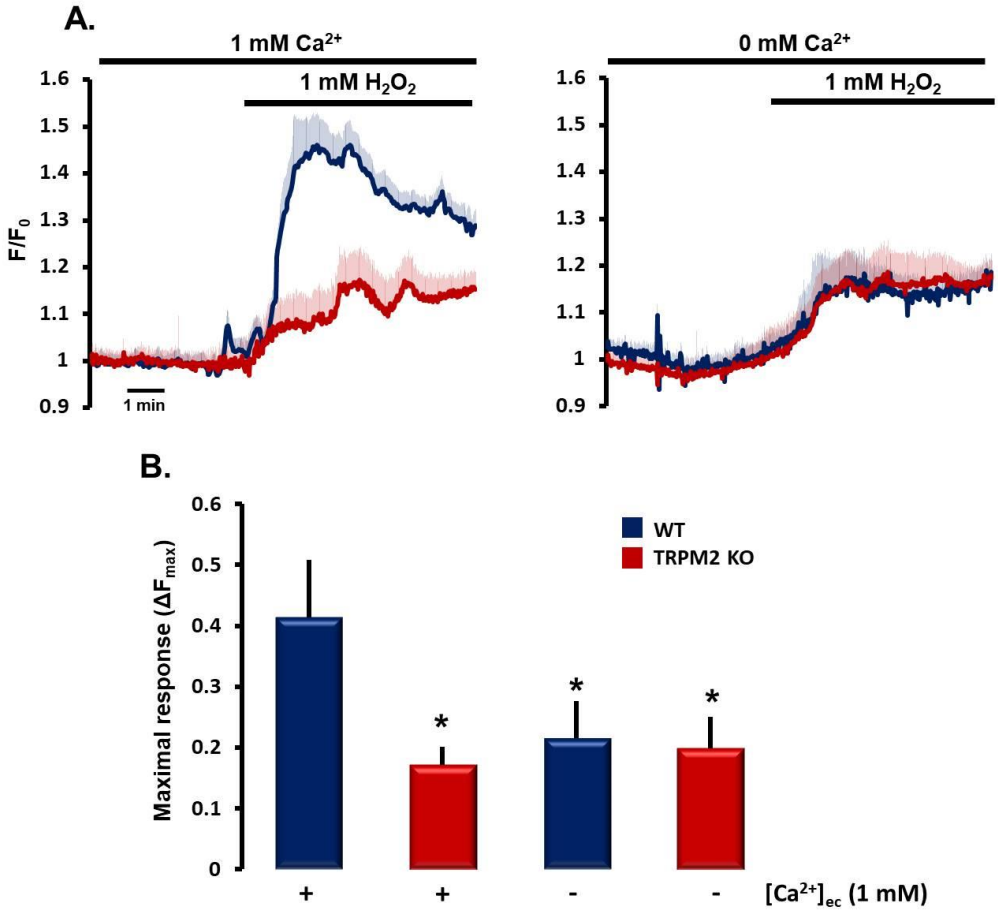

Figure 6. Functional activity of TRPM2 in pancreatic acinar cells. A. Average traces of 5–6 individual experiments demonstrating the effect of 1 mM H_2O_2 on pancreatic acinar cells in the presence or absence of extracellular Ca^{2+}. **B.** Bar charts summarize the maximal Ca^{2+} responses to H_2O_2, which was significantly reduced in TRPM2 KO acini. *: $p < 0.05$ vs WT.

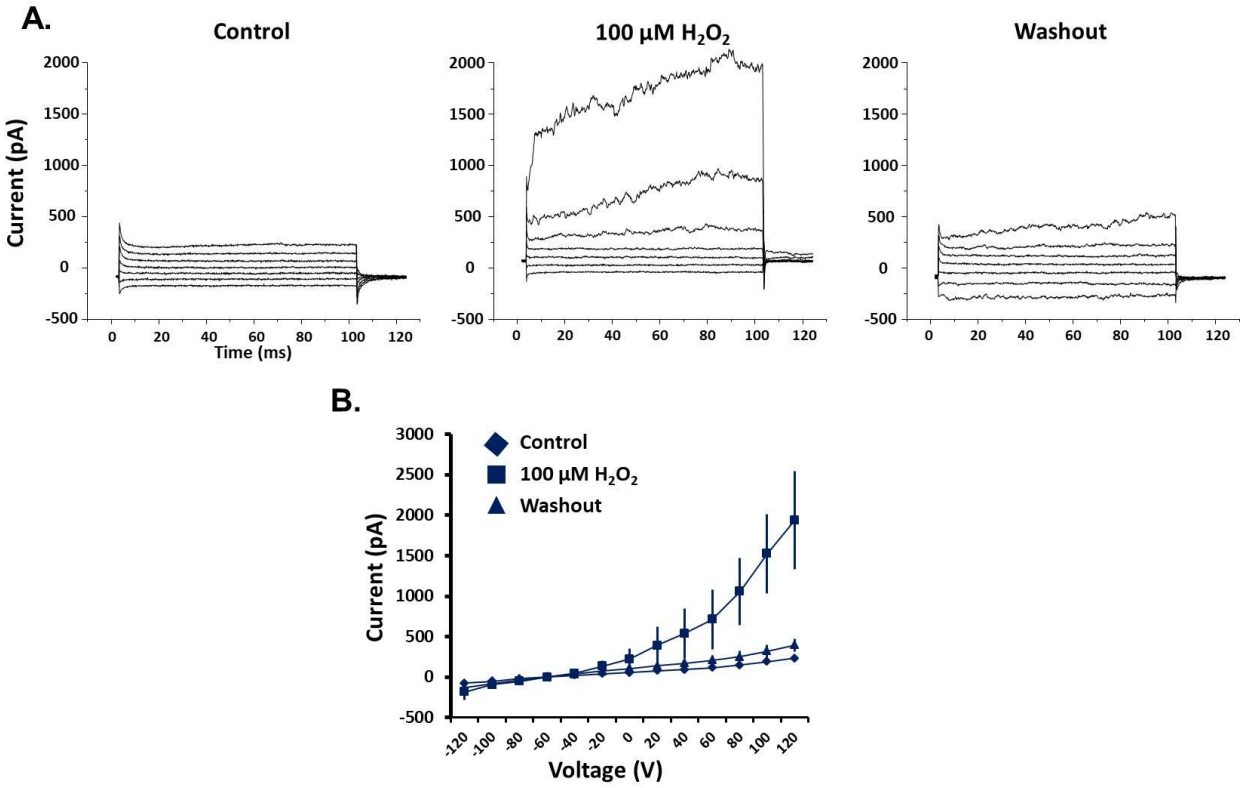

Figure 7. TRPM2 current measurement in pancreatic acinar cells. A. Representative whole cell current recordings and current–voltage relationships in isolated pancreatic acini. **B.** I-V relationship of TRPM2 current. H_2O_2 activated a reversible cationic membrane current, with a relative linear I–V relationship. n = 4/group.

4.3. TRPM2 contributes to bile-acid-induced extracellular Ca^{2+} influx in pancreatic acinar cells

Bile acids have an important pathogenetic role in the development of biliary pancreatitis and can cause the release of Ca^{2+} from intracellular stores and trigger extracellular Ca^{2+} influx. Therefore, to study the role of TRPM2 in this process, the intracellular Ca^{2+} elevation in response to bile acid treatment was examined in pancreatic acini of WT and TRPM2 KO mice. Administration of 250 µM CDC was found to trigger a rapid, sustained increase in $[Ca^{2+}]$ I, which was markedly impaired in the TRPM2 KO acinar cells (0.834 ± 0.02 vs 0.655 ± 0.04) (Figure 8.A-B). These results highlight that TRPM2 plays an important role in bile-acid induced extracellular Ca^{2+} influx in pancreatic acinar cells.

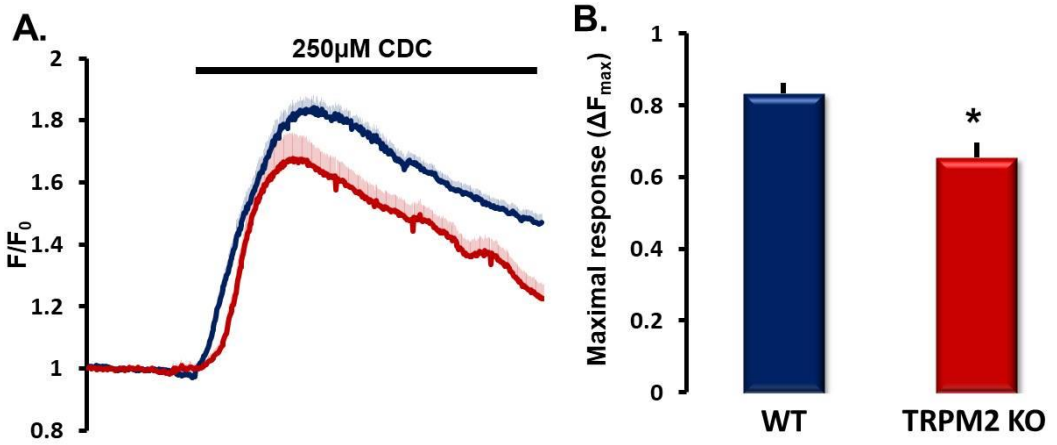

Figure 8. The role of TRPM2 in bile-acid-evoked Ca^{2+} signal generation. A. Average traces of 5–6 individual experiments comparing intracellular Ca^{2+} elevations evoked by 250 μM CDC in WT and TRPM2 KO acini and isolated ducts. **B.** Bar charts of the Ca^{2+} elevations evoked by bile acid. Genetic deletion of TRPM2 reduced the bile-acid-induced Ca^{2+} elevation in pancreatic acini. *: $p < 0.05$ vs WT.

4.4. Lack of TRPM2 decreases acinar cell necrosis during bile acid exposure

Pancreatic acinar cell fate determines the severity of AP. Because of this, it was also important to characterize the role of TRPM2 in acinar cell death. In the untreated control samples, ~85% of the acinar cells were viable in both the WT and TRPM2 KO samples, which is comparable to previously published results [43]. Incubation of WT and TRPM2 KO acini with 1 mM H_2O_2 for 30 min remarkably decreased the number of viable cells, and necrotic cell death was significantly increased (Figure 9.A-B). A lack of TRPM2 was observed to protect acinar cells from oxidative stress- induced cell necrosis during H_2O_2 treatment (% of viable cells: 19.4 ± 0.4 in WT vs 49.1 ± 1.2 in TRPM2 KO). The rate of apoptosis was similar in TRPM2 KO and WT acini (% of apoptotic cells: 9.1 ± 4.3 in WT vs 10.8 ± 2.5 in TRPM2 KO), whereas necrosis was significantly impaired in TRPM2 KO acini (% of necrotic cells: 71.5 ± 4.2 in WT vs 40.1 ± 3.2 in TRPM2 KO). Similarly, incubation of acinar cells with 250 μM CDC for 30 min decreased the number of live cells in WT sample, however overall cell survival was remarkably improved by TRPM2 deletion (% of viable cells: 48.3 ± 0.9 in WT vs 74.1 ± 1.3 in TRPM2 KO) (Figure 9.A-B). TRPM2 deletion significantly decreased booth apoptotic and necrotic cell death in the CDC treated group (WT: 15.4 ± 2.5% vs KO: 8.5 ± 1.3% and WT: 36.3 ± 2.2% vs KO:17.4 ± 1.3%, respectively). Importantly, the lack of

TRPM2 channels resulted in a ~30% decrease in acinar cell death, suggesting that TRPM2 has an important contribution to acinar cell death during biliary AP.

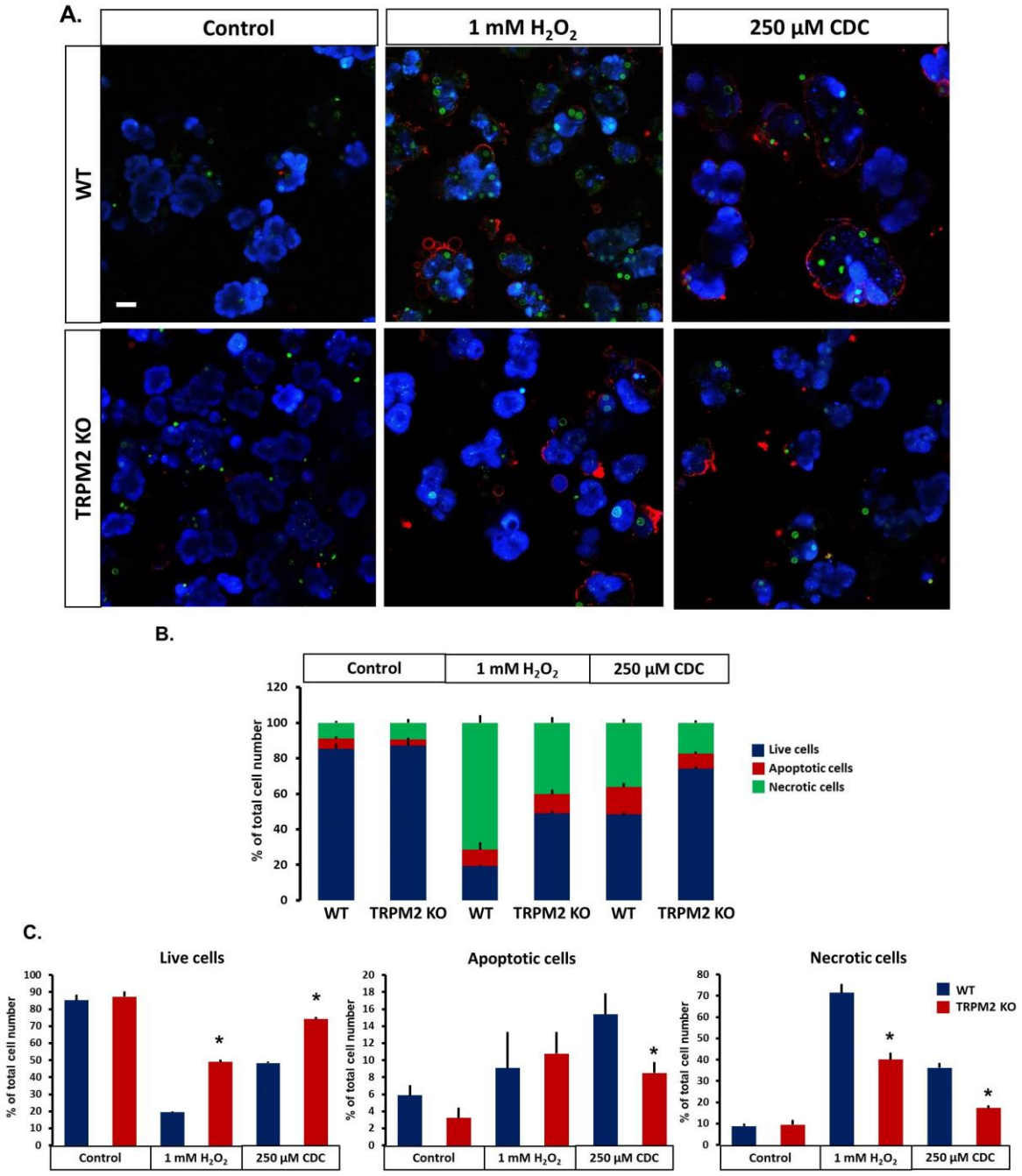

Figure 9. The role of TRPM2 in acinar cell necrosis during bile acid exposure. A. Representative images of different conditions (blue: live cells labelled with CytoCalcein 450, green: necrotic cells labelled with Nuclear Green, and red: apoptotic cells labelled with Apopxin Deep Red). Scale bar: 20 µm. **B.** Bar chart representing the ratio of live, apoptotic and necrotic

cells. Incubation of WT and TRPM2 KO acini with 1 mM H_2O_2 or with 250 μM CDC for 30 min markedly decreased the number of viable cells, whereas necrosis was significantly increased. TRPM2 KO acinar cells displayed a significantly decreased rate of apoptosis in the bile acid treated group, whereas cell necrosis was impaired in both cases. n: 4-5 experiment/group. **C.** Bar charts representing the ratio of live, apoptotic and necrotic cells. TRPM2 knockout significantly improved acinar cell survival in 1 mM H_2O_2 or with 250 μM CDC treated groups. *: $p< 0.05$ vs WT treated sample (H_2O_2 or CDC); n: 4-5 experiment/group.

4.5. Lack of TRPM2 does not prevent mitochondrial damage during bile acid exposure

We wanted to further characterize the intracellular mechanisms that play a role in TRPM2-channel mediated cell necrosis. As TRPM2 has been reported to induce mitochondrial damage [60], therefore we compared the mitochondrial membrane potential (Δψm) in WT and TRPM2 KO pancreatic acinar cells. Administration of 1 mM H_2O_2 related in a marked drop of Δψm in WT cells (Figure 10.A). The decrease of Δψm was significantly lower in TRPM2 KO cells, whereas removal of the extracellular Ca^{2+} impaired the loss of Δψm in WT cells to the level of TRPM2 KO acini. This suggests that extracellular Ca^{2+} influx through TRPM2 plays a crucial role in the oxidative stress induced mitochondrial damage seen in pancreatic acinar cells. The decrease of Δψm in response to 250 μM CDC was also compared. However, no difference was seen between WT and TRPM2 KO cells (Figure 10.B). This may be due to the Ca^{2+} -independent direct mitochondrial toxicity of bile acids [76]. Previously, TRPM2 channels have been suggested to be key mediators of diabetic stress-induced mitochondrial fragmentation in endothelial cells [61]. Notably, in pancreatic acinar cells, fragmentation of mitochondria was not observed in response to either H_2O_2 or bile acid treatment (Figure 11.).

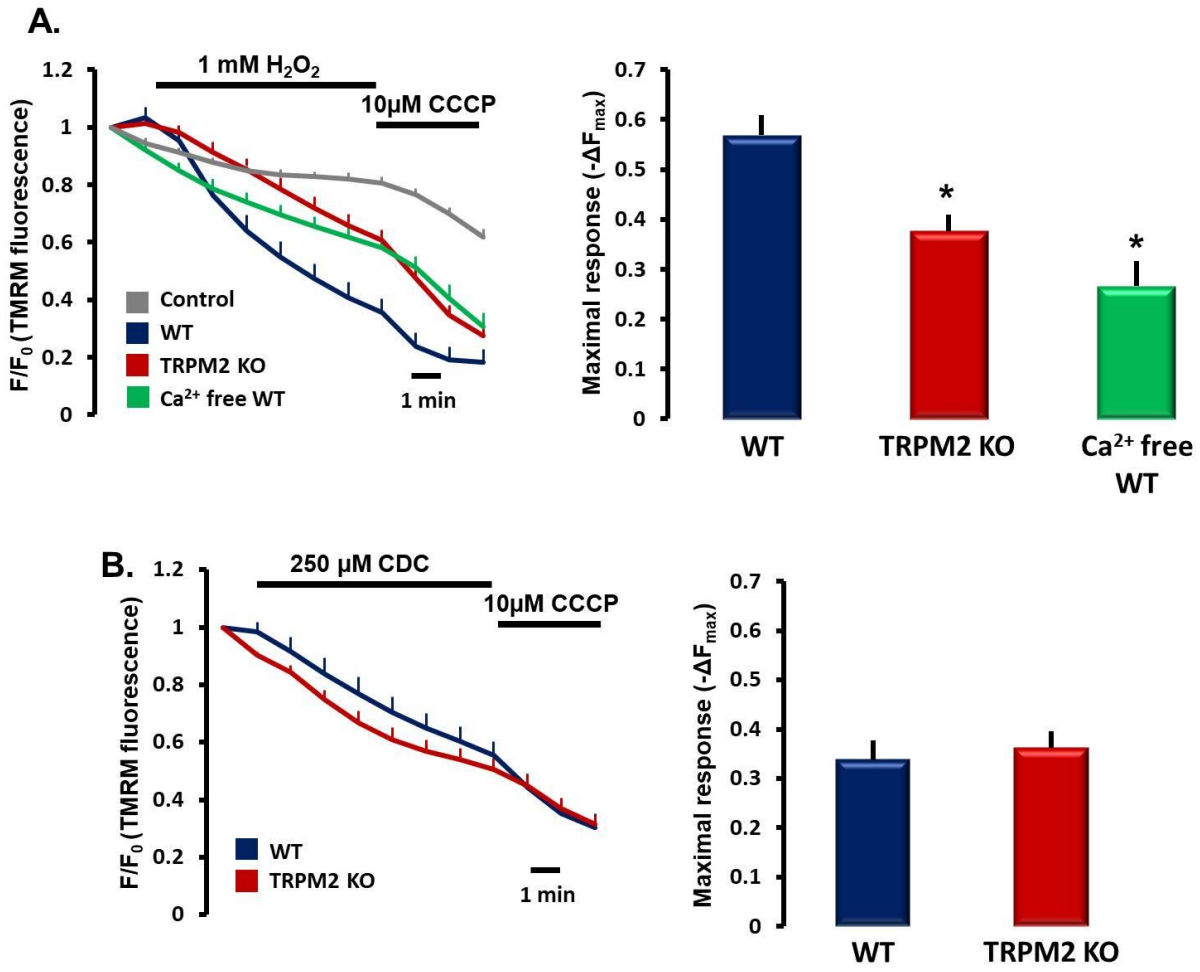

Figure 10. The effect of TRPM2 on the development of mitochondrial damage. A. Average traces and bar charts of the changes of Δψm in WT and TRPM2 pancreatic acinar cells. 1 mM H_2O_2 markedly decreased Δψm in WT cells (blue trace), which was impaired by TRPM2 knockout (red trace) or removal of the extracellular Ca^{2+} (green trace). For control cells were perfused with standard HEPES solution (grey trace). **B.** By contrast, no difference was observed when acinar cells were challenged by 250 μM CDC. n: 6–7 experiments/groups; *: $p < 0.05$ vs WT.

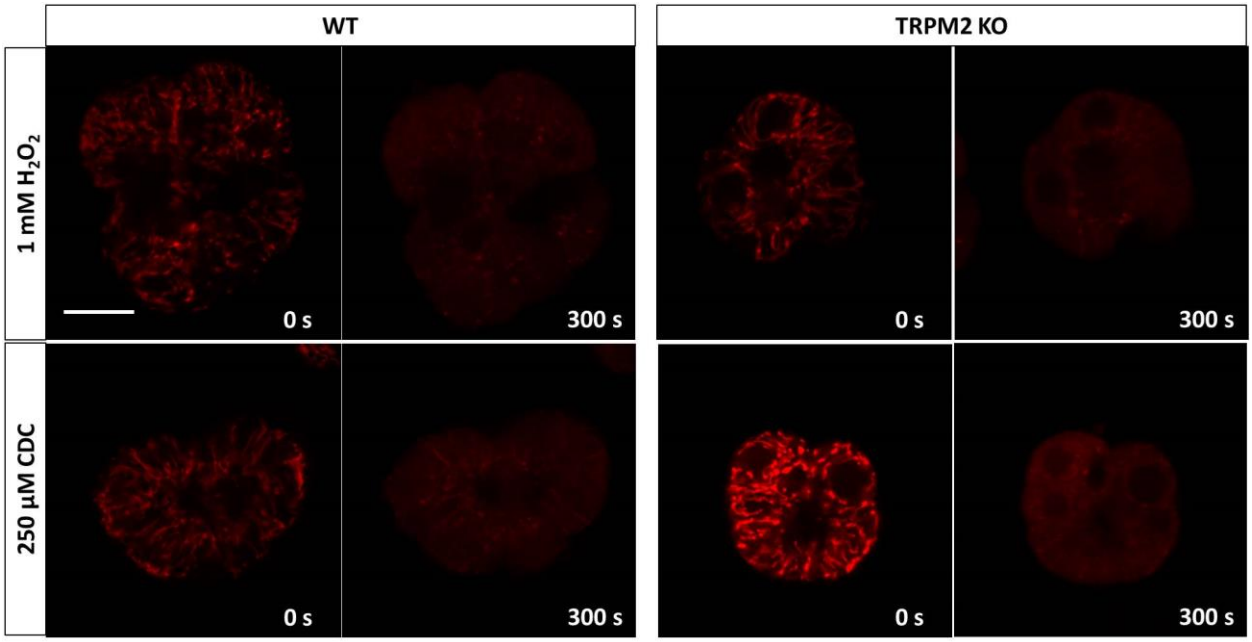

Figure 11. The role of TRPM2 in mitochondrial morphology changes. Representative confocal images of labelled mitochondria in pancreatic acinar cells. Mitochondrial fragmentation was not observed in response to H_2O_2, or to bile acid treatment. Scale bar: 10 µm.

4.6. Lack of TRPM2 decreases the severity of experimental biliary pancreatitis

To determine the role of TRPM2 in the pathogenesis of AP, the disease severity of WT and TRPM2 KO animals was compared in two well-established experimental AP models. In the first series of experiments, mice were given 10 hourly i.p. injections of either physiological saline (control group) or 50 µg/bwkg cerulein to induce AP (Figure 12.A). Overall, in this experimental model, no significant differences were detected between WT and TRPM2 KO mice. The control animals had normal pancreatic histology in both groups (Figure 12.A), whereas cerulein hyperstimulation caused extensive pancreatic damage. Despite this, no significant differences were observed between the histological parameters of WT and TRPM2 KO animals. The extent of interstitial oedema (3.14 ± 0.25 for WT vs 3.03 ± 0.34 for KO), leukocyte infiltration (2.74 ± 0.53 for WT vs 3.04 ± 0.23 for KO, p = 0.08) or necrosis(18.64 ± 3.16 for WT vs 21.32 ± 3.58 for KO) showed no significant difference in the cerulein-treated groups (Figure 12.B). More importantly, the role of TRPM2 channel in the pathogenesis of biliary AP was also examined. In this model, pancreatitis was induced by intraductal infusion of 4% Na-taurocholate (control animals received physiological saline) as described previously [74]. The infusion of 4% Na-taurocholate induced necrotizing

pancreatitis in both WT and TRPM2 KO mice, accompanied by elevated histological and laboratory parameters (Figures 13.A). The extent of interstitial oedema (2.8 ± 0.16 for WT vs 2.7 ± 0.2 for KO) or leukocyte infiltration (3.3 ± 0.38 for WT vs 2.7 ± 0.29 for KO, p = 0.08) was not significantly different in the Na-taurocholate-treated groups. Notably, the extent of necrosis was significantly higher in the WT group in comparison to the TRPM2 KO animals (41.3% ± 7.13% for WT vs 26.4% ± 5.5% for KO) (Figures 13.B). In accordance with these findings, serum amylase activities were also significantly higher in the Na-taurocholate-treated WT animals versus the TRPM2 KO group. This perfectly mimicked the *in vitro* results obtained in this study, further confirming the crucial role of the TRPM2 channel in the pathogenesis of biliary AP.

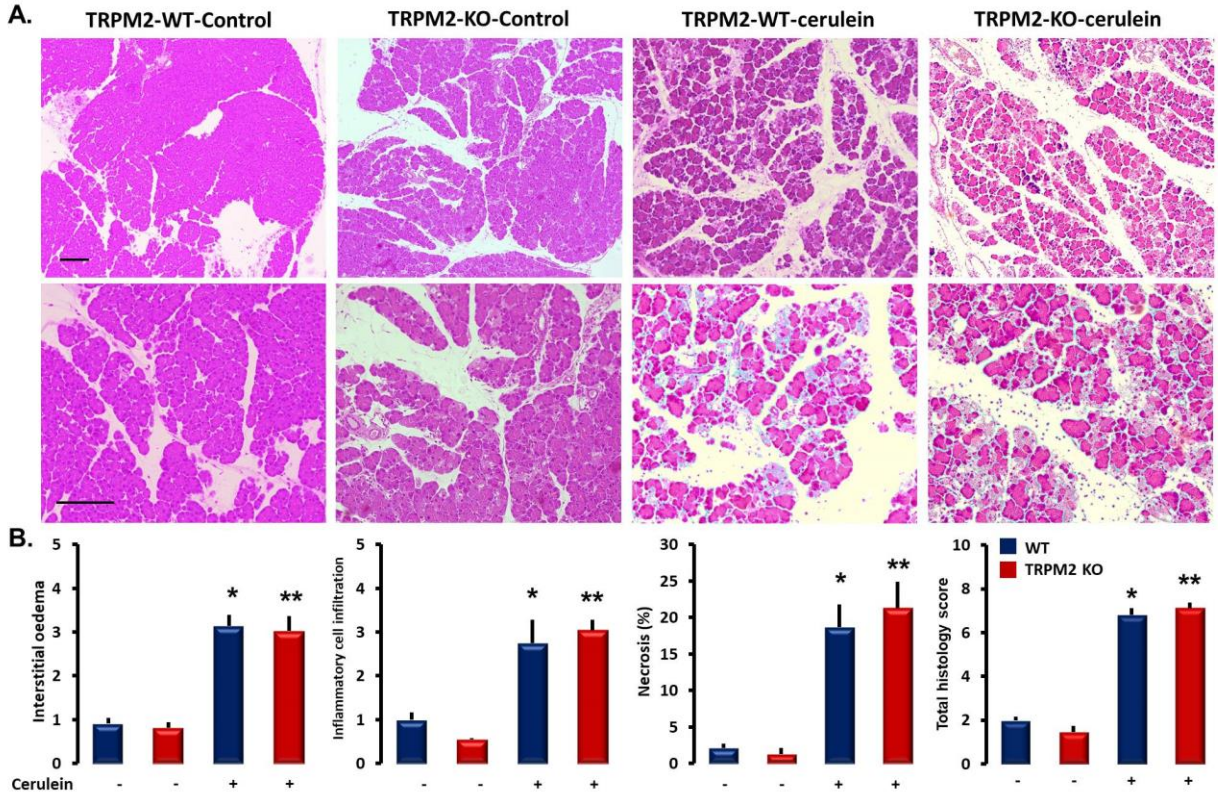

Figure 12. Genetic knockout of TRPM2 does not decrease the severity of cerulean-induced acute pancreatitis. A. Representative images of pancreatic histology in cerulein-induced pancreatitis. Mice were given 10 hourly i.p. injections of either physiological saline (control group) or 50 μg/bwkg cerulein. Scale bar: 100 μm. **B.** The graphs show cerulein administration caused extensive pancreatic damage; however, no significant differences were observed in the histological parameters of WT and TRPM2 KO animals. n: 6–7 animals/groups; *: $p < 0.05$ vs WT; **: $p < 0.05$ vs TRPM2 KO.

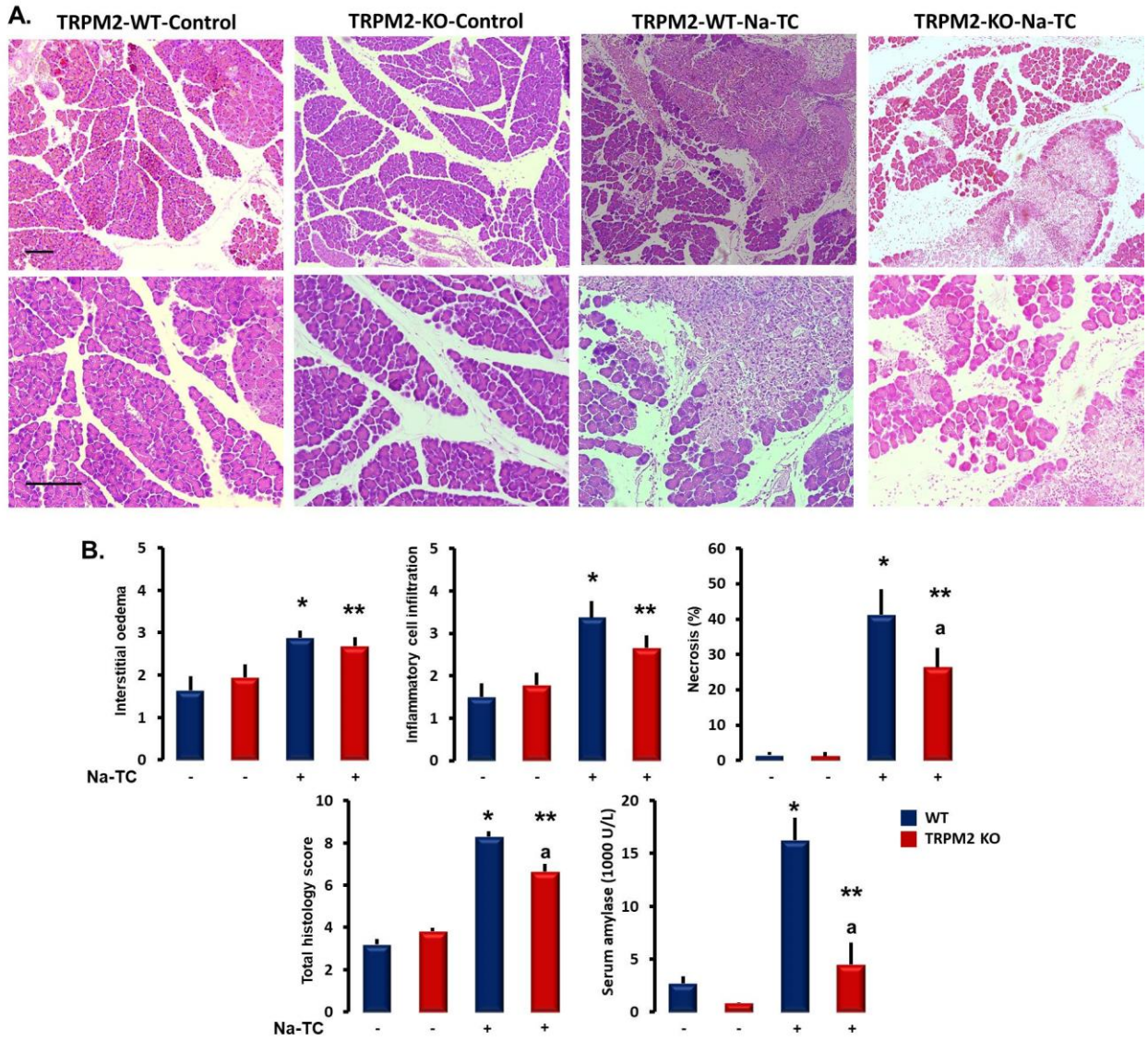

Figure 13. Genetic knockout of TRPM2 decreases the severity of biliary acute pancreatitis. **A.** Representative images of pancreatic histology in Na-taurocholate-induced pancreatitis. Pancreatitis was induced by intraductal infusion of 4% Na-taurocholate. Scale bar: 100 µm. **B.** The graphs show the infusion of 4% Na-taurocholate-induced necrotizing pancreatitis in WT and TRPM2 KO mice accompanied by elevated histological and laboratory parameters. Although the extent of interstitial oedema or leukocyte infiltration was not different, the extent of necrosis was significantly impaired in the TRPM2 KO animals. n: 6–7 animals/groups; *: $p < 0.05$ vs WT control; **: $p < 0.05$ vs TRPM2 KO control; a: $p < 0.05$ vs WT Na-TC treated.

4.7. Intracellular Ca^{2+} signaling in pancreatic organoids

Organoid cultures emerged as novel 3D models of epithelial physiology and pathology, which have several advantages (see in the Introduction). Therefore, OCs might be a better model in exocrine pancreatic research, however we have only limited information about the functional properties (like Ca^{2+} signaling) of OCs. To investigate this, we compared Ca^{2+} signaling in primary pancreatic ducts and in OCs. For the release of Ca^{2+} from the endoplasmic reticulum Ca^{2+} stores, we used two Ca^{2+} mobilizing agonists (ATP and carbachol). We observed that both agonists induced peak-plateau type Ca^{2+} elevation in the tested concentrations (Figure 14.A). These signals showed no significant differences in the maximal response (Figure. 14.B bar chart). We also compared the store operated Ca^{2+} entry caused by the ER store depletion (Figure 15.A). Applying this assay, we detected that the ER Ca^{2+} release induced by 25 µM cyclopiazonic acid (CPA) was significantly higher in isolated ducts, whereas the Ca^{2+} influx was significantly higher in OCs (Figure 15.B bar chart). These observations need further investigation to determine the biological relevance of this phenomena.

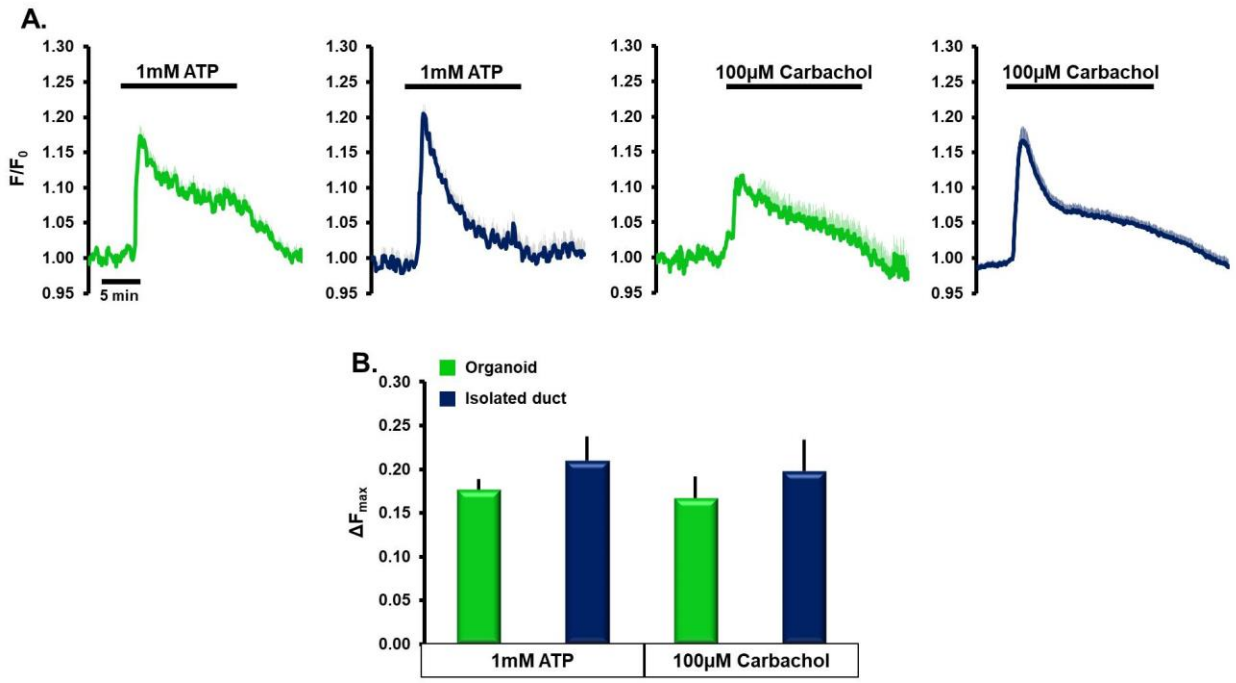

Figure 14. Agonist induced intracellular Ca^{2+} elevation in isolated pancreatic ducts and organoids. **A**, Average traces of 4–6 experiments demonstrating the effect of 1 mM ATP, or 100 µM carbachol on pancreatic epithelial cells. Both agonists induced peak-plateau Ca^{2+} signals. **B.** Summary of the maximal Ca^{2+} responses to agonist stimulation. . n: 6–7 experiments/groups.

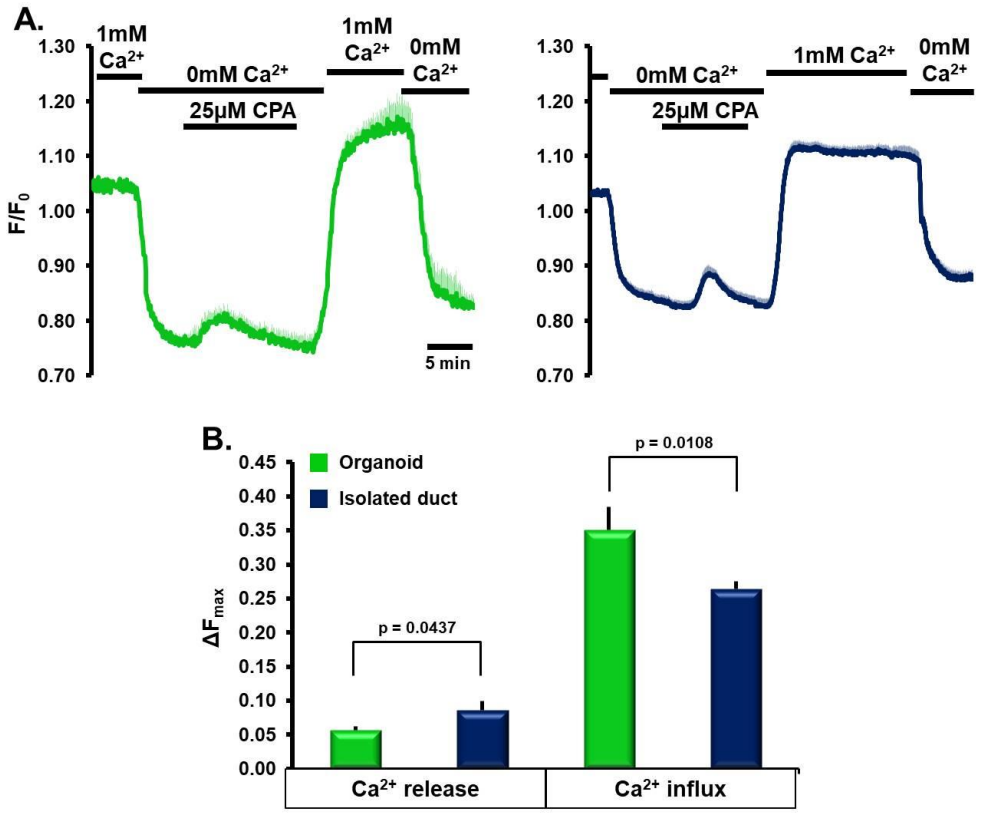

Figure 15. Intracellular Ca^{2+} release and extracellular Ca^{2+} influx in isolated pancreatic ducts and organoids. **A.** Ca^{2+} influx in pancreatic ducts and OCs (average traces of 4–6 experiments). ER Ca^{2+} release induced by 25 μM CPA and Ca^{2+} influx was measured by the maximal response to re-addition of Ca^{2+}. **B.** ER Ca^{2+} release (first two columns) and extracellular Ca^{2+} influx (second two columns).

5. Discussion

5.1. TRPM2-mediated extracellular Ca^{2+} entry promotes acinar cell necrosis in biliary acute pancreatitis

Several publications suggested that bile acids can generate prolonged intracellular Ca^{2+} elevation, increase ROS production and damage the mitochondria in pancreatic acini. These pathologic changes can trigger the development of AP, which is a severe inflammatory disease of the gastrointestinal tract that has no specific treatment. The role of TRPM2 emerged in the development of Ca^{2+}-dependent cell injury as a ROS-sensitive non-specific cation channel, however the possible role of TRPM2 in the pathogenesis of AP has yet to be investigated.

Though the expression of TRPM2 has been demonstrated previously in different cell types, including inflammatory cells [55], myocytes [77] and epithelial cells [59], to our knowledge, this is the first report demonstrating the expression of TRPM2 in the exocrine pancreas. Using conventional PCR and immunolabelling techniques, the expression of TRPM2 in the basolateral membrane of acinar cells was confirmed. In addition, increased intracellular ROS was found to trigger TRPM2-mediated extracellular Ca^{2+} influx in acinar cells. This study did not show any alterations in acinar cell function between WT and TRPM2 KO mice. However, intracellular Ca^{2+} signalling is one of the major signalling pathways in the exocrine pancreas [78, 79] which regulates the secretion of digestive enzymes in acinar cells as well as ion and fluid secretion in ductal cells. Therefore, it might be possible that TRPM2-mediated Ca^{2+} entry could contribute to physiological signalling, though further studies are required in order to confirm this. In other cell types, redox signals have been demonstrated to sensitise TRPM2 and increase the intracellular Ca^{2+} concentration at physiological body temperature, which plays an important role in the regulation of macrophage functions [80]. In TRPM2 KO mice, blood glucose levels were significantly higher, whereas insulin secretion was significantly impaired, suggesting a potential role of TRPM2-mediated Ca^{2+} increase in insulin secretion [81]. On the other hand, activation of TRPM2 channels in pancreatic β-cells increased intracellular Ca^{2+} concentration and release of sequestered intracellular Zn^{2+} from lysosomes [82]. In these experiments, gene knockout of TRPM2 protected mice from β-cell death. Previously, TRPM2 facilitated extracellular Ca^{2+} influx in monocytes in response to H_2O_2 and thus regulated the production of the macrophage inflammatory protein-2

(CXCL2), which, in turn, regulated the inflammatory response in a dextran sulphate sodium-induced colitis inflammation model in mice [55]. In another experimental model, the lack of TRPM2-regulated CXCL2 production in TRPM2 KO mice suppressed neutrophil infiltration into the central nervous system and slowed the progression of experimental autoimmune encephalomyelitis [83]. The role of TRPM2 has also been indicated in irradiation-induced side effects in cancer patients. In salivary gland epithelial cells, irradiation increased ROS production during radiotherapy of head and neck cancers, which activated TRPM2-mediated extracellular Ca^{2+} influx in acinar cells [59]. The sustained intracellular Ca^{2+} entry leads to impaired secretory function of acinar cells and to the development of xerostomia–a frequent side effect of radiotherapy in these patients. In a downstream study, the same group demonstrated that irradiation increased the mitochondrial Ca^{2+} concentration and the production of ROS, impaired the $\Delta\psi_m$ and activated caspase-3. These changes lead to a sustained decrease in STIM1 expression and consequently decreased the store-operated Ca^{2+} entry [60].

Disturbed intracellular Ca^{2+} homeostasis has been suggested by several studies to play a pivotal role in bile-acid-induced exocrine pancreatic cell damage. In pancreatic acini, bile acids trigger dose-dependent intracellular Ca^{2+} elevation via the activation of IP_3 and ryanodine receptors [30]. In addition, Perides et al. showed that activation of the G-protein-coupled cell surface bile acid receptor (Gpbar1 or TGR5) at the apical membrane of pancreatic acinar cells leads to sustained Ca^{2+} elevation, intracellular activation of digestive enzymes and cell injury [33]. Moreover, the genetic deletion of Gpbar1 specifically reduced the severity of TLCS-induced AP. On the other hand, however, in pancreatic ductal cells, CDC dose-dependently elevated the intracellular Ca^{2+} level and inhibited HCO_3^- secretion [34]. In our experiments, CDC increased the $[Ca^{2+}]_I$ both in acinar and ductal cells, but genetic deletion of TRPM2 decreased Ca^{2+} elevation only in acinar cells. The results of this study show that the TRPM2 channel has a ~22% contribution to the bile-acid-generated Ca^{2+} signal in acinar cells. In pancreatic acini, other plasma membrane Ca^{2+} channels were also demonstrated to contribute to cell damage during AP. Gerasimenko et al. showed that the inhibition of extracellular Ca^{2+} entry via Orai1 decreases acinar cell necrosis *in vitro* [15]. Moreover, inhibition of Orai1 by selective inhibitors markedly impaired the extracellular Ca^{2+} influx and sustained Ca^{2+} overload in pancreatic acinar cells upon bile acid stimulation, which significantly impaired pancreatic oedema, inflammation and necrosis in

experimental models of AP [16]. Others found that deletion of TRPC3 markedly reduced the bile-acid-evoked Ca^{2+} signals and decreased the intracellular trypsin activation *in vitro* and the severity of cerulein-induced AP *in vivo* [17]. In addition, Kim et al. described that transporter-mediated bile acid uptake results in a specific and significant of the sarco/endoplasmic reticulum Ca^{2+} ATPase pump function and thus deplete the endoplasmic reticulum Ca^{2+} stores leading cell damage and necrosis [84].

Intracellular Ca^{2+} overload can lead to premature activation of trypsinogen [1], mitochondrial damage and cell necrosis in acinar cells [14]. In this study, a knockout of TRPM2 resulted in a significant protection of pancreatic acinar cells from H_2O_2 and bile-acid-induced necrosis. Importantly, this protection was also observed in TC-induced AP as the extent of necrosis was significantly lower in TRPM2 knockout mice compared to the WT littermates. In line with our results, in a previous study, Booth et al. reported that incubation of pancreatic acinar cells with TLC-S *in vitro* induced Ca^{2+}-dependent necrosis, which was abolished by BAPTA-AM pre-treatment [43]. Using different inhibitors to prevent apoptosis and necrosis, the authors suggested that elevated intracellular and intramitochondrial ROS are the major triggers of apoptosis, whereas increases in intracellular and intramitochondrial Ca^{2+} induce necrosis. As bile acids inhibited cellular ATP production [31] and decreased $\Delta\Psi_m$ [32], we also compared the changes of $\Delta\Psi_m$ in response to bile acid treatment in TRPM2 KO and WT acinar cells. The genetic knockout of TRPM2 and removal of the extracellular Ca^{2+} markedly reduced the drop of $\Delta\psi_m$, suggesting that extracellular Ca^{2+} influx through TRPM2 plays a crucial role in oxidative-stress-induced mitochondrial damage. Despite this, we did not detect this protective effect in bile-acid-treated cells a result which might be explained by the Ca^{2+}-independent direct mitochondrial toxicity of bile acids. Direct mitochondrial toxicity of bile acids was described in an experimental model of cholestasis. In these series of experiments Schultz et al. found that bile acids impaired the mitochondrial membrane potential and induced mitochondrial permeability transition pore opening [76]. Another group showed that physiologically relevant concentrations of bile acids can induce alterations in the mitochondria outer membrane (MOM) order, which again can lead to the opening of the mitochondrial membrane permeability transition pore in isolated mitochondria [85]. Previously, we [34] and others also reported [32] that the toxic effects of bile acids cannot be completely abolished by the removal of intracellular Ca^{2+} elevation. Mitochondrial fragmentation,

which has been previously linked to the activation of TRPM2 [61], was not observed in our experiments. These results suggest that bile acids can induce mitochondrial damage in several different ways independently form intracellular Ca^{2+} overload. On the other hand, independently from mitochondrial damage, other Ca^{2+}-dependent toxic effects of bile acids have been described, which could also contribute to acinar cell necrosis. Bile acids were shown to activate calcineurin via the elevation of intracellular Ca^{2+} in pancreatic acinar cells, leading to intra-acinar activation of chymotrypsinogen and NF-κB activation, and acinar cell death [26]. In addition, genetic or pharmacological inhibition of calcineurin reduced the severity of TLC-S-induced AP, and pharmacologic and genetic inhibition of calcineurin abolished the translocation of protein kinase C, which is a critical upstream regulator of NF-κB activation [27].

In our study general TRPM2 knockout mice were used, therefore other factors might contribute to the observed protective effect of TRPM2 deletion in acute biliary pancreatitis. It is well described that inflammatory cells contribute to the severity of acute pancreatitis [86, 87]. Previously, TRPM2 was identified as a crucial contributor of monocyte response to oxidative stress, which in turn regulated the production of CXCL2 and inflammatory response in experimental colitis in mice [55]. Although inflammatory cell infiltration of the damaged area peaks several days (on day 3-4) after the initial injury, therefore these cell types do not contribute to the early events in acute pancreatitis pathogenesis. In our series of experiments, the animals were sacrificed 24 hours after the bile acid infusion, therefore we concluded that the observed difference is primarily due to the lack of TRPM2 expression in the acinar cells.

Taken together, to the best of our knowledge, this is the first report of the expression and pathological function of the TRPM2 channel in the exocrine pancreas. We demonstrated that pancreatic acinar cells express functionally active TRPM2, which can be activated by increased oxidative stress. Importantly, we also provided evidence that TRPM2 activity contributes to bile-acid-induced extracellular Ca^{2+} influx in acinar cells, which promotes acinar cell necrosis independently from mitochondrial damage and increases the severity of bile-acid-induced experimental pancreatitis. These results suggest that inhibition of TRPM2 might be a potential option for use in treating biliary pancreatitis.

5.2. Intracellular Ca^{2+} signaling in pancreatic organoids

Pancreatic exocrine, secretory processes are challenging to investigate on primary epithelial cells. In pancreatic research currently OCs are studied as relevant human models of tissue development [69] and carcinogenesis [70]. OCs have recently emerged as promising *ex vivo* models of tissue physiology and pathophysiology. OCs are 3D self-organizing, organ like *in vitro* grown cell cultures where the cell-to cell contact is maintained. Reports suggest that cells in OCs maintain tissue specific gene expression, cell morphology and function and may represent features of malignant diseases. Although organoids are used in an increased number of studies, we only have limited experimental data about their physiological relevance, especially in case of pancreatic OCs. Pancreatic organoid cultures may help to overcome shortcomings of the current models, however their physiological relevance or their utility in disease modeling are not known. To answer these questions, we provide side by side comparison of Ca^{2+} signaling of epithelial cells in primary mouse isolated pancreatic ducts and organoids. To release the Ca^{2+} from the ER we used two Ca^{2+} mobilizing agonist ATP and carbachol, where both agonists induced a peak-plateau type Ca^{2+} elevation. There were no significant differences in the maximal response, but Ca^{2+} release was slightly lower in organoid than in the isolated ducts. The ER Ca^{2+} released by CPA was higher in isolated duct, whereas the Ca^{2+} influx was significantly higher in OCs. These observations need further investigation to get to know the biological relevance of this fact. The changes of extracellular Ca^{2+} concentration regulates ion secretion in physiology [88] and impairs transport function via complex mechanism in pathology [78]. In ductal cells intracellular Ca^{2+} signaling play a central role in the regulation of HCO_3^- secretion, however aberrant calcium signaling can lead to intracellular Ca^{2+} overload and toxicity, including mitochondrial damage and impaired ATP production [78]. To investigate a potential drug target, we needed to observe the Ca^{2+} signaling in an advanced *in vitro* model. Therefore our model could be utilized in drug screening models as well as in basic and translational pancreatic research.

6. Summary

Background: Biliary pancreatitis is one of the most common forms of acute pancreatitis. Aberrant intracellular Ca^{2+} signaling is the hallmark of acute pancreatitis inducing mitochondrial damage, intra-acinar digestive enzyme activation and cell death. Thus, prevention of toxic cellular Ca^{2+} overload is a promising therapeutic target. The TRPM2 is a non-selective cation channel that plays major role in oxidative stress induced cellular Ca^{2+} overload in different cell types. Although likely, its role in pancreatic acinar cells and the pathogenesis of AP was not investigated yet.

The **aim** of this study to investigate the expression of TRPM2 and characterize the functional activity of the channel in pancreatic acinar cells and its possible role in acute pancreatitis.

Methods: In our experiments pancreatic acinar cells were isolated from WT and TRPM2 knockout KO mice with enzymatic digestion. Besides mouse pancreatic ductal fragments were isolated by enzymatic digestion. The isolated ducts were grown in Matrigel on 37 ℃ for a week in OC media. The changes of the intracellular Ca^{2+} level was measured whit fluorescent microscopy using FURA2-AM. The mitochondrial membrane potential in acinar cells was measured with confocal microscopy using TMRM and generation of intracellular ROS was measured by H2DCFDA ROS indicator. The type of cell death in acinar cells was measured by confocal microscopy using an Apoptosis/Necrosis kit. To detect the two different AP model were used cerulein induced where the mice were given 10 hourly I.P. injection of 50 µg/bwkg cerulein and sodium taurocholate-treated which was induced by intraductal infusion of 4% Na-taurocholate. The control mice were given physiological saline.

Results: We found that TRPM2 is expressed in the plasma membrane of mouse pancreatic acinar cells, which can be activated by increased oxidative stress induced by H_2O_2 treatment. TRPM2 activity was found to contribute to bile acid induced extracellular Ca^{2+} influx in acinar cells but did not have the same effect in ductal cells. This activity promoted acinar cell necrosis *in vitro* independently from mitochondrial damage or mitochondrial fragmentation. In addition, bile-acid-induced experimental pancreatitis was less severe in TRPM2 knockout mice, whereas the lack of TRPM2 had no protective effect in cerulein induced acute pancreatitis. Our results suggest that the inhibition of TRPM2 may be a potential treatment option for biliary pancreatitis.

Conclusion: To best of our knowledge this is the first study of the expression and the pathological

function of TRPM2 channel in the exocrine pancreas. Our results confirmed the expression and the functional activity of the TRPM2 channel in PAC, which can be activated by increased oxidative stress. TRPM2 activity contributes to bile acid - induced Ca^{2+} influx in PAC, which promotes acinar cell necrosis independently of mitochondrial damage. We also observed the Ca^{2+} signaling in an advanced 3D *in vitro* model, although observations need further investigation to determine the biological relevance of this phenomenon. The presence of TRPM2 also increases the severity of bile-acid induced experimental pancreatitis. These results suggest that the inhibition of TRPM2 might be a potential pharmacological therapeutic target for use in treating biliary pancreatitis.

New observations

- This is the first study demonstrating the expression of TRPM2 in the exocrine pancreas
- We described that TRPM2 is localized in the plasma membrane of pancreatic acinar cells
- H_2O_2 activated TRPM2 in pancreatic acinar cells as demonstrated by the intracellular Ca^{2+} elevation and characteristic cationic currents, which was absent in TRPM2 knockout acini
- Bile acids activate TRPM2 mediated extracellular Ca^{2+} influx
- H_2O_2 and bile acid -induced necrotic cell death was markedly reduced in acinar cells from TRPM2 knockout mice suggesting a remarkable role of TRPM2 in acinar cell fate
- the severity of bile induced (but not cerulean induced) experimental AP was lower in TRPM2 knockout mice suggesting that TRPM2 may represent a new pharmaceutical drug target for the treatment of biliary pancreatitis
- the agonist induced intracellular Ca^{2+} signaling was similar in isolated pancreatic ducts and pancreatic organoids, although the ER Ca^{2+} release induced by CPA was higher in isolated ducts than in organoids, whereas the Ca^{2+} influx was significantly higher in organoids.

7. Acknowledgement

I would like to thank all the people who have helped and inspired me during my doctoral studies. I would like to express my deep and most sincere thanks to my mentor and supervisor **Dr. József Maléth** for all his help, support, guidance throughout these years**.** Without his outstanding supervision this dissertation would not have been possible**.** I also grateful and I would like to thank to my other supervisor **Prof. Dr. Péter Hegyi** chairman of the Institute for Translational Medicine, University of Pécs for his support and scientific advices.

I am grateful to **Prof. Dr. Csaba Lengyel** and **Prof. Dr. György Ábrahám,** the current and former head of First Department of Medicine, University of Szeged and **Prof. Dr. Varró András** (former head of Department of Pharmacology and Pharmacotherapy University of Szeged) who gave me the opportunity to work at their Departments.

I owe a special thanks to **Dr. Pallagi Petra** for her collaboration and scientific advices throughout the last year. I also would like to thank to Prof. **Dr. Zoltán Rakonczay Jr.** (Department of Pathophysiology, University of Szeged) for the scientific advices during these years.

I would also like to thank to my colleagues and friends (in alphabetic order) **Kitti Ancsányi, ,Emese Réka Bálint, Dr. Eszter Becskeházi, Orsolya Berczeli, Dr. Péter Csernay-Bíró, Dr. Zsolt Balla, Szilvia Déri, Klaudia Dobai, Attila Ébert, Gréta Elekes, Gabriella Fűr, Eleonóra Gál, Zsuzsanna Gyömbér, Marietta Görög, Anna Grassalkovich, Xénia Katona, Evelyin Kelemen, Balázs Koncz, Dr. Eszter Kormányos, Anett Lőrincz, Tamara Madácsy, Réka Molnár, Dr. Szentesi Andrea, Dávid Tàlas, Àrpád Tóth, Emese Tóth, Dr. Viktória Venglovecz** for all the help, encouragement, support, entertainment and great time what we had without them it would not be possible.

This work would not have been possible to accomplish without the assistance work of **Tünde Pritz, Miklósné Àrva, Rea Fritz, Tóth Zsolt, Nikoletta Szabó, Edit Magyarné Pálfi and †Erzsébet Zoltánné Fuksz.**

I deeply grateful to **Gyula Diszházi** and Dr. **János Almássy** (Department of Physiology, University of Debrecen) for the outstanding collaboration.

I have to say a special thanks to my boyfriend **Dr. Ernesto Ruivo** for all the support, help, patience all along these years. Last, but not least I owe warm thanks to **my parents, Julianna Rácz Fanczalné, István Fanczal my siblings Bence Fanczal, Dr. Eszter Fanczal, Sára Fanczal and my whole family** for all their love, support, never-ending patience, encouragement and for always being there.

I dedicate this thesis to them!

8. References

1. Kruger, B., E. Albrecht, and M.M. Lerch, *The role of intracellular calcium signaling in premature protease activation and the onset of pancreatitis.* Am J Pathol, 2000. **157**(1): p. 43-50.
2. Pearson, G.T., et al., *Control of enzyme secretion by non-cholinergic, non-adrenergic nerves in guinea pig pancreas.* Nature, 1981. **290**(5803): p. 259-61.
3. Razzini, G., et al., *The role of the pleckstrin homology domain in membrane targeting and activation of phospholipase Cbeta(1).* J Biol Chem, 2000. **275**(20): p. 14873-81.
4. Berridge, M.J., *Inositol trisphosphate and calcium signalling.* Nature, 1993. **361**(6410): p. 315-25.
5. Burgess, G.M., et al., *The second messenger linking receptor activation to internal Ca release in liver.* Nature, 1984. **309**(5963): p. 63-6.
6. Lee, K.P., et al., *An endoplasmic reticulum/plasma membrane junction: STIM1/Orai1/TRPCs.* FEBS Lett, 2010. **584**(10): p. 2022-7.
7. Yuan, J.P., et al., *SOAR and the polybasic STIM1 domains gate and regulate Orai channels.* Nat Cell Biol, 2009. **11**(3): p. 337-43.
8. Yuan, J.P., et al., *STIM1 heteromultimerizes TRPC channels to determine their function as store-operated channels.* Nat Cell Biol, 2007. **9**(6): p. 636-45.
9. Peery, A.F., et al., *Burden of gastrointestinal disease in the United States: 2012 update.* Gastroenterology, 2012. **143**(5): p. 1179-87 e1-3.
10. Parniczky, A., et al., *Prospective, Multicentre, Nationwide Clinical Data from 600 Cases of Acute Pancreatitis.* PLoS One, 2016. **11**(10): p. e0165309.
11. Pandol, S.J., et al., *Acute pancreatitis: bench to the bedside.* Gastroenterology, 2007. **132**(3): p. 1127-51.
12. Crockett, S.D., et al., *American Gastroenterological Association Institute Guideline on Initial Management of Acute Pancreatitis.* Gastroenterology, 2018. **154**(4): p. 1096-1101.
13. Maleth, J. and P. Hegyi, *Ca2+ toxicity and mitochondrial damage in acute pancreatitis: translational overview.* Philos Trans R Soc Lond B Biol Sci, 2016. **371**(1700).
14. Criddle, D.N., et al., *Fatty acid ethyl esters cause pancreatic calcium toxicity via inositol trisphosphate receptors and loss of ATP synthesis.* Gastroenterology, 2006. **130**(3): p. 781-93.
15. Gerasimenko, J.V., et al., *Ca2+ release-activated Ca2+ channel blockade as a potential tool in antipancreatitis therapy.* Proc Natl Acad Sci U S A, 2013. **110**(32): p. 13186-91.
16. Wen, L., et al., *Inhibitors of ORAI1 Prevent Cytosolic Calcium-Associated Injury of Human Pancreatic Acinar Cells and Acute Pancreatitis in 3 Mouse Models.* Gastroenterology, 2015. **149**(2): p. 481-492 e7.
17. Kim, M.S., et al., *Deletion of TRPC3 in mice reduces store-operated Ca2+ influx and the severity of acute pancreatitis.* Gastroenterology, 2009. **137**(4): p. 1509-17.
18. Rizzuto, R., et al., *Close contacts with the endoplasmic reticulum as determinants of mitochondrial Ca2+ responses.* Science, 1998. **280**(5370): p. 1763-6.
19. Halestrap, A.P., *What is the mitochondrial permeability transition pore?* J Mol Cell Cardiol, 2009. **46**(6): p. 821-31.

20. Bender, T. and J.C. Martinou, *Where killers meet--permeabilization of the outer mitochondrial membrane during apoptosis.* Cold Spring Harb Perspect Biol, 2013. **5**(1): p. a011106.

21. Halestrap, A.P. and P. Pasdois, *The role of the mitochondrial permeability transition pore in heart disease.* Biochim Biophys Acta, 2009. **1787**(11): p. 1402-15.

22. Halestrap, A.P., *Mitochondrial calcium in health and disease.* Biochim Biophys Acta, 2009. **1787**(11): p. 1289-90.

23. Barrow, S.L., et al., *ATP depletion inhibits Ca2+ release, influx and extrusion in pancreatic acinar cells but not pathological Ca2+ responses induced by bile.* Pflugers Arch, 2008. **455**(6): p. 1025-39.

24. Fischer, L., et al., *Phosphatidylinositol 3-kinase facilitates bile acid-induced Ca(2+) responses in pancreatic acinar cells.* Am J Physiol Gastrointest Liver Physiol, 2007. **292**(3): p. G875-86.

25. Voronina, S., et al., *Bile acids induce calcium signals in mouse pancreatic acinar cells: implications for bile-induced pancreatic pathology.* J Physiol, 2002. **540**(Pt 1): p. 49-55.

26. Muili, K.A., et al., *Bile acids induce pancreatic acinar cell injury and pancreatitis by activating calcineurin.* J Biol Chem, 2013. **288**(1): p. 570-80.

27. Muili, K.A., et al., *Pancreatic acinar cell nuclear factor kappaB activation because of bile acid exposure is dependent on calcineurin.* J Biol Chem, 2013. **288**(29): p. 21065-73.

28. Lerch, M.M. and A.A. Aghdassi, *The role of bile acids in gallstone-induced pancreatitis.* Gastroenterology, 2010. **138**(2): p. 429-33.

29. Lerch, M.M., et al., *Pancreatic duct obstruction triggers acute necrotizing pancreatitis in the opossum.* Gastroenterology, 1993. **104**(3): p. 853-61.

30. Gerasimenko, J.V., et al., *Bile acids induce Ca2+ release from both the endoplasmic reticulum and acidic intracellular calcium stores through activation of inositol trisphosphate receptors and ryanodine receptors.* J Biol Chem, 2006. **281**(52): p. 40154-63.

31. Voronina, S.G., et al., *Dynamic changes in cytosolic and mitochondrial ATP levels in pancreatic acinar cells.* Gastroenterology, 2010. **138**(5): p. 1976-87.

32. Voronina, S.G., et al., *Effects of secretagogues and bile acids on mitochondrial membrane potential of pancreatic acinar cells: comparison of different modes of evaluating DeltaPsim.* Journal of Biological Chemistry, 2004. **279**(26): p. 27327-38.

33. Perides, G., et al., *Biliary acute pancreatitis in mice is mediated by the G-protein-coupled cell surface bile acid receptor Gpbar1.* Gastroenterology, 2010. **138**(2): p. 715-25.

34. Venglovecz, V., et al., *Effects of bile acids on pancreatic ductal bicarbonate secretion in guinea pig.* Gut, 2008. **57**(8): p. 1102-12.

35. Maleth, J., et al., *Non-conjugated chenodeoxycholate induces severe mitochondrial damage and inhibits bicarbonate transport in pancreatic duct cells.* Gut, 2011. **60**(1): p. 136-8.

36. Lerch, M.M. and A.A. Aghdassi, *The role of bile acids in gallstone-induced pancreatitis*, in *Gastroenterology*. 2010: United States. p. 429-33.

37. Adam-Vizi, V. and C. Chinopoulos, *Bioenergetics and the formation of mitochondrial reactive oxygen species.* Trends Pharmacol Sci, 2006. **27**(12): p. 639-45.

38. Hamanaka, R.B. and N.S. Chandel, *Mitochondrial reactive oxygen species regulate cellular signaling and dictate biological outcomes.* Trends Biochem Sci, 2010. **35**(9): p. 505-13.

39. Booth, D.M., et al., *Redox Nanodomains Are Induced by and Control Calcium Signaling at the ER-Mitochondrial Interface.* Mol Cell, 2016. **63**(2): p. 240-248.

40. Criddle, D.N., *Reactive oxygen species, Ca(2+) stores and acute pancreatitis; a step closer to therapy?* Cell Calcium, 2016. **60**(3): p. 180-9.

41. Forkink, M., et al., *Detection and manipulation of mitochondrial reactive oxygen species in mammalian cells.* Biochim Biophys Acta, 2010. **1797**(6-7): p. 1034-44.

42. Criddle, D.N., et al., *Menadione-induced reactive oxygen species generation via redox cycling promotes apoptosis of murine pancreatic acinar cells.* J Biol Chem, 2006. **281**(52): p. 40485-92.

43. Booth, D.M., et al., *Reactive oxygen species induced by bile acid induce apoptosis and protect against necrosis in pancreatic acinar cells.* Gastroenterology, 2011. **140**(7): p. 2116-25.

44. Booth, D.M., et al., *Calcium and reactive oxygen species in acute pancreatitis: friend or foe?* Antioxid Redox Signal, 2011. **15**(10): p. 2683-98.

45. Perez, S., et al., *Redox signaling in acute pancreatitis.* Redox Biol, 2015. **5**: p. 1-14.

46. Hara, Y., et al., *LTRPC2 Ca2+-permeable channel activated by changes in redox status confers susceptibility to cell death.* Mol Cell, 2002. **9**(1): p. 163-73.

47. Wang, L., et al., *Structures and gating mechanism of human TRPM2.* Science, 2018. **362**(6421).

48. Yamamoto, S. and S. Shimizu, *Targeting TRPM2 in ROS-Coupled Diseases.* Pharmaceuticals (Basel), 2016. **9**(3).

49. Toth, B. and L. Csanady, *Identification of direct and indirect effectors of the transient receptor potential melastatin 2 (TRPM2) cation channel.* J Biol Chem, 2010. **285**(39): p. 30091-102.

50. Uchida, K. and M. Tominaga, *The role of TRPM2 in pancreatic beta-cells and the development of diabetes.* Cell Calcium, 2014. **56**(5): p. 332-9.

51. Turlova, E., Z.P. Feng, and H.S. Sun, *The role of TRPM2 channels in neurons, glial cells and the blood-brain barrier in cerebral ischemia and hypoxia.* Acta Pharmacol Sin, 2018. **39**(5): p. 713-721.

52. Fonfria, E., et al., *Tissue distribution profiles of the human TRPM cation channel family.* J Recept Signal Transduct Res, 2006. **26**(3): p. 159-78.

53. Hoffman, N.E., et al., *Ca(2)(+) entry via Trpm2 is essential for cardiac myocyte bioenergetics maintenance.* Am J Physiol Heart Circ Physiol, 2015. **308**(6): p. H637-50.

54. Togashi, K., et al., *TRPM2 activation by cyclic ADP-ribose at body temperature is involved in insulin secretion.* Embo j, 2006. **25**(9): p. 1804-15.

55. Yamamoto, S., et al., *TRPM2-mediated Ca2+influx induces chemokine production in monocytes that aggravates inflammatory neutrophil infiltration.* Nat Med, 2008. **14**(7): p. 738-47.

56. Lange, I., et al., *Synergistic regulation of endogenous TRPM2 channels by adenine dinucleotides in primary human neutrophils.* Cell Calcium, 2008. **44**(6): p. 604-15.

57. Toth, B., I. Iordanov, and L. Csanady, *Putative chanzyme activity of TRPM2 cation channel is unrelated to pore gating.* Proc Natl Acad Sci U S A, 2014. **111**(47): p. 16949-54.

58. Kashio, M., *Redox-Sensitive TRP channels: TRPA$_1$ and TRPM2*, M. Tomigana, Editor. 2017, IntechOpen: Redox - Principles and Advanced Applications.

59. Liu, X., et al., *Loss of TRPM2 function protects against irradiation-induced salivary gland*

dysfunction. Nat Commun, 2013. **4**: p. 1515.

60. Liu, X., et al., *Radiation inhibits salivary gland function by promoting STIM1 cleavage by caspase-3 and loss of SOCE through a TRPM2-dependent pathway.* Sci Signal, 2017. **10**(482).
61. Abuarab, N., et al., *High glucose-induced ROS activates TRPM2 to trigger lysosomal membrane permeabilization and Zn(2+)-mediated mitochondrial fission.* Sci Signal, 2017. **10**(490).
62. Sato, T., et al., *Long-term expansion of epithelial organoids from human colon, adenoma, adenocarcinoma, and Barrett's epithelium.* Gastroenterology, 2011. **141**(5): p. 1762-72.
63. Clevers, H., *Modeling Development and Disease with Organoids.* Cell, 2016. **165**(7): p. 1586-1597.
64. Nusse, R. and H. Clevers, *Wnt/beta-Catenin Signaling, Disease, and Emerging Therapeutic Modalities.* Cell, 2017. **169**(6): p. 985-999.
65. Kretzschmar, K. and H. Clevers, *Organoids: Modeling Development and the Stem Cell Niche in a Dish.* Dev Cell, 2016. **38**(6): p. 590-600.
66. Sato, T., et al., *Single Lgr5 stem cells build crypt-villus structures in vitro without a mesenchymal niche.* Nature, 2009. **459**(7244): p. 262-5.
67. Huch, M., et al., *Unlimited in vitro expansion of adult bi-potent pancreas progenitors through the Lgr5/R-spondin axis.* EMBO J, 2013. **32**(20): p. 2708-21.
68. Simian, M. and M.J. Bissell, *Organoids: A historical perspective of thinking in three dimensions.* J Cell Biol, 2017. **216**(1): p. 31-40.
69. Dahl-Jensen, S.B., et al., *Deconstructing the principles of ductal network formation in the pancreas.* PLoS Biol, 2018. **16**(7): p. e2002842.
70. Boj, S.F., et al., *Organoid models of human and mouse ductal pancreatic cancer.* Cell, 2015. **160**(1-2): p. 324-38.
71. Gout, J., et al., *Isolation and culture of mouse primary pancreatic acinar cells.* J Vis Exp, 2013(78).
72. Maleth, J., et al., *Alcohol disrupts levels and function of the cystic fibrosis transmembrane conductance regulator to promote development of pancreatitis.* Gastroenterology, 2015. **148**(2): p. 427-39 e16.
73. Geyer, N., et al., *Bile acids activate ryanodine receptors in pancreatic acinar cells via a direct allosteric mechanism.* Cell Calcium, 2015. **58**(2): p. 160-70.
74. Pallagi, P., et al., *The role of pancreatic ductal secretion in protection against acute pancreatitis in mice*.* Crit Care Med, 2014. **42**(3): p. e177-88.
75. Perides, G., et al., *Experimental acute biliary pancreatitis induced by retrograde infusion of bile acids into the mouse pancreatic duct.* Nat Protoc, 2010. **5**(2): p. 335-41.
76. Schulz, S., et al., *Progressive stages of mitochondrial destruction caused by cell toxic bile salts.* Biochim Biophys Acta, 2013. **1828**(9): p. 2121-33.
77. Miller, B.A., et al., *Trpm2 enhances physiological bioenergetics and protects against pathological oxidative cardiac injury: Role of Pyk2 phosphorylation.* J Cell Physiol, 2019.
78. Maleth, J. and P. Hegyi, *Calcium signaling in pancreatic ductal epithelial cells: an old friend and a nasty enemy.* Cell Calcium, 2014. **55**(6): p. 337-45.
79. Ahuja, M., et al., *cAMP and Ca(2)(+) signaling in secretory epithelia: crosstalk and synergism.* Cell Calcium, 2014. **55**(6): p. 385-93.

80. Kashio, M., et al., *Redox signal-mediated sensitization of transient receptor potential melastatin 2 (TRPM2) to temperature affects macrophage functions.* Proc Natl Acad Sci U S A, 2012. **109**(17): p. 6745-50.

81. Uchida, K., et al., *Lack of TRPM2 impaired insulin secretion and glucose metabolisms in mice.* Diabetes, 2011. **60**(1): p. 119-26.

82. Manna, P.T., et al., *TRPM2-mediated intracellular Zn2+ release triggers pancreatic beta-cell death.* Biochem J, 2015. **466**(3): p. 537-46.

83. Tsutsui, M., et al., *TRPM2 Exacerbates Central Nervous System Inflammation in Experimental Autoimmune Encephalomyelitis by Increasing Production of CXCL2 Chemokines.* J Neurosci, 2018. **38**(39): p. 8484-8495.

84. Kim, J.Y., et al., *Transporter-mediated bile acid uptake causes Ca2+-dependent cell death in rat pancreatic acinar cells.* Gastroenterology, 2002. **122**(7): p. 1941-53.

85. Sousa, T., et al., *Deoxycholic acid modulates cell death signaling through changes in mitochondrial membrane properties.* J Lipid Res, 2015. **56**(11): p. 2158-71.

86. Sendler, M., et al., *Cathepsin B-Mediated Activation of Trypsinogen in Endocytosing Macrophages Increases Severity of Pancreatitis in Mice.* Gastroenterology, 2018. **154**(3): p. 704-718 e10.

87. Sendler, M., et al., *NLRP3 Inflammasome Regulates Development of Systemic Inflammatory Respoes in Mice With Acute Pancreatitis.* Gastroenterology, 2019.

88. Yang, D., et al., *IRBIT governs epithelial secretion in mice by antagonizing the WNK/SPAK kinase pathway.* J Clin Invest, 2011. **121**(3): p. 956-65.

I.

The Journal of Physiology

TRPM2-mediated extracellular Ca^{2+} entry promotes acinar cell necrosis in biliary acute pancreatitis

Júlia Fanczal[1,*], Petra Pallagi[1,2,*], Marietta Görög[1,2], Gyula Diszházi[3], János Almássy[3], Tamara Madácsy[1,2], Árpád Varga[1,2], Péter Csernay-Biró[1], Xénia Katona[1,2], Emese Tóth[1], Réka Molnár[1], Zoltán Rakonczay Jr[4], Péter Hegyi[5,6] and József Maléth[1,2,7]

[1] *First Department of Internal Medicine, University of Szeged, Szeged, Hungary*
[2] *HAS-USZ Momentum Epithelial Cell Signalling and Secretion Research Group, University of Szeged, Szeged, Hungary*
[3] *Department of Physiology, University of Debrecen, Debrecen, Hungary*
[4] *Department of Pathophysiology, University of Szeged, Szeged, Hungary*
[5] *HAS-USZ Momentum Translational Gastroenterology Research Group, University of Szeged, Szeged, Hungary*
[6] *Institute for Translational Medicine, Medical School, University of Pécs, Pécs, Hungary*
[7] *Department of Public Health, University of Szeged, Szeged, Hungary*

Edited by: Kim Barrett & Pawel Ferdek

Key points

- Acute biliary pancreatitis is a significant clinical challenge as currently no specific pharmaceutical treatment exists.
- Intracellular Ca^{2+} overload, increased reactive oxygen species (ROS) production, mitochondrial damage and intra-acinar digestive enzyme activation caused by bile acids are hallmarks of acute biliary pancreatitis.
- Transient receptor potential melastatin 2 (TRPM2) is a non-selective cation channel that has recently emerged as an important contributor to oxidative-stress-induced cellular Ca^{2+} overload across different diseases.
- We demonstrated that TRPM2 is expressed in the plasma membrane of mouse pancreatic acinar and ductal cells, which can be activated by increased oxidative stress induced by H_2O_2 treatment and contributed to bile acid-induced extracellular Ca^{2+} influx in acinar cells, which promoted acinar cell necrosis *in vitro* and *in vivo*.
- These results suggest that the inhibition of TRPM2 may be a potential treatment option for biliary pancreatitis.

Abstract Acute biliary pancreatitis poses a significant clinical challenge as currently no specific pharmaceutical treatment exists. Disturbed intracellular Ca^{2+} signalling caused by bile acids is

Júlia Fanczal is a PhD candidate at the University of Szeged, First Department of Medicine, supervised by Dr József Maléth. Júlia holds an MSc degree in Biology, specialized in Molecular- Immuno- and Microbiology. Currently, her research focuses on understanding the role of oxidative stress in exocrine pancreatic diseases. She found that the non-selective cation channel TRPM2 is an important contributor of the oxidative stress-induced pancreatic acinar cell damage during biliary acute pancreatitis. **Petra Pallagi** is a research fellow at the First Department of Internal Medicine at the University of Szeged. She earned her PhD under the supervision of Peter Hegyi and Zoltan Rakonczay at the University of Szeged for her work on the role of pancreatic ductal secretion in acute pancreatitis pathogenesis. She also investigated how activated trypsin inhibits pancreatic ductal secretion. Her current work is focusing on intracellular signalling and secretion in the exocrine pancreas.

*These authors contributed equally

 DOI: 10.1113/JP279047

a hallmark of the disease, which induces increased reactive oxygen species (ROS) production, mitochondrial damage, intra-acinar digestive enzyme activation and cell death. Because of this mechanism of action, prevention of toxic cellular Ca^{2+} overload is a promising therapeutic target. Transient receptor potential melastatin 2 (TRPM2) is a non-selective cation channel that has recently emerged as an important contributor to oxidative-stress-induced cellular Ca^{2+} overload across different diseases. However, the expression and possible functions of TRPM2 in the exocrine pancreas remain unknown. Here we found that TRPM2 is expressed in the plasma membrane of mouse pancreatic acinar and ductal cells, which can be activated by increased oxidative stress induced by H_2O_2 treatment. TRPM2 activity was found to contribute to bile acid-induced extracellular Ca^{2+} influx in acinar cells, but did not have the same effect in ductal cells. The generation of intracellular ROS in response to bile acids was remarkably higher in pancreatic acinar cells compared to isolated ducts, which can explain the difference between acinar and ductal cells. This activity promoted acinar cell necrosis *in vitro* independently from mitochondrial damage or mitochondrial fragmentation. In addition, bile-acid-induced experimental pancreatitis was less severe in TRPM2 knockout mice, whereas the lack of TRPM2 had no protective effect in cerulein-induced acute pancreatitis. Our results suggest that the inhibition of TRPM2 may be a potential treatment option for biliary pancreatitis.

(Received 1 October 2019; accepted after revision 24 December 2019; first published online 9 January 2020)
Corresponding author: Jozsef Maleth MD, PhD, HAS-USZ Momentum Epithelial Cell Signalling and Secretion Research Group, First Department of Medicine and Department of Public Health, University of Szeged, H6720, Szeged; Hungary. Email: jozsefmaleth1@gmail.com

Introduction

Acute pancreatitis (AP) is one of the most common inflammatory diseases of the gastrointestinal tract (Yadav & Lowenfels, 2013), and is primarily caused by impacted gallstones or heavy alcohol consumption (Parniczky *et al.* 2016). Despite intense efforts in both basic and clinical research, no specific pharmaceutical treatment exists, and the mortality associated with severe forms of AP (∼10% of all cases) remains remarkably high (∼28%) (Parniczky *et al.* 2016). The 'common channel' theory of biliary pancreatitis suggests that communication between the common bile duct and the pancreatic duct may exist because of impacted gallstones. Theoretically, bile acids could reach the pancreatic ductal system and the acinar cells through this channel (Lerch & Aghdassi, 2010). Although this hypothesis remains unproven (DiMagno *et al.* 1982; Lerch *et al.* 1993), several studies have shown that bile acids disturb intracellular Ca^{2+} homeostasis and trigger mitochondrial damage in the exocrine pancreas. Bile acids are known to increase the intracellular Ca^{2+} concentration ($[Ca^{2+}]_I$) in isolated pancreatic acinar (Gerasimenko *et al.* 2006) and ductal cells (Venglovecz *et al.* 2008) *in vitro* via Ca^{2+} release from intracellular stores, sarco-endoplasmic reticulum Ca^{2+} pump (SERCA) inhibition (Kim *et al.* 2002) and extracellular Ca^{2+} influx (Hong *et al.* 2011). This sustained elevation of $[Ca^{2+}]_I$ can induce intra-acinar trypsinogen activation (Halangk *et al.* 2002; Sherwood *et al.* 2007), mitochondrial damage (Voronina *et al.* 2010; Maleth *et al.* 2011) and, consequently, cell necrosis in the exocrine pancreas. In addition, Booth *et al.* (2011) have demonstrated that taurolithocholic acid sulphate (TLC-S) increases production of intracellular and mitochondrial reactive oxygen species (ROS), which was dependent on increases in $[Ca^{2+}]_I$ and mitochondrial Ca^{2+} concentration (Booth *et al.* 2011). They also showed that bile acid induced the increased generation of ROS and promoted apoptosis, whereas increased intracellular and intramitochondrial Ca^{2+} initiated necrosis.

In recent years, transient potential melastatin-like 2 (TRPM2), a Ca^{2+}-permeable non-selective cation channel, has been identified to act as a cellular redox-sensor (Hara *et al.* 2002; Di *et al.* 2011), which plays an important role in physiological functions as well as in various diseases (Takahashi *et al.* 2011). Activation of TRPM2 by H_2O_2 is suggested to occur indirectly through intracellular production of adenosine diphosphate ribose (ADPR), which then binds to and stimulates the C-terminal ADPR pyrophosphatase Nudix-like domain (NUDT9-H motif) of TRPM2 (Perraud *et al.* 2005). In monocytes, Ca^{2+} influx via TRPM2 was shown to increase chemokine production, leading to enhanced neutrophil infiltration in inflammatory bowel diseases (Yamamoto *et al.* 2008). More recently, TRPM2 has been implicated in the pathogenesis of irradiation-induced xerostomia. Liu *et al.* (2013) demonstrated that irradiation followed by increased ROS production activates TRPM2, leading to extracellular Ca^{2+} influx and a consequent loss of acinar cell function in the salivary glands. In a downstream study, the authors also showed that irradiation activated a TRPM2-dependent mitochondrial pathway,

leading to caspase-3 activation and mediated cleavage of stromal interaction molecule 1, which then attenuated store-operated Ca^{2+} entry (Liu *et al.* 2017). In the endocrine pancreas, TRPM2 has been suggested to play a role in diabetic stress-induced mitochondrial fragmentation. Abuarab *et al.* (2017) demonstrated that ROS production induced by high glucose concentrations activates TRPM2 and triggers lysosomal membrane permeabilization, leading to Zn^{2+}-mediated mitochondrial fission. These studies demonstrate the expression of TRPM2 in various epithelial cells, and this protein plays a central role in the pathogenesis of oxidative-stress-related diseases. Despite this knowledge, the expression or function of TRPM2 in exocrine pancreatic cells has never been investigated.

In this study, TRPM2 was shown to be expressed in the acinar and ductal cells of the exocrine pancreas. In both cell types, TRPM2 was also found to mediate extracellular Ca^{2+} influx during oxidative stress conditions. The non-conjugated bile acid chenodeoxycholate (CDC) was found to activate TRPM2-mediated Ca^{2+} influx in acinar cells, but did not do the same in ductal cells, contributing to acinar cell damage and increased acinar cell necrosis that was independent of mitochondrial damage. Importantly, a knockout of the gene encoding TRPM2 was found to significantly decrease tissue necrosis in an experimental model of acute biliary pancreatitis. Taken together, these results are the first description of the expression and functional activity of TRPM2 in the exocrine pancreas. Moreover, evidence was demonstrated for the important role that the activation of this channel plays in biliary pancreatitis.

Materials and methods

Animals

TRPM2 knockout mice were generously provided by Yasuo Mori (Kyoto University, Kyoto, Japan). The knockout mice were generated from a C57BL/6 background as described previously (Yamamoto *et al.* 2008). $TRPM2^{+/+}$ and $TRPM2^{-/-}$ mice were bred from $TRPM2^{+/-}$ animals and were used for experiments between the age of 8 and 12 weeks. Mice were kept in a standard 12 h light–dark cycle and on standard rodent food *ad libitum*. Mice were genotyped using a standard PCR assay (Liu *et al.* 2013). Experiments on live animals were carried out with adherence to NIH guidelines and EU directive 2010/63/EU for the protection of animals used for scientific purposes. The study was authorized by the National Scientific Ethical Committee on Animal Experimentation under licence number XXI./2523/2018. Terminal anaesthesia was induced in mice with 250 mg $bwkg^{-1}$ sodium pentobarbital. Before surgery, mice were anaesthetised with 125 mg kg^{-1} ketamine and 12.5 mg kg^{-1} xylazine. After operation the animals were placed on a heating pad until they regained consciousness, following which they were given buprenorphine (0.075 mg kg^{-1}) I.P. to reduce pain.

Isolation of pancreatic acinar cells

Pancreatic acinar cells from wild-type and TRPM2 knockout mice were isolated as described previously (Gout *et al.* 2013). Briefly, mice were killed, and the pancreas was removed and placed into ice-cold Hank's balanced salt solution (HBSS; Sigma-Aldrich, St Louis, MO, USA; Cat. No.: 8264). The tissue was then cut into small pieces in a 1.5 ml centrifuge tube and placed into a sterile flask with 10 ml of isolation solution [10 ml HBSS, 200 U ml^{-1} collagenase (Worthington, Lakewood, NJ, USA; Cat. No.: 5273), 10 mM HEPES (Sigma-Aldrich; Cat. No.: 3375)]. The tissue was incubated for 25–30 min at 37°C and was vigorously shaken every 5 min. After digestion, the pancreas was placed into a 50 ml tube (Sarstedt, Nümbrecht, Germany; Cat. No.: 62.559.205) with 10 ml of ice-cold washing solution (containing 10 ml HBSS, 10 mM HEPES, 5% fetal bovine serum Cat. No.: Gibco, Waltham, MA, USA; 10500-064) and centrifuged at 90 relative centrifugal force (RCF) at 4°C for 2 min. This step was repeated twice. The supernatant was removed, and the pellet was resuspended in 1 ml HBSS solution. Until experimental use, the acinar cells were kept in an incubator at 37°C with 5% CO_2.

Isolation of pancreatic ductal fragments

Isolation of inter- and intralobular pancreatic ductal fragments was performed as described previously (Maleth *et al.* 2015). Terminal anaesthesia was induced in mice with 250 mg $bwkg^{-1}$ sodium pentobarbital and the removed pancreas was digested for 15 min with 100 U ml^{-1} purified collagenase (Worthington, Cat. No.: LS005273) containing solution at 37°C applying gentle shaking. The isolation solution also contained 0.1 mg ml^{-1} trypsin inhibitor (ThermoFisher Scientific, Cat. No.: 17075029) and 1 mg ml^{-1} bovine serum albumin (VWR, Radnor, PA, USA, Cat. No.: 9048-46-8) in DMEM Nutrient Mixture F-12 Ham (Sigma, Cat. No.: D6421). Pancreatic ducts were separated from the acinar lobules under a stereomicroscope and used for downstream analysis.

Gene expression analysis

Gene expression was investigated by the combination of reverse-transcription (RT-PCR) and conventional PCR. Total mRNA was isolated from three independent biological replicates of mouse brain, isolated pancreatic acini or isolated pancreatic ducts with the NucleoSpin RNA XS kit (Macherey-Nagel, Ref.: 740902.50) according to the manufacturer's instructions. The mRNA

concentrations were measured with a NanoDrop 2000 (ThermoFisher Scientific). In total, 1 μg purified mRNA was used to synthetize cDNA using an iScript cDNA Synthesis kit (Bio-Rad, Hercules, CA, USA; Cat. No.: 1708890). Conventional PCR amplification was performed by DreamTaq Hot Start DNA Polymerase (ThermoFisher Scientific, Cat. No.: EP1702) with cDNA-specific primers (forward: ACGGGCAATATGGTGTGGAG; reverse: CACCTCCCCTTTCCTTCGTT) for 35 cycles. Mouse brain lysate was used to validate the primers.

Immunofluorescence labelling

For immunostaining, pancreatic acinar cells were isolated and attached to poly-L-lysine-coated cover glasses, whereas pancreatic ducts were frozen in Shandon Cryomatrix (ThermoFisher Scientific, Cat. No.: 6769006) and 7 μm thick sections were cut with a cryostat (Leica CM 1860 UV). Antibody labelling was performed as previously described (Molnar *et al.* 2020). Briefly, sections were fixed in 4% PFA-PBS and after antigen retrieval with sodium citrate–Tween 20 buffer sections were blocked for 1 h. Sections were incubated with anti-TRPM2-ATTO-594 (Alomone Labs, Jerusalem, Israel, Cat. No.: ACC-043-AR) conjugated primary rabbit polyclonal antibody overnight at 4°C (1:100 dilution). Nuclei were labelled with Hoechst 33342 and sections were kept in a Fluoromount mounting medium (Sigma-Aldrich; Cat. No.: F4680) until imaging. Sections were imaged with a Zeiss LSM880 laser scanning confocal microscope using a 40× oil immersion objective (Zeiss, NA: 1.4).

Electrophysiology

For electrophysiology recordings, pancreatic acinar cells were isolated from mouse pancreas as described previously (Geyer *et al.* 2015), with slight modifications. The pancreas was removed and injected with an F12/DMEM (ThermoFisher Scientific, Cat. No.: 11320033) medium containing 100 U ml^{-1} collagenase P (Roche, Indianapolis, IN, USA), 0.1 mg ml^{-1} trypsin inhibitor and 2.5 mg ml^{-1} BSA. These were then incubated in a 5 ml volume of the same solution in a 37°C shaking water bath for 30 min, which was continuously gassed with carbogen. The tissue was dissociated by pipetting with a serological pipette 4–6 times before filtering through a 150 μm mesh. Cells were layered on top of 400 mg ml^{-1} BSA and washed through the medium by gentle centrifugation. The pellet was resuspended in Ca^{2+}-free, collagenase-containing Tyrode's solution before being further digested for 10 min. Following this, cell clumps were gently agitated with a 1 ml pipette tip attached to a serological pipette. The resulting cells were collected by centrifugation, resuspended in DMEM medium and kept gassed at room temperature until use in patch clamp experiments. Whole cell currents were acquired at room temperature using an Axopatch 200B amplifier and a Digidata 1322A digitiser (Axon Instruments) at a 50 kHz sampling rate and filtered online at 5 kHz using a low-pass Bessel filter. Data acquisition was performed using pClamp 9 software package (Axon Instruments, Union City, CA, USA). Pipettes of ∼6 MΩ resistance were used with the intracellular solution containing 130 mM caesium glutamate, 5 mM $CaCl_2$, 10 mM EGTA (resulting in 135 nM ionised Ca^{2+}), 5 mM $MgCl_2$ and 10 mM HEPES (pH 7.3). Pancreatic acinar cells were continuously perfused with extracellular saline solution (140 mM sodium glutamate, 4 mM CsCl, 2 mM $CaCl_2$, 2 mM $MgCl_2$, 10 mM HEPES, pH 7.4) with or without 100 μM H_2O_2. Cation currents were recorded during 100 ms long test pulses at step potentials between −60 and +120 mV both under control conditions and during treatment.

Fluorescence microscopy

Isolated pancreatic acinar clusters or ductal fragments were placed on poly-l-lysine-coated cover glasses and incubated with BCECF-AM (1.5 μmol l^{-1}) or Fura2-AM (5 μmol l^{-1}) for 30 min at 37°C (Hegyi *et al.* 2004). The loaded cells were imaged with an Olympus IX71 inverted microscope equipped with a Hamamatsu ORCA-ER CCD camera through a 20× oil immersion objective (Olympus; NA: 0.8). Samples were excited with an Olympus MT-20 illumination system equipped with a 150 W xenon arc light source. Filter combinations for BCECF and Fura2 were as described previously (Molnar *et al.* 2020). Ratiometric image analysis was performed using Olympus excellence software with a temporal resolution of 1 s.

Investigation of acinar cell fate

To investigate acinar cell fate, an apoptosis/necrosis detection kit was used according to the manufacturer's instructions (Abcam, Cambridge, MA, USA; Cat. No.: ab176750). CytoCalcein Violet 450 is sequestered in the cytoplasm of live cells. In apoptosis, phosphatidylserine (PS) is transferred to the outer leaflet of the plasma membrane, which can be detected by the PS sensor Apopxin Deep Red. During necrosis the cell membrane integrity is lost and thus the DNA Nuclear Green DCS1, a membrane-impermeable dye, can label the nucleus of damaged cells. Briefly, pancreatic acinar cells from wild-type (WT) and TRPM2 knockout (KO) mice were isolated as described above with modifications to improve overall cell survival (shorter tissue digestion and gentle centrifugation was applied) and incubated with 1 mM H_2O_2 or 250 μM CDC for 30 min.

Cells were then centrifuged at 500 RCF for 5 min at 4°C and washed twice with PBS. Cells were then resuspended in 200 μl of Assay Buffer and loaded with CytoCalcein 450, Nuclear Green and Apopxin Deep Red at room temperature for 30–60 min. Following this, cells were collected and centrifuged at 500 RCF for 5 min at 4°C before being placed on a Cellview cell culture slide (Greiner Bio-One, Kremsmünster, Austria; cat. no.: 543979) for imaging. Images were captured using a Zeiss LSM880 confocal microscope with different channels and wavelengths according to each dye: CytoCalcein 450 (Ex/Em = 405/450 nm), Nuclear Green (Ex/Em = 490/520 nm) and Apopxin Deep Red (Ex/Em = 630/660 nm). For each condition, five images were captured, and the total number of cells was counted by two independent investigators. Cells with Nuclear Green staining were considered necrotic, with Apopxin Deep Red staining apoptotic, whereas double stained cells were considered necrotic.

Confocal imaging of live acinar cells

Changes of the mitochondrial membrane potential ($\Delta\Psi_m$) were followed by using tertamethylrhodamine-methyl ester (TMRM), which accumulates in the mitochondria depending on $\Delta\Psi_m$. Generation of intracellular ROS was measured by H2DCFDA ROS indicator. Isolated pancreatic acinar cells were incubated with 100 nM TMRM (ThermoFisher Scientific Cat. No.: T668), or 4 μM H2DCFDA (ThermoFisher Scientific Cat. No.: D399) in standard HEPES solution for 20 min at 37°C on a poly-L-lysine-coated cover glass. The solutions were complemented with 100 nM TMRM to avoid dye leakage. Changes in $\Delta\Psi_m$ or intracellular ROS were monitored using a Zeiss LSM880 confocal microscope. The cells loaded with TMRM were excited at 543 nm, and the emitted light was captured between 560 and 650 nm. Five to 10 regions of interest (ROIs) were placed on the mitochondria of pancreatic acinar cells. H2DCFDA was excited at 490 nm and the emitted fluorescence was captured between 500 and 550 nm. Fluorescence signals were normalised to initial fluorescence intensity (F/F_0) and expressed as relative fluorescence.

In vivo acute pancreatitis models

Cerulein-induced AP was induced by 10, hourly intraperitoneal injections of 50 μg bwkg^{-1} cerulein (Bachem, Bubendorf, Switzerland; Cat. No.: H-3220) (control groups received physiological saline) (Pallagi *et al.* 2014). Two hours after the last cerulein injection, mice were killed with 85 mg kg^{-1} pentobarbital. Biliary AP was triggered by the administration of 4% sodium taurocholate (Sigma-Aldrich Cat. No.: 86339) into the common bile duct as described previously (Perides *et al.* 2010*b*). Briefly, mice were anaesthetised with 125 mg kg^{-1} ketamine and 12.5 mg kg^{-1} xylazine, and median laparotomy was performed, where the papilla of Vater was cannulated by a 0.4 mm diameter needle connected to an infusion pump. Mice were administered 4% sodium taurocholate or physiological saline at a perfusion rate of 10 μl min^{-1} (TSE System GmbH, Bad Homburg, Germany; cat. no.: 540060-HP) for 5 min. After the abdominal wall and the skin were closed separately, the animals were placed on a heating pad until they regained consciousness, following which they were given buprenorphine (0.075 mg kg^{-1}) I.P. to reduce pain. Mice were killed 24 h later using pentobarbital (85 mg kg^{-1} I.P.). In both cases, blood samples were collected after terminal anaesthesia through the inferior vena cava, and the pancreata were removed immediately. Blood samples were placed on ice and then centrifuged at 2500 RCF for 15 min at 4°C. Serum samples were collected and stored at −20°C. Pancreas samples were placed into a 4% formaldehyde solution and stored at 4°C until histology. A colorimetric kit (A Amylase Assay) was used to measure serum amylase activity (Diagnosticum, Budapest, Hungary; Cat. No.: 47462). Absorbance of the samples was detected at 405 nm using a FLUOstar OPTIMA (BMG Labtech, Offenburg, Germany) microplate reader. Formaldehyde-fixed pancreas samples were embedded in paraffin, and 4 μm thick sections were cut and stained with haematoxylin–eosin. Histological parameters such as oedema, inflammatory cell infiltration and necrosis were scored (0–5 points for oedema, leukocyte infiltration and necrosis for the total histological score, or % of total area for necrosis) by three independent investigators blinded to the protocol (Pallagi *et al.* 2014). Averages of the scores were calculated and included to the manuscript. The total histological score was calculated by adding the individual scores together.

Statistics

Statistical analysis was performed by Graphpad Prism software. All data are expressed as means ± SD. Both parametric (one-way ANOVA) and non-parametric (Mann–Whitney test, Kruskal–Wallis test – for analysis of the acinar cell survival assay) tests were used based on the normality of data distribution. A P value <0.05 was accepted as statistically significant.

Results

TRPM2 channel is expressed in the exocrine pancreas

End-point PCR analysis of isolated acini and ductal fragments confirmed that the TRPM2 gene was expressed in the exocrine pancreatic cells (Fig. 1*A*). When

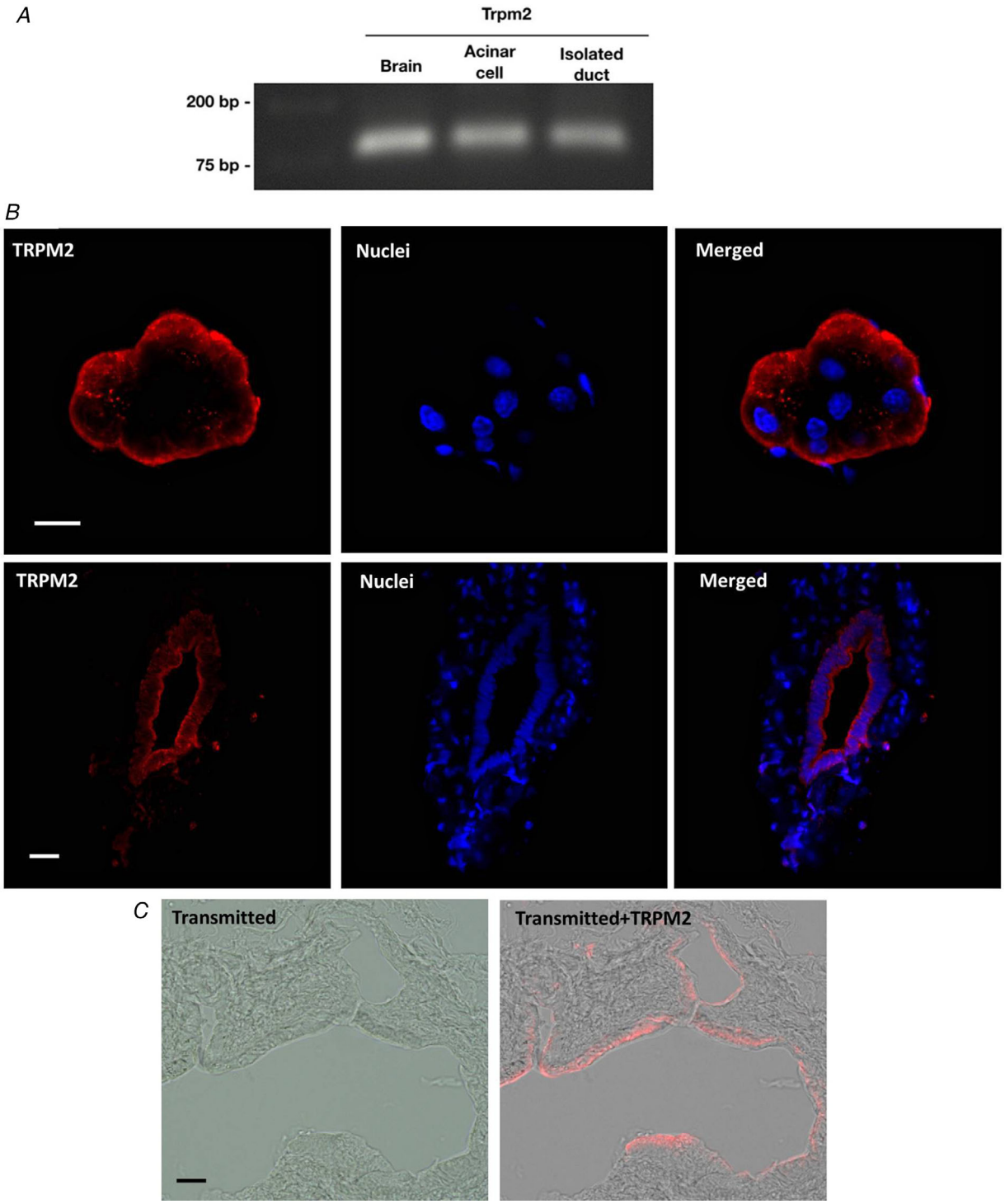

Figure 1. Expression of TRPM2 in the exocrine pancreas
A, agarose gel images of cDNA samples derived from isolated acini and ductal fragments confirmed that the TRPM2 gene is expressed in the exocrine pancreas. *B* and *C*, immunofluorescence labelling of TRPM2 on isolated acinar clusters and cross-sections of isolated ducts. TRPM2 channels are expressed on the basolateral membrane of the pancreatic acinar cells and on the apical membrane in ductal cells, which is also demonstrated on the transmitted light images Scale bar: 10 μm.

immunofluorescence labelling of TRPM2 was performed on isolated acinar clusters and cross-sections of isolated ducts, the confocal images showed that TRPM2 channels were expressed on the basolateral membrane of the pancreatic acinar cells, whereas an apical expression pattern was seen in ductal cells (Fig. 1*B*, *C*).

Functional TRPM2 channels are present in pancreatic acinar and ductal cells

When isolated WT pancreatic acini were challenged with 1 mM H_2O_2 to increase ROS, a rapid and sustained increase of $[Ca^{2+}]_I$ was observed (Fig. 2*A*), which was significantly reduced in the TRPM2 KO acini (0.41 ± 0.09 *vs.* 0.17 ± 0.029, respectively). In cells treated in an extracellular Ca^{2+}-free medium, Ca^{2+} elevation was found to be significantly impaired, and no difference was detected between WT and TRPM2 KO cells. This suggests that the sustained elevation of $[Ca^{2+}]_I$ in response to H_2O_2 was largely due to TRPM2-channel-mediated influx of extracellular Ca^{2+}. In addition, H_2O_2 activated a reversible cationic membrane current, with a relative linear *I–V* relationship as was reported previously for TRPM2 (Liu *et al.* 2013) (Fig. 2*B*). Similarly to acinar cells, treatment of isolated WT pancreatic ductal fragments with 1 mM H_2O_2 induced a sustained elevation of $[Ca^{2+}]_I$ (Fig. 2*C*), which was significantly lower in TRPM2 KO ductal cells (0.30 ± 0.06 *vs.* 0.10 ± 0.013, respectively). In these cells as well, Ca^{2+} elevation was significantly lower in Ca^{2+}-free conditions (Fig. 2*C*). As the intracellular Ca^{2+} level of pancreatic ductal cells decrease in response to extracellular Ca^{2+} removal, we normalised the maximal Ca^{2+} responses to the same initial value. Genetic inhibition of TRPM2

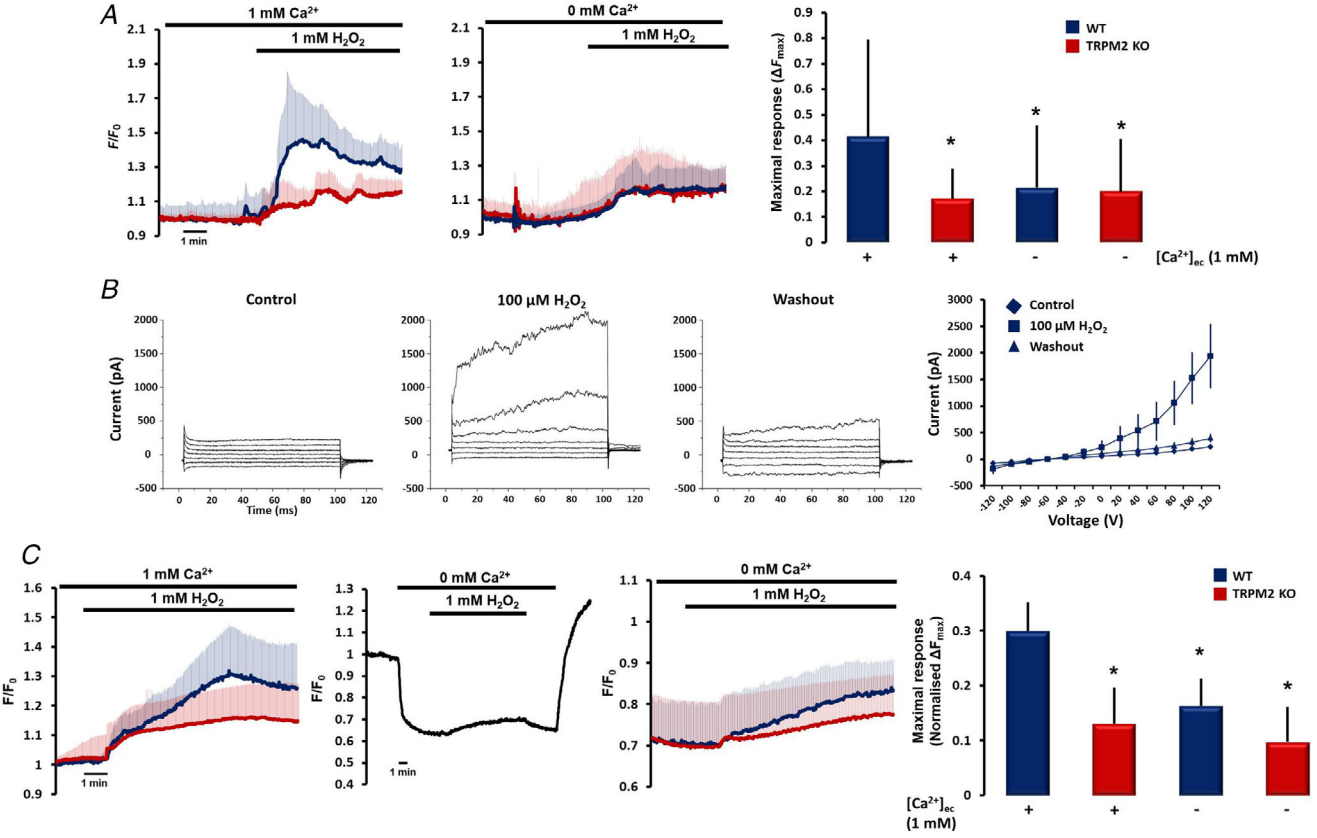

Figure 2. Functional activity of TRPM2 in the exocrine pancreas
A, average traces of 5–6 individual experiments demonstrating the effect of 1 mM H_2O_2 on pancreatic acinar cells in the presence or absence of extracellular Ca^{2+}. Bar charts summarise the maximal Ca^{2+} responses to H_2O_2, which was significantly reduced in TRPM2 KO acini. $^*P < 0.05$ *vs.* WT. *B*, representative whole cell current recordings and *I–V* relationships in isolated pancreatic acini. H_2O_2 activated a reversible cationic membrane current, with a relative linear *I–V* relationship. $n = 4$ per group. *C*, averages of intracellular Ca^{2+} recordings in isolated pancreatic ducts (5–6 experiments per group) in the presence or absence of extracellular Ca^{2+}. The intracellular Ca^{2+} level decreases in response to extracellular Ca^{2+} removal, as demonstrated by the representative trace of intracellular Ca^{2+} recordings in isolated pancreatic duct (wild type). Bar charts summarise the maximal Ca^{2+} elevations evoked by H_2O_2, which was significantly lower in TRPM2 KO ductal cells. These results suggest that TRPM2 mediates extracellular Ca^{2+} influx under an oxidative stress condition in pancreatic acinar and ductal cells. $^*P < 0.05$ *vs.* WT.

channels had no effect on amylase release from pancreatic acinar cells (data not shown) or on the HCO_3^- secretion by pancreatic ductal cells (described below, Fig. 3*C*, *D*). Therefore, the physiological relevance and function of TRPM2 in the exocrine pancreas still require further characterisation and study.

TRPM2 contributes to bile-acid-induced extracellular Ca^{2+} influx in pancreatic acinar cells

Bile acids can cause the release of Ca^{2+} from intracellular stores and can trigger extracellular Ca^{2+} influx. To study this, the intracellular Ca^{2+} elevation in response to bile acid treatment was compared in pancreatic acini and ducts. Administration of 250 μM CDC was found to trigger a rapid, sustained increase in $[Ca^{2+}]_I$, which was markedly impaired in the TRPM2 KO acinar cells (0.834 $\pm$ 0.02 *vs.* 0.655 $\pm$ 0.04) (Fig. 3*A*). These results highlight that TRPM2 plays an important role in bile-acid-induced extracellular Ca^{2+} influx in pancreatic acinar cells. By contrast, no significant difference was detected in isolated ductal fragments between the Ca^{2+} response of WT and TRPM2 KO ducts to 250 μM CDC, suggesting that, in ductal cells, TRPM2 plays no role in bile-acid-induced cell injury (Fig. 3*B*).

Because HCO_3^- secretion is the primary function of the ductal epithelia, the HCO_3^- efflux across the apical membrane was compared between WT and TRPM2 KO ducts using fluorescence intracellular pH (pH_i) measurements (Maleth *et al.* 2015). Ductal cells were exposed to 20 mM NH_4Cl in HCO_3^-/CO_2-buffered solution from the basolateral membrane, triggering a rapid alkalisation because of the influx of NH_3 (Fig. 3*D*), followed by a slower recovery of the alkaline pH to the resting pH_i. This recovery phase depends on the HCO_3^-

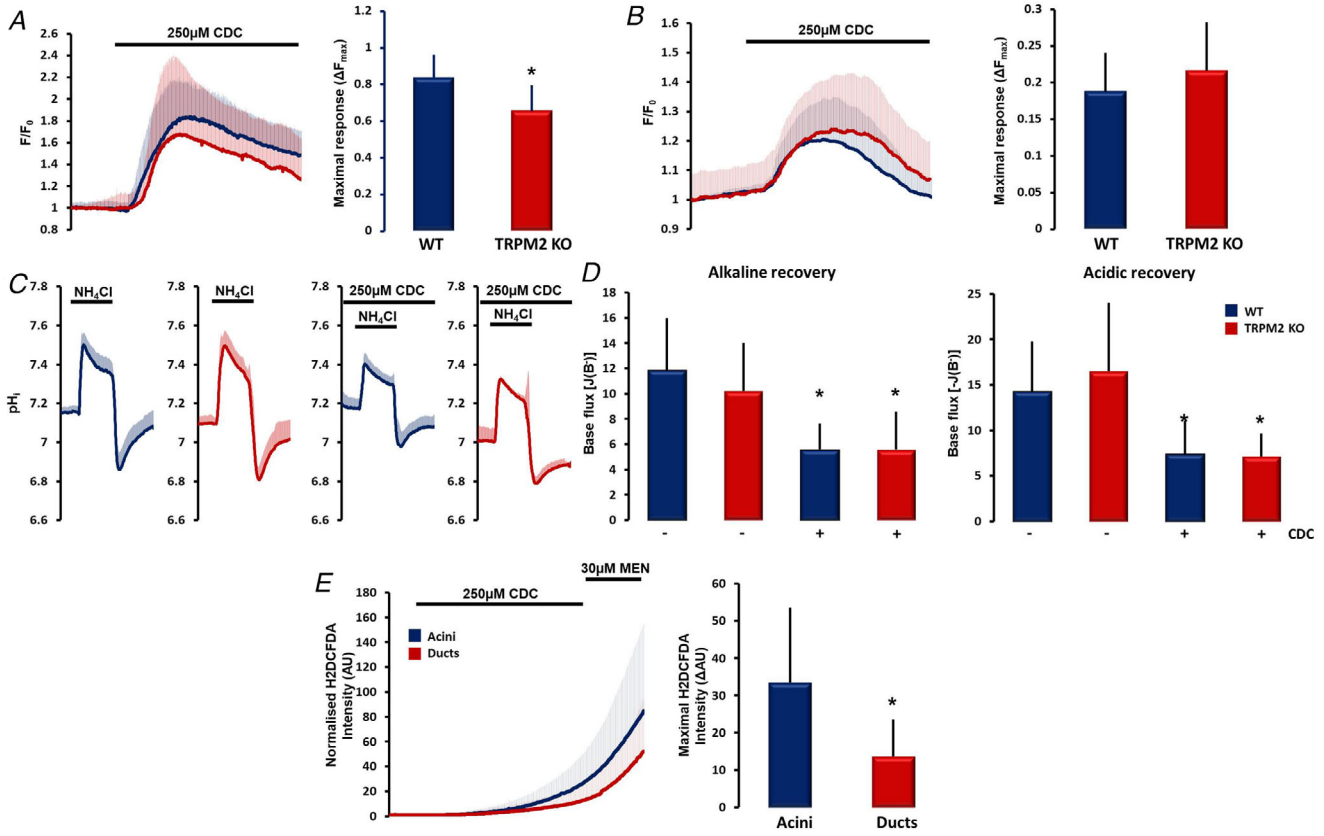

Figure 3. The role of TRPM2 in bile acid-evoked Ca^{2+} signal generation
A and *B*, average traces and bar charts of 5–6 individual experiments comparing intracellular Ca^{2+} elevations evoked by 250 μM CDC in WT and TRPM2 KO acini and isolated ducts. Genetic deletion of TRPM2 reduced the bile-acid-induced Ca^{2+} elevation in pancreatic acini, but not in ducts. $^*P < 0.05$ *vs.* WT. *C*, average pH_i traces of 4–6 experiments for each condition. Pancreatic ducts were perfused with HCO_3^-/CO_2-buffered extracellular solution, and intracellular alkalisation was achieved via administration of 20 mM NH_4Cl. *D*, bar charts of the calculated base fluxes of HCO_3^-. CDC at 250 μM significantly decreased both alkaline and acidic recovery; however, no significant difference was detected in WT and TRPM2 KO ducts. *E*, average traces of H2DCFDA intensities and bar charts of the maximal fluorescence intensity changes in isolated acini and ducts. ROS generation induced by bile acid treatment was measured in 5–6 individual experiments. $^*P < 0.05$ *vs.* acini.

efflux (i.e. secretion) from the ductal epithelia via the SLC26 Cl^-/HCO_3^- exchangers and cystic fibrosis transmembrane conductance regulator (CFTR) (Maleth *et al.* 2015). Removal of NH_4Cl rapidly decreased pH_i below the resting value, which is restored by the activities of the basolateral NHE1 and NBCe1 (Maleth *et al.* 2015). The initial recovery rates were measured (calculated as $\Delta pH/\Delta t$) over the first 30 s to calculate the base flux [$J(B^-)$] values as described (Maleth *et al.* 2015). With this assay, no difference in the activities of the apical and basolateral proteins was found between WT and TRPM2 KO ducts (Fig. 3*D*, *E*). Although the administration of CDC markedly inhibited ion secretion, as has been previously described (Maleth *et al.* 2011), the genetic knockout of TRPM2 demonstrated no protective effect, suggesting that bile acids affect ductal cells via a TRPM2-independent mechanism (Fig. 3*D*, *E*).

To provide a mechanistic explanation for the different contribution of TRPM2 in bile acid-generated Ca^{2+} response in acinar and ductal cells, we measured the intracellular ROS using H2DCFDA. In accordance with the findings of Booth *et al.* (2011), we showed that 250 μM CDC increased the intracellular ROS level in pancreatic acini. Interestingly, ROS production during bile acid treatment in ductal epithelial cells was significantly lower compared to acinar cells (13.6 ± 2 *vs.* 33.4 ± 4 arbitrary units).

Lack of TRPM2 decreases acinar cell necrosis during bile acid exposure

Pancreatic acinar cell fate determines the severity of AP. It was therefore also important to characterise the role of TRPM2 in acinar cell death. In the untreated control samples, ∼85% of the acinar cells were viable in both the WT and the TRPM2 KO samples, which is comparable to previously published results (Booth *et al.* 2011). Incubation of WT and TRPM2 KO acini with 1 mM H_2O_2 for 30 min remarkably decreased the number of viable cells, and necrotic cell death was significantly increased (Fig. 4*A*, *B*). A lack of TRPM2 was observed to protect acinar cells from oxidative-stress-induced cell necrosis during H_2O_2 treatment (% of viable cells: 19.4 ± 0.4 in WT *vs.* 49.1 ± 1.2 in TRPM2 KO). The rate of apoptosis was similar in TRPM2 KO and WT acini (% of apoptotic cells: 9.1 ± 4.3 in WT *vs.* 10.8 ± 2.5 in TRPM2 KO), whereas necrosis was significantly impaired in TRPM2 KO acini (% of necrotic cells: 71.5 ± 4.2 in WT *vs.* 40.1 ± 3.2 in TRPM2 KO). Similarly, incubation of acinar cells with 250 μM CDC for 30 min decreased the number of live cells in the WT sample, although overall cell survival was remarkably improved by TRPM2 deletion (% of viable cells: 48.3 ± 0.9 in WT *vs.* 74.1 ± 1.3 in TRPM2 KO) (Fig. 4*A*, *B*). TRPM2 deletion significantly decreased both apoptotic and necrotic cell death in the CDC-treated group (WT: 15.4 ± 2.5% *vs.* KO: 8.5 ± 1.3% and WT: 36.3 ± 2.2% *vs.* KO: 17.4 ± 1.3%, respectively). Importantly, the lack of TRPM2 channels resulted in a ∼30% decrease in acinar cell death, suggesting that TRPM2 has an important contribution to acinar cell death during biliary AP.

Lack of TRPM2 does not prevent mitochondrial damage during bile acid exposure

We wanted to further characterise the intracellular mechanisms that play a role in TRPM2-channel-mediated cell necrosis. As TRPM2 has been reported to induce mitochondrial damage (Liu *et al.* 2017), the mitochondrial membrane potential was measured ($\Delta\Psi_m$) in WT and TRPM2 pancreatic acinar cells. Administration of 1 mM H_2O_2 resulted in a marked drop of $\Delta\Psi_m$ in WT cells (Fig. 5*A*). The decrease of $\Delta\Psi_m$ was significantly lower in TRPM2 KO cells, whereas removal of the extracellular Ca^{2+} impaired the loss of $\Delta\Psi_m$ in WT cells to the level of TRPM2 KO acini. This suggests that extracellular Ca^{2+} influx through TRPM2 plays a crucial role in the oxidative-stress-induced mitochondrial damage seen in pancreatic acinar cells. The decrease of $\Delta\Psi_m$ in response to 250 μM CDC was also compared. However, no difference was seen between WT and TRPM2 KO cells (Fig. 5*B*). This may be due to the Ca^{2+}-independent direct mitochondrial toxicity of bile acids (Schulz *et al.* 2013). Previously, TRPM2 channels have been suggested to be key mediators of diabetic stress-induced mitochondrial fragmentation in endothelial cells (Abuarab *et al.* 2017). Notably, in pancreatic acinar cells, fragmentation of mitochondria was not observed in response to either H_2O_2 or bile acid treatment (Fig. 5*C*).

Lack of TRPM2 decreases the severity of experimental biliary pancreatitis

To determine the role of TRPM2 in the pathogenesis of AP, the disease severity of WT and TRPM2 KO animals was compared in two standard experimental AP models. In the first series of experiments, mice were given 10 hourly I.P. injections of either physiological saline (control group) or 50 μg bwkg^{-1} cerulein to induce AP (Fig. 6*A*). Overall, in this experimental model, no significant differences were detected between WT and TRPM2 KO mice. The control animals had normal pancreatic histology in both groups (Fig. 6*A*), whereas cerulein hyperstimulation caused extensive pancreatic damage. Despite this, no significant differences were observed in the histological parameters between the WT and TRPM2 KO animals. The extent of interstitial oedema (3.14 ± 0.25 for WT *vs.* 3.03 ± 0.34 for KO), leukocyte infiltration (2.74 ± 0.53 for WT *vs.* 3.04 ± 0.23 for KO, $P = 0.08$) or necrosis

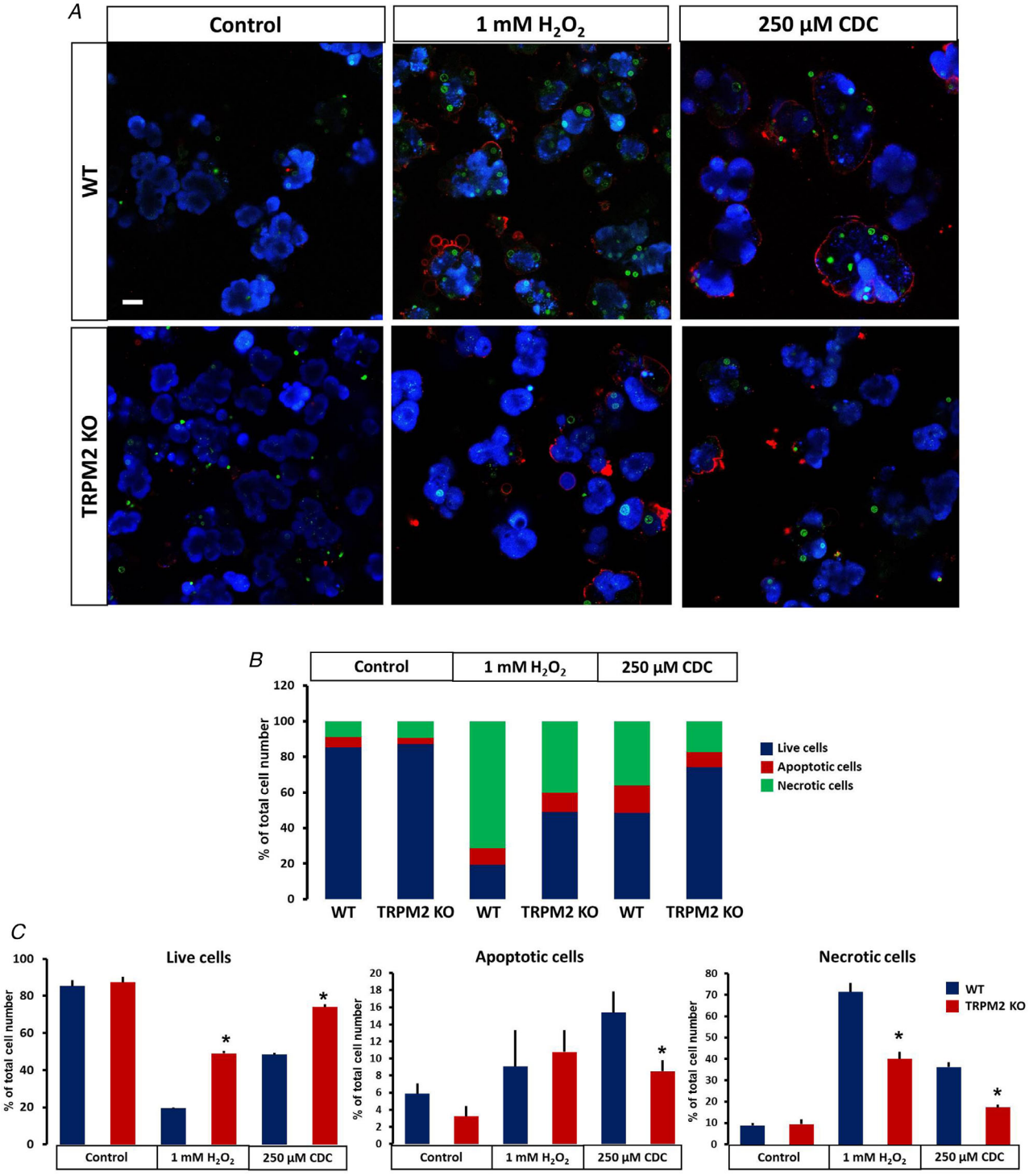

Figure 4. The role of TRPM2 in acinar cell necrosis during bile acid exposure
A, representative images of different conditions (blue: live cells labelled with CytoCalcein 450, green: necrotic cells labelled with Nuclear Green, and red: apoptotic cells labelled with Apopxin Deep Red). Scale bar: 20 μm. B, bar chart representing the ratio of live, apoptotic and necrotic cells. Incubation of WT and TRPM2 KO acini with 1 mM H_2O_2 or with 250 μM CDC for 30 min markedly decreased the number of viable cells, whereas necrosis was significantly increased. TRPM2 KO acinar cells displayed a significantly decreased rate of apoptosis in the bile acid-treated group, whereas cell necrosis was impaired in both cases. n = 4–5 experiments/group. C, bar charts representing the ratio of live, apoptotic and necrotic cells. TRPM2 knockout significantly improved acinar cell survival in the 1 mM H_2O_2 or 250 μM CDC-treated groups. *$P < 0.05$ *vs.* WT treated sample (H_2O_2 or CDC); n = 4–5 experiments/group.

(18.64 ± 3.16 for WT *vs.* 21.32 ± 3.58 for KO) was not found to be significantly different in the cerulein-treated groups (Fig. 6*B*).

More importantly, the role of the TRPM2 channel in the pathogenesis of biliary AP was also examined. In this model, pancreatitis was induced by intraductal infusion of 4% sodium taurocholate (control animals received physiological saline) as described previously (Pallagi *et al.* 2014). The infusion of 4% sodium taurocholate induced necrotising pancreatitis in both WT and TRPM2 KO

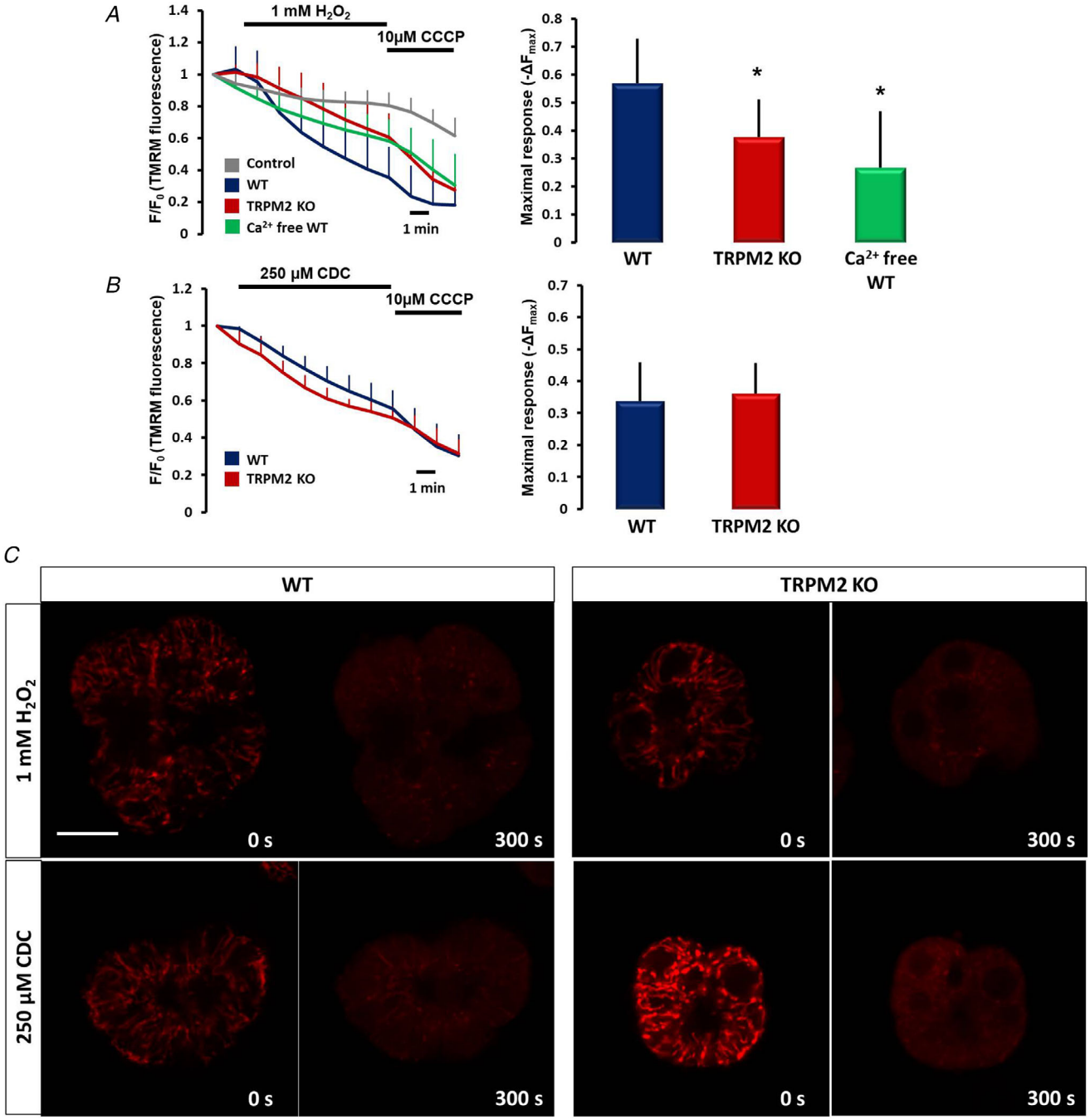

Figure 5. The effect of TRPM2 on the development of mitochondrial damage
A, average traces and bar charts of the changes of $\Delta\Psi_m$ in WT and TRPM2 pancreatic acinar cells. H_2O_2 at 1 mM markedly decreased $\Delta\Psi_m$ in WT cells (blue trace), which was impaired by TRPM2 knockout (red trace) or removal of the extracellular Ca^{2+} (green trace). Control cells were perfused with standard HEPES solution (grey trace). *B*, by contrast, no difference was observed when acinar cells were challenged by 250 μM CDC. *C*, representative confocal images of labelled mitochondria in pancreatic acinar cells. Mitochondrial fragmentation was not observed in response to H_2O_2, or to bile acid treatment. Scale bar: 10 μm. $n = 6$–7 experiments/groups; $^*P < 0.05$ *vs.* WT.

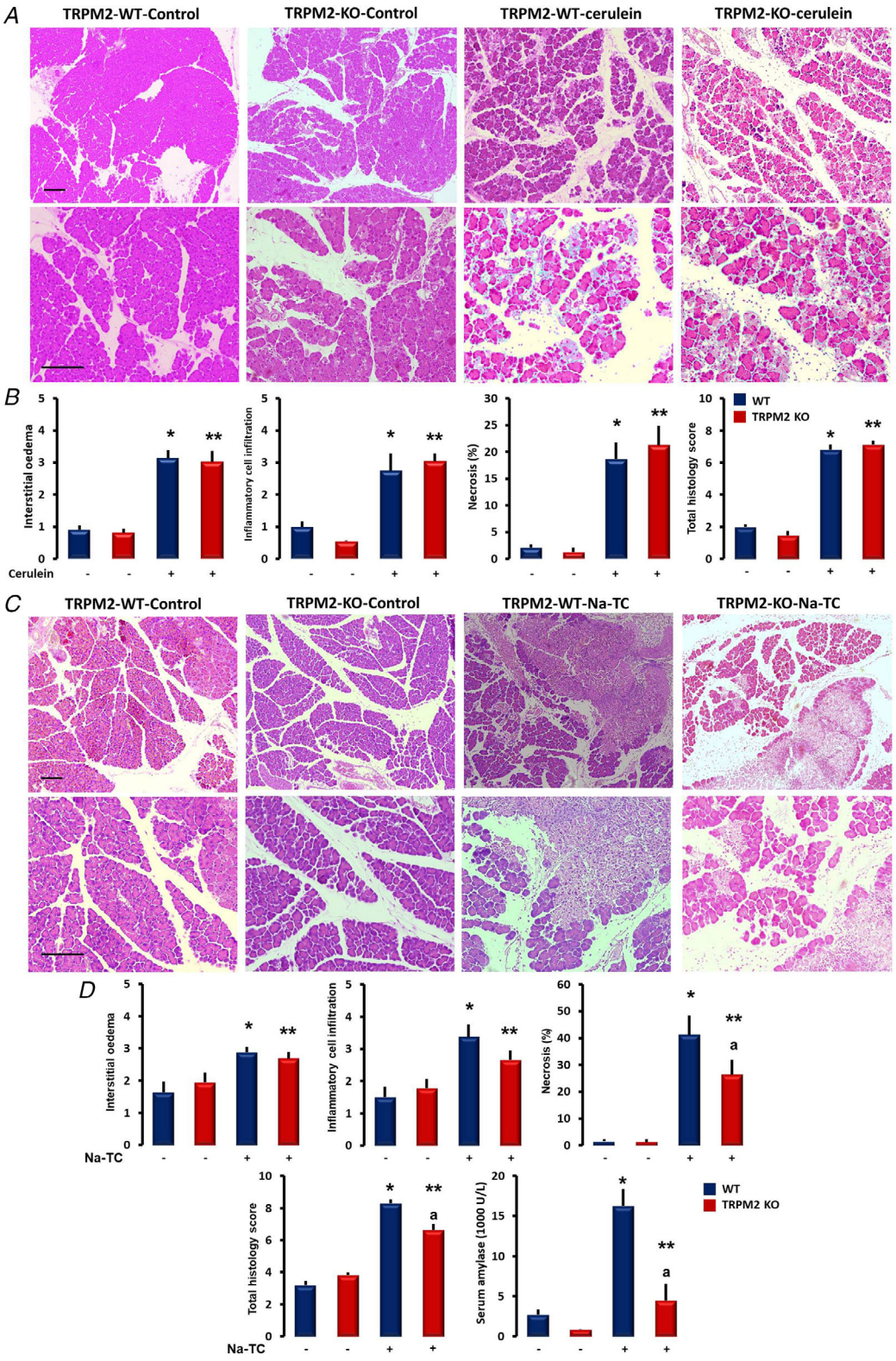

Figure 6. Genetic knockout of TRPM2 decreases the severity of biliary, but not cerulein-induced, acute pancreatitis

A, representative images of pancreatic histology in cerulein-induced pancreatitis. Mice were given 10 hourly I.P. injections of either physiological saline (control group) or 50 μg bwkg^{-1} cerulein. Scale bar: 100 μm. *B*, cerulein administration caused extensive pancreatic damage; however, no significant differences were observed

mice, accompanied by elevated histological and laboratory parameters (Fig. 6*C*, *D*). The extent of interstitial oedema (2.8 ± 0.16 for WT *vs.* 2.7 ± 0.2 for KO) or leukocyte infiltration (3.3 ± 0.38 for WT *vs.* 2.7 ± 0.29 for KO, $P = 0.08$) was not significantly different in the sodium taurocholate-treated groups. Notably, the extent of necrosis was significantly higher in the WT group in comparison to the TRPM2 KO animals (41.3% ± 7.13% for WT *vs.* 26.4% ± 5.5% for KO). In accordance with these findings, serum amylase activities were also significantly higher in the sodium taurocholate-treated WT animals *versus* the TRPM2 KO group. This perfectly mimicked the *in vitro* results obtained in this study, further confirming the crucial role of the TRPM2 channel in the pathogenesis of biliary AP.

Discussion

Previous reports suggest that bile acids can trigger sustained intracellular Ca^{2+} elevation, increase intracellular and intramitochondrial ROS production and damage the mitochondrial network in both pancreatic acinar and ductal cells. These subcellular changes can eventually lead to AP, which is a severe inflammatory disease of the gastrointestinal tract that has no specific treatment. Although the TRPM2 channel has recently emerged as an ROS-sensitive non-specific cation channel that mediates Ca^{2+}-dependent injury, the possible role that this channel plays in the pathogenesis of AP has yet to be investigated.

Although the expression of TRPM2 has been demonstrated previously in different cell types, including inflammatory cells (Yamamoto *et al.* 2008), myocytes (Miller *et al.* 2019) and epithelial cells (Liu *et al.* 2013), to our knowledge, this is the first report demonstrating the expression of TRPM2 in the exocrine pancreas. Using conventional PCR and immunolabelling techniques, the expression of TRPM2 in the basolateral membrane of acinar cells and on the luminal membrane of ductal cells was confirmed. In addition, increased intracellular ROS was found to trigger TRPM2-mediated extracellular Ca^{2+} influx in both cell types. This study did not show any alterations in acinar and ductal cell function between WT and TRPM2 KO mice. However, intracellular Ca^{2+} signalling is one of the major signalling pathways in the exocrine pancreas (Ahuja *et al.* 2014; Maleth & Hegyi, 2014) which regulates the secretion of digestive enzymes in acinar cells as well as ion and fluid secretion in ductal cells. Therefore, it might be possible that TRPM2-mediated Ca^{2+} entry could contribute to physiological signalling, although further studies are required to confirm this. In other cell types, redox signals have been demonstrated to sensitise TRPM2 and increase the intracellular Ca^{2+} concentration at physiological body temperature, which plays an important role in the regulation of macrophage functions (Kashio *et al.* 2012). In TRPM2 KO mice, blood glucose levels were significantly higher, whereas insulin secretion was significantly impaired, suggesting a potential role of TRPM2-mediated Ca^{2+} increase in insulin secretion (Uchida *et al.* 2011). On the other hand, activation of TRPM2 channels in pancreatic β-cells increased intracellular Ca^{2+} concentration and release of sequestered intracellular Zn^{2+} from lysosomes (Manna *et al.* 2015). In these experiments, gene knockout of TRPM2 protected mice from β-cell death. Previously, TRPM2 was shown to facilitate extracellular Ca^{2+} influx in monocytes in response to H_2O_2 and thus regulate the production of the macrophage inflammatory protein-2 (CXCL2), which in turn regulated the inflammatory response in a dextran sulphate sodium-induced colitis inflammation model in mice (Yamamoto *et al.* 2008). In another experimental model, the lack of TRPM2-regulated CXCL2 production in TRPM2 KO mice suppressed neutrophil infiltration into the CNS and slowed the progression of experimental autoimmune encephalomyelitis (Tsutsui *et al.* 2018). The role of TRPM2 has also been indicated in irradiation-induced side effects in cancer patients. In salivary gland epithelial cells, irradiation increased ROS production during radiotherapy of head and neck cancers, which activated TRPM2-mediated extracellular Ca^{2+} influx in acinar cells (Liu *et al.* 2013). The sustained intracellular Ca^{2+} entry leads to impaired secretory function of acinar cells and to the development of xerostomia, a frequent side effect of radiotherapy in these patients. In a downstream study, the same group demonstrated that irradiation increased the mitochondrial Ca^{2+} concentration and the production of ROS, impaired the $\Delta\Psi_m$ and activated caspase-3. These changes led to a sustained decrease in STIM1 expression and consequently decreased the store-operated Ca^{2+} entry (Liu *et al.* 2017).

Disturbed intracellular Ca^{2+} homeostasis has been suggested by several studies to play a pivotal role

in the histological parameters of WT and TRPM2 KO animals. n = 6–7 animals/groups; $^*P < 0.05$ *vs.* WT; $^{**}P < 0.05$ *vs.* TRPM2 KO. *C*, representative images of pancreatic histology in sodium taurocholate (Na-TC)-induced pancreatitis. Pancreatitis was induced by intraductal infusion of 4% Na-TC. Scale bar: 100 μm. *D*, the infusion of 4% Na-TC-induced necrotising pancreatitis in WT and TRPM2 KO mice accompanied by elevated histological and laboratory parameters. Although the extent of interstitial oedema or leukocyte infiltration was not different, the extent of necrosis was significantly impaired in the TRPM2 KO animals. n = 6–7 animals/groups; $^*P < 0.05$ *vs.* WT control; $^{**}P < 0.05$ *vs.* TRPM2 KO control; $^aP < 0.05$ *vs.* WT Na-TC treated.

in bile-acid-induced exocrine pancreatic cell damage. In pancreatic acini, bile acids trigger dose-dependent intracellular Ca^{2+} elevation via the activation of $InsP_3$ and ryanodine receptors (Gerasimenko *et al.* 2006). In addition, Perides *et al.* (2010*a*) showed that activation of the G-protein-coupled cell surface bile acid receptor (Gpbar1 or TGR5) at the apical membrane of pancreatic acinar cells leads to sustained Ca^{2+} elevation, intracellular activation of digestive enzymes and cell injury. Moreover, the genetic deletion of Gpbar1 specifically reduced the severity of TLC-S-induced AP. However, in pancreatic ductal cells, CDC dose-dependently elevated the intracellular Ca^{2+} level and inhibited HCO_3^- secretion (Venglovecz *et al.* 2008). In our experiments, CDC increased the $[Ca^{2+}]_I$ both in acinar and in ductal cells, but genetic deletion of TRPM2 decreased Ca^{2+} elevation only in acinar cells. The results of this study show that the TRPM2 channel has a ∼22% contribution to the bileacid-generated Ca^{2+} signal in acinar cells. Interestingly, our results highlighted that the generation of intracellular ROS in response to bile acids is remarkably different in pancreatic acinar and ductal cells, which can provide a mechanistic explanation for the different involvement of TRPM2 in bile acid-generated Ca^{2+} response in these cell types. This different response might be caused by the difference in the mitochondrial mass in acinar *versus* ductal cells (Park *et al.* 2001; Maleth *et al.* 2011). As expected from this, the genetic deletion of TRPM2 had no protective effect against bile acid-induced inhibition of ductal secretion. By contrast, in acini, other plasma membrane Ca^{2+} channels were also demonstrated to contribute to cell damage during AP. Gerasimenko *et al.* (2013) showed that the inhibition of extracellular Ca^{2+} entry via Orai1 decreases acinar cell necrosis *in vitro*. Moreover, inhibition of Orai1 by selective inhibitors markedly impaired the extracellular Ca^{2+} influx and sustained Ca^{2+} overload in pancreatic acinar cells upon bile acid stimulation, which significantly impaired pancreatic oedema, inflammation and necrosis in experimental models of AP (Wen *et al.* 2015). Others found that deletion of TRPC3 markedly reduced the bile acid-evoked Ca^{2+} signals and decreased the intracellular trypsin activation *in vitro* and the severity of cerulein-induced AP *in vivo* (Kim *et al.* 2009). In addition, Kim *et al.* (2002) described that transporter-mediated bile acid uptake results in a specific and significant sarco/endoplasmic reticulum Ca^{2+} ATPase pump function and thus depletes the endoplasmic reticulum Ca^{2+} stores, leading to cell damage and necrosis.

Intracellular Ca^{2+} overload can lead to premature activation of trypsinogen (Kruger *et al.* 2000), mitochondrial damage and cell necrosis in acinar cells (Criddle *et al.* 2006). In the present study, knockout of TRPM2 resulted in a significant protection of pancreatic acinar cells from H_2O_2 and bile acid-induced necrosis. Importantly, this protection was also observed in TC-induced AP as the extent of necrosis was significantly lower in TRPM2 KO mice compared to the WT littermates. In line with our results, Booth *et al.* (2011) reported that incubation of pancreatic acinar cells with TLC-S *in vitro* induced Ca^{2+}-dependent necrosis, which was abolished by pre-treatment with BAPTA-AM. Using different inhibitors to prevent apoptosis and necrosis, the authors suggested that elevated intracellular and intramitochondrial ROS are the major triggers of apoptosis, whereas increases in intracellular and intramitochondrial Ca^{2+} induce necrosis. As bile acids inhibited cellular ATP production (Voronina *et al.* 2010) and decreased $\Delta\Psi_m$ (Voronina *et al.* 2004), we also compared the changes of $\Delta\Psi_m$ in response to bile acid treatment in TRPM2 KO and WT acinar cells. The genetic knockout of TRPM2 and removal of the extracellular Ca^{2+} markedly reduced the drop of $\Delta\Psi_m$, suggesting that extracellular Ca^{2+} influx through TRPM2 plays a crucial role in oxidative stress-induced mitochondrial damage. Despite this, we did not detect this protective effect in bile acid-treated cells, a result which might be explained by the Ca^{2+}-independent direct mitochondrial toxicity of bile acids. Direct mitochondrial toxicity of bile acids was described in an experimental model of cholestasis. In these series of experiments, Schulz *et al.* (2013) found that bile acids impaired the mitochondrial membrane potential and induced mitochondrial permeability transition pore opening. Another group showed that physiologically relevant concentrations of bile acids can induce alterations in the mitochondria outer membrane order, which again can lead to opening of the mitochondrial membrane permeability transition pore in isolated mitochondria (Sousa *et al.* 2015). Previously, we (Venglovecz *et al.* 2008) and others (Voronina *et al.* 2004) also reported that the toxic effects of bile acids cannot be completely abolished by the removal of intracellular Ca^{2+} elevation. Mitochondrial fragmentation, which has been previously linked to the activation of TRPM2 (Abuarab *et al.* 2017), was not observed in our experiments. These results suggest that bile acids can induce mitochondrial damage in several different ways independently of intracellular Ca^{2+} overload. On the other hand, independently of mitochondrial damage, other Ca^{2+}-dependent toxic effects of bile acids have been described, which could also contribute to acinar cell necrosis. Bile acids were shown to activate calcineurin via the elevation of intracellular Ca^{2+} in pancreatic acinar cells, leading to intra-acinar activation of chymotrypsinogen and NF-κB activation, and acinar cell death (Muili *et al.* 2013*b*). In addition, genetic or pharmacological inhibition of calcineurin reduced the severity of TLC-S-induced AP, and pharmacological and genetic inhibition of calcineurin abolished the translocation of protein kinase C, which is a critical upstream regulator of NF-κB activation (Muili *et al.* 2013*a*).

In our study, general TRPM2 KO mice were used, so other factors might contribute to the observed protective effect of TRPM2 deletion in acute biliary pancreatitis. It is well described that inflammatory cells contribute to the severity of AP (Sendler *et al.* 2018, 2020). Previously, TRPM2 was identified as a crucial contributor of monocyte response to oxidative stress, which in turn regulated the production of the macrophage inflammatory protein-2 (CXCL2) and inflammatory response in experimental colitis in mice (Yamamoto *et al.* 2008). Although inflammatory cell infiltration of the damaged area peaks several days (on day 3–4) after the initial injury, these cell types do not contribute to the early events in AP pathogenesis. In our series of experiments, the animals were killed 24 h after the bile acid infusion, and therefore we concluded that the observed difference is primarily due to the lack of TRPM2 expression in the acinar cells.

Taken together, to the best of our knowledge, this is the first report of the expression and pathological function of the TRPM2 channel in the exocrine pancreas. We demonstrated that both pancreatic acinar and ductal cells express functionally active TRPM2, which can be activated by increased oxidative stress. Importantly, we have also provided evidence that TRPM2 activity contributes to bile acid-induced extracellular Ca^{2+} influx in acinar but not ductal cells, which promotes acinar cell necrosis independently of mitochondrial damage and increases the severity of bile acid-induced experimental pancreatitis. These results suggest that inhibition of TRPM2 might be a potential option for use in treating biliary pancreatitis.

References

Abuarab N, Munsey TS, Jiang LH, Li J & Sivaprasadarao A (2017). High glucose-induced ROS activates TRPM2 to trigger lysosomal membrane permeabilization and Zn^{2+}-mediated mitochondrial fission. *Sci Signal* **10**.

Ahuja M, Jha A, Maleth J, Park S & Muallem S (2014). cAMP and Ca^{2+} signaling in secretory epithelia: crosstalk and synergism. *Cell Calcium* **55**, 385–393.

Booth DM, Murphy JA, Mukherjee R, Awais M, Neoptolemos JP, Gerasimenko OV, Tepikin AV, Petersen OH, Sutton R & Criddle DN (2011). Reactive oxygen species induced by bile acid induce apoptosis and protect against necrosis in pancreatic acinar cells. *Gastroenterology* **140**, 2116–2125.

Criddle DN, Murphy J, Fistetto G, Barrow S, Tepikin AV, Neoptolemos JP, Sutton R & Petersen OH (2006). Fatty acid ethyl esters cause pancreatic calcium toxicity via inositol trisphosphate receptors and loss of ATP synthesis. *Gastroenterology* **130**, 781–793.

Di A, Gao XP, Qian F, Kawamura T, Han J, Hecquet C, Ye RD, Vogel SM & Malik AB (2011). The redox-sensitive cation channel TRPM2 modulates phagocyte ROS production and inflammation. *Nat Immunol* **13**, 29–34.

DiMagno EP, Shorter RG, Taylor WF & Go VL (1982). Relationships between pancreaticobiliary ductal anatomy and pancreatic ductal and parenchymal histology. *Cancer* **49**, 361–368.

Gerasimenko JV, Flowerdew SE, Voronina SG, Sukhomlin TK, Tepikin AV, Petersen OH & Gerasimenko OV (2006). Bile acids induce Ca^{2+} release from both the endoplasmic reticulum and acidic intracellular calcium stores through activation of inositol trisphosphate receptors and ryanodine receptors. *J Biol Chem* **281**, 40154–40163.

Gerasimenko JV, Gryshchenko O, Ferdek PE, Stapleton E, Hebert TO, Bychkova S, Peng S, Begg M, Gerasimenko OV & Petersen OH (2013). Ca^{2+} release-activated Ca^{2+} channel blockade as a potential tool in antipancreatitis therapy. *Proc Natl Acad Sci U S A* **110**, 13186–13191.

Geyer N, Diszhazi G, Csernoch L, Jona I & Almassy J (2015). Bile acids activate ryanodine receptors in pancreatic acinar cells via a direct allosteric mechanism. *Cell Calcium* **58**, 160–170.

Gout J, Pommier RM, Vincent DF, Kaniewski B, Martel S, Valcourt U & Bartholin L (2013). Isolation and culture of mouse primary pancreatic acinar cells. *J Vis Exp* **78**.

Halangk W, Kruger B, Ruthenburger M, Sturzebecher J, Albrecht E, Lippert H & Lerch MM (2002). Trypsin activity is not involved in premature, intrapancreatic trypsinogen activation. *Am J Physiol Gastrointest Liver Physiol* **282**, G367–374.

Hara Y, Wakamori M, Ishii M, Maeno E, Nishida M, Yoshida T, Yamada H, Shimizu S, Mori E, Kudoh J, Shimizu N, Kurose H, Okada Y, Imoto K & Mori Y (2002). LTRPC2 Ca^{2+}-permeable channel activated by changes in redox status confers susceptibility to cell death. *Mol Cell* **9**, 163–173.

Hegyi P, Rakonczay Z, Jr, Gray MA & Argent BE (2004). Measurement of intracellular pH in pancreatic duct cells: a new method for calibrating the fluorescence data. *Pancreas* **28**, 427–434.

Hong JH, Li Q, Kim MS, Shin DM, Feske S, Birnbaumer L, Cheng KT, Ambudkar IS & Muallem S (2011). Polarized but differential localization and recruitment of STIM1, Orai1 and TRPC channels in secretory cells. *Traffic* **12**, 232–245.

Kashio M, Sokabe T, Shintaku K, Uematsu T, Fukuta N, Kobayashi N, Mori Y & Tominaga M (2012). Redox signal-mediated sensitization of transient receptor potential melastatin 2 (TRPM2) to temperature affects macrophage functions. *Proc Natl Acad Sci U S A* **109**, 6745–6750.

Kim JY, Kim KH, Lee JA, Namkung W, Sun AQ, Ananthanarayanan M, Suchy FJ, Shin DM, Muallem S & Lee MG (2002). Transporter-mediated bile acid uptake causes Ca^{2+}-dependent cell death in rat pancreatic acinar cells. *Gastroenterology* **122**, 1941–1953.

Kim MS, Hong JH, Li Q, Shin DM, Abramowitz J, Birnbaumer L & Muallem S (2009). Deletion of TRPC3 in mice reduces store-operated Ca^{2+} influx and the severity of acute pancreatitis. *Gastroenterology* **137**, 1509–1517.

Kruger B, Albrecht E & Lerch MM (2000). The role of intracellular calcium signaling in premature protease activation and the onset of pancreatitis. *Am J Pathol* **157**, 43–50.

Lerch MM & Aghdassi AA (2010). The role of bile acids in gallstone-induced pancreatitis. *Gastroenterology* **138**, 429–433.

Lerch MM, Saluja AK, Runzi M, Dawra R, Saluja M & Steer ML (1993). Pancreatic duct obstruction triggers acute necrotizing pancreatitis in the opossum. *Gastroenterology* **104**, 853–861.

Liu X, Cotrim A, Teos L, Zheng C, Swaim W, Mitchell J, Mori Y & Ambudkar I (2013). Loss of TRPM2 function protects against irradiation-induced salivary gland dysfunction. *Nat Commun* **4**, 1515.

Liu X, Gong B, de Souza LB, Ong HL, Subedi KP, Cheng KT, Swaim W, Zheng C, Mori Y & Ambudkar IS (2017). Radiation inhibits salivary gland function by promoting STIM1 cleavage by caspase-3 and loss of SOCE through a TRPM2-dependent pathway. *Sci Signal* **10**, eaal4064.

Maleth J, Balazs A, Pallagi P, Balla Z, Kui B, Katona M, Judak L, Nemeth I, Kemeny LV, Rakonczay Z, Jr, Venglovecz V, Foldesi I, Peto Z, Somoracz A, Borka K, Perdomo D, Lukacs GL, Gray MA, Monterisi S, Zaccolo M, Sendler M, Mayerle J, Kuhn JP, Lerch MM, Sahin-Toth M & Hegyi P (2015). Alcohol disrupts levels and function of the cystic fibrosis transmembrane conductance regulator to promote development of pancreatitis. *Gastroenterology* **148**, 427–439 e416.

Maleth J & Hegyi P (2014). Calcium signaling in pancreatic ductal epithelial cells: an old friend and a nasty enemy. *Cell Calcium* **55**, 337–345.

Maleth J, Venglovecz V, Razga Z, Tiszlavicz L, Rakonczay Z, Jr & Hegyi P (2011). Non-conjugated chenodeoxycholate induces severe mitochondrial damage and inhibits bicarbonate transport in pancreatic duct cells. *Gut* **60**, 136–138.

Manna PT, Munsey TS, Abuarab N, Li F, Asipu A, Howell G, Sedo A, Yang W, Naylor J, Beech DJ, Jiang LH & Sivaprasadarao A (2015). TRPM2-mediated intracellular Zn^{2+} release triggers pancreatic beta-cell death. *Biochem J* **466**, 537–546.

Miller BA, Wang J, Song J, Zhang XQ, Hirschler-Laszkiewicz I, Shanmughapriya S, Tomar D, Rajan S, Feldman AM, Madesh M, Sheu SS & Cheung JY (2019). Trpm2 enhances physiological bioenergetics and protects against pathological oxidative cardiac injury: role of Pyk2 phosphorylation. *J Cell Physiol* **234**, 15048–15060.

Molnar R, Madacsy T, Varga A, Nemeth M, Katona X, Gorog M, Molnar B, Fanczal J, Rakonczay Z, Jr, Hegyi P, Pallagi P & Maleth J (2020). Mouse pancreatic ductal organoid culture as a relevant model to study exocrine pancreatic ion secretion. *Lab Invest* **100**, 84–97.

Muili KA, Jin S, Orabi AI, Eisses JF, Javed TA, Le T, Bottino R, Jayaraman T & Husain SZ (2013*a*). Pancreatic acinar cell nuclear factor kappaB activation because of bile acid exposure is dependent on calcineurin. *J Biol Chem* **288**, 21065–21073.

Muili KA, Wang D, Orabi AI, Sarwar S, Luo Y, Javed TA, Eisses JF, Mahmood SM, Jin S, Singh VP, Ananthanaravanan M, Perides G, Williams JA, Molkentin JD & Husain SZ (2013*b*). Bile acids induce pancreatic acinar cell injury and pancreatitis by activating calcineurin. *J Biol Chem* **288**, 570–580.

Pallagi P, Balla Z, Singh AK, Dosa S, Ivanyi B, Kukor Z, Toth A, Riederer B, Liu Y, Engelhardt R, Jarmay K, Szabo A, Janovszky A, Perides G, Venglovecz V, Maleth J, Wittmann T, Takacs T, Gray MA, Gacser A, Hegyi P, Seidler U & Rakonczay Z, Jr (2014). The role of pancreatic ductal secretion in protection against acute pancreatitis in mice. *Crit Care Med* **42**, e177–188.

Park MK, Ashby MC, Erdemli G, Petersen OH & Tepikin AV (2001). Perinuclear, perigranular and sub-plasmalemmal mitochondria have distinct functions in the regulation of cellular calcium transport. *EMBO J* **20**, 1863–1874.

Parniczky A, Kui B, Szentesi A, Balazs A, Szucs A, Mosztbacher D, Czimmer J, Sarlos P, Bajor J, Godi S, Vincze A, Illes A, Szabo I, Par G, Takacs T, Czako L, Szepes Z, Rakonczay Z, Izbeki F, Gervain J, Halasz A, Novak J, Crai S, Hritz I, Gog C, Sumegi J, Golovics P, Varga M, Bod B, Hamvas J, Varga-Muller M, Papp Z, Sahin-Toth M & Hegyi P (2016). Prospective, multicentre, nationwide clinical data from 600 cases of acute pancreatitis. *PLoS One* **11**, e0165309.

Perides G, Laukkarinen JM, Vassileva G & Steer ML (2010*a*). Biliary acute pancreatitis in mice is mediated by the G-protein-coupled cell surface bile acid receptor Gpbar1. *Gastroenterology* **138**, 715–725.

Perides G, van Acker GJ, Laukkarinen JM & Steer ML (2010*b*). Experimental acute biliary pancreatitis induced by retrograde infusion of bile acids into the mouse pancreatic duct. *Nat Protoc* **5**, 335–341.

Perraud AL, Takanishi CL, Shen B, Kang S, Smith MK, Schmitz C, Knowles HM, Ferraris D, Li W, Zhang J, Stoddard BL & Scharenberg AM (2005). Accumulation of free ADP-ribose from mitochondria mediates oxidative stress-induced gating of TRPM2 cation channels. *J Biol Chem* **280**, 6138–6148.

Schulz S, Schmitt S, Wimmer R, Aichler M, Eisenhofer S, Lichtmannegger J, Eberhagen C, Artmann R, Tookos F, Walch A, Krappmann D, Brenner C, Rust C & Zischka H (2013). Progressive stages of mitochondrial destruction caused by cell toxic bile salts. *Biochim Biophys Acta* **1828**, 2121–2133.

Sendler M, van den Brandt C, Glaubitz J, Wilden A, Golchert J, Weiss FU, Homuth G, De Freitas Chama LL, Mishra N, Mahajan UM, Bossaller L, Volker U, Broker BM, Mayerle J & Lerch MM (2020). NLRP3 inflammasome regulates development of systemic inflammatory respoes in mice with acute pancreatitis. *Gastroenterology* **158**, 253–269.e14.

Sendler M, Weiss FU, Golchert J, Homuth G, van den Brandt C, Mahajan UM, Partecke LI, Doring P, Gukovsky I, Gukovskaya AS, Wagh PR, Lerch MM & Mayerle J (2018). Cathepsin B-mediated activation of trypsinogen in endocytosing macrophages increases severity of pancreatitis in mice. *Gastroenterology* **154**, 704–718.e710.

Sherwood MW, Prior IA, Voronina SG, Barrow SL, Woodsmith JD, Gerasimenko OV, Petersen OH & Tepikin AV (2007). Activation of trypsinogen in large endocytic vacuoles of pancreatic acinar cells. *Proc Natl Acad Sci U S A* **104**, 5674–5679.

Sousa T, Castro RE, Pinto SN, Coutinho A, Lucas SD, Moreira R, Rodrigues CM, Prieto M & Fernandes F (2015). Deoxycholic acid modulates cell death signaling through changes in mitochondrial membrane properties. *J Lipid Res* **56**, 2158–2171.

Takahashi N, Kozai D, Kobayashi R, Ebert M & Mori Y (2011). Roles of TRPM2 in oxidative stress. *Cell Calcium* **50**, 279–287.

Tsutsui M, Hirase R, Miyamura S, Nagayasu K, Nakagawa T, Mori Y, Shirakawa H & Kaneko S (2018). TRPM2 exacerbates central nervous system inflammation in experimental autoimmune encephalomyelitis by increasing production of CXCL2 chemokines. *J Neurosci* **38**, 8484–8495.

Uchida K, Dezaki K, Damdindorj B, Inada H, Shiuchi T, Mori Y, Yada T, Minokoshi Y & Tominaga M (2011). Lack of TRPM2 impaired insulin secretion and glucose metabolisms in mice. *Diabetes* **60**, 119–126.

Venglovecz V, Rakonczay Z, Jr, Ozsvari B, Takacs T, Lonovics J, Varro A, Gray MA, Argent BE & Hegyi P (2008). Effects of bile acids on pancreatic ductal bicarbonate secretion in guinea pig. *Gut* **57**, 1102–1112.

Voronina SG, Barrow SL, Gerasimenko OV, Petersen OH & Tepikin AV (2004). Effects of secretagogues and bile acids on mitochondrial membrane potential of pancreatic acinar cells: comparison of different modes of evaluating $\Delta\Psi_m$. *J Biol Chem* **279**, 27327–27338.

Voronina SG, Barrow SL, Simpson AW, Gerasimenko OV, da Silva Xavier G, Rutter GA, Petersen OH & Tepikin AV (2010). Dynamic changes in cytosolic and mitochondrial ATP levels in pancreatic acinar cells. *Gastroenterology* **138**, 1976–1987.

Wen L, Voronina S, Javed MA, Awais M, Szatmary P, Latawiec D, Chvanov M, Collier D, Huang W, Barrett J, Begg M, Stauderman K, Roos J, Grigoryev S, Ramos S, Rogers E, Whitten J, Velicelebi G, Dunn M, Tepikin AV, Criddle DN & Sutton R (2015). Inhibitors of ORAI1 prevent cytosolic calcium-associated injury of human pancreatic acinar cells and acute pancreatitis in 3 mouse models. *Gastroenterology* **149**, 481–492 e487.

Yadav D & Lowenfels AB (2013). The epidemiology of pancreatitis and pancreatic cancer. *Gastroenterology* **144**, 1252–1261.

Yamamoto S, Shimizu S, Kiyonaka S, Takahashi N, Wajima T, Hara Y, Negoro T, Hiroi T, Kiuchi Y, Okada T, Kaneko S, Lange I, Fleig A, Penner R, Nishi M, Takeshima H & Mori Y (2008). TRPM2-mediated Ca^{2+} influx induces chemokine production in monocytes that aggravates inflammatory neutrophil infiltration. *Nat Med* **14**, 738–747.

Additional information

Competing interests

The authors have no conflicts of interest to declare.

Author contributions

P.P. and J.M. designed the research project; J.F., M.G., G.yD., J.A., T.M., Á.V., P.C.S.B., E.T., R.M., X.K., H.P. and R.Z. contributed to acquisition, analysis and interpretation of data for the work; P.P. and J.M. drafted the work, H.P. and R.Z. revised the manuscript critically for important intellectual content. All of the authors revised the final version of the manuscript. All authors approved the final version of the manuscript, and agree to be accountable for all aspects of the work in ensuring that questions related to the accuracy or integrity of any part of the work are appropriately investigated and resolved. All persons designated as authors qualify for authorship, and all those who qualify for authorship are listed.

Funding

The research was supported by funding from the Hungarian National Research, Development and Innovation Office (PD115974 and GINOP-2.3.2-15-2016-00048 to J.M., PD116553 to P.P., K119938 to R.Z.), the Ministry of Human Capacities (EFOP 3.6.2-16-2017-00006 to J.M.), Bolyai Research Fellowship (BO/00440/16/5 to J.M., BO/00569/17 to P.P.), the Hungarian Academy of Sciences (LP2017-18/2017 to J.M.), by the National Excellence Programme (20391-3/2018/FEKUSTRAT to J.M.), by the New National Excellence Program of the Ministry of Human Capacities (UNKP-18-4-SZTE-85 to P.P., UNKP-18-3-I-SZTE-66 to M.T., UNKP-19-3-I-DE-186 G.yD., UNKP-19-3-SZTE-318 to Á.V.) and EFOP 3.6.3-VEKOP-16-2017-00009 to M.T.

Acknowledgements

We are grateful to Yasuo Mori for generously providing the TRPM2 KO mice. The authors are also grateful to Indu Ambudkar for the scientific discussions.

Translational perspective

Inflammatory disorders of the pancreas (such as acute and chronic pancreatitis) pose a significant clinical challenge as currently no specific pharmaceutical treatment exists. Basic science studies can identify pathogenic disease mechanisms as novel drug targets, which can support drug discovery and therapy development in pancreatic diseases. Disturbed intracellular Ca^{2+} signalling caused by bile acids is a hallmark of the disease, which induces increased reactive oxygen species production, mitochondrial damage, intra-acinar digestive enzyme activation and cell death. Because of this mechanism of action, prevention of toxic cellular Ca^{2+} overload might be a promising therapeutic target. Transient receptor potential melastatin 2 (TRPM2) is a non-selective cation channel that has recently emerged as an important contributor to oxidative stress-induced cellular Ca^{2+} overload across different diseases. In our study, we are the first to report that TRPM2 is expressed in the acinar and ductal cells of the exocrine pancreas, which can be activated by increased oxidative stress. Activation of TRPM2 contributed to bile acid-induced extracellular Ca^{2+} influx in acinar cells, which promoted necrosis *in vitro* and *in vivo*. In an experimental model of biliary AP, genetic knockout of TRPM2 significantly decreased the disease severity and protected acinar cell. Based on these results we suggest that the inhibition of TRPM2 may be a potential treatment option for biliary

pancreatitis and development of novel TRPM2 inhibitors can be translated to patient benefit.

Keywords

acinar cell necrosis, acute pancreatitis, bile acid, Ca^{2+} signalling, epithelial ion transport, TRPM2 channel

Supporting information

Additional supporting information may be found online in the Supporting Information section at the end of the article.

Statistical Summary Document

II.

Laboratory Investigation
https://doi.org/10.1038/s41374-019-0300-3

TECHNICAL REPORT

Mouse pancreatic ductal organoid culture as a relevant model to study exocrine pancreatic ion secretion

Réka Molnár[1] · Tamara Madácsy[1,2] · Árpád Varga[1,2] · Margit Németh[1,2] · Xénia Katona[1,2] · Marietta Görög[1,2] · Brigitta Molnár[1] · Júlia Fanczal[1] · Zoltán Rakonczay Jr.[3] · Péter Hegyi[4,5] · Petra Pallagi[1,2] · József Maléth[1,2,6]

Received: 10 May 2019 / Revised: 19 June 2019 / Accepted: 19 June 2019

Abstract

Pancreatic exocrine secretory processes are challenging to investigate on primary epithelial cells. Pancreatic organoid cultures may help to overcome shortcomings of the current models, however the ion secretory processes in pancreatic organoids—and therefore their physiological relevance or their utility in disease modeling—are not known. To answer these questions, we provide side-by-side comparison of gene expression, morphology, and function of epithelial cells in primary isolated pancreatic ducts and organoids. We used mouse pancreatic ductal fragments for experiments or were grown in Matrigel to obtain organoid cultures. Using PCR analysis we showed that gene expression of ion channels and transporters remarkably overlap in primary ductal cells and organoids. Morphological analysis with scanning electron microscopy revealed that pancreatic organoids form polarized monolayers with brush border on the apical membrane. Whereas the expression and localization of key proteins involved in ductal secretion (cystic fibrosis transmembrane conductance regulator, Na^+/H^+ exchanger 1 and electrogenic Na^+/HCO_3^- cotransporter 1) are equivalent to the primary ductal fragments. Measurements of intracellular pH and Cl^- levels revealed no significant difference in the activities of the apical Cl^-/HCO_3^- exchange, or in the basolateral Na^+ dependent HCO_3^- uptake. In summary we found that ion transport activities in the mouse pancreatic organoids are remarkably similar to those observed in freshly isolated primary ductal fragments. These results suggest that organoids can be suitable and robust model to study pancreatic ductal epithelial ion transport in health and diseases and facilitate drug development for secretory pancreatic disorders like cystic fibrosis, or chronic pancreatitis.

Introduction

Pancreatic ductal epithelia (PDE) have been known to provide the structural framework of the exocrine pancreas, but more importantly they secrete HCO_3^- and fluid that play pivotal role in the pancreatic physiology [1]. Exocrine ductal secretion flushes out bioactive molecules, including pancreatic enzymes secreted by acinar cells to the duodenum [2]. In addition, the alkaline ductal fluid neutralizes protons co-secreted during acinar exocytosis, which prevents the premature activation of pancreatic proenzymes in the ductal lumen by inhibiting the autoactivation of trypsinogen [3]. On the other hand, in disease conditions—such as cystic fibrosis or acute pancreatitis—the impaired ductal secretion could lead to the functional and morphological damage of the acinar cells [4, 5], enhanced inflammatory response [6], or complete destruction of the gland leading to exocrine pancreatic insufficiency [7]. Standard isolation techniques of pancreatic ducts [8]—based on digestion of the pancreas with collagenase and manual isolation of the

Supplementary information The online version of this article (https://doi.org/10.1038/s41374-019-0300-3) contains supplementary material, which is available to authorized users.

✉ József Maléth
maleth.jozsef@med.u-szeged-hu

1 First Department of Medicine, University of Szeged, Szeged, Hungary

2 HAS-USZ Momentum Epithelial Cell Signaling and Secretion Research Group, University of Szeged, Szeged, Hungary

3 Department of Pathophysiology, University of Szeged, Szeged, Hungary

4 HAS-USZ Momentum Translational Gastroenterology Research Group, University of Szeged, Szeged, Hungary

5 Institute for Translational Medicine and First Department Medicine, Medical School, University of Pécs, Pécs, Hungary

6 Department of Public Health, University of Szeged, Szeged, Hungary

Published online: 13 August 2019

ductal fragments under stereomicroscope—have been used extensively to study pancreatic ductal physiology and pathology and led to a better understanding of the ductal epithelia in health and disease. This technique made the study of primary PDE cells possible, including physiologically relevant measurements, such as forskolin induced swelling [5] or fluorescent indicator-based intracellular pH measurements [9]. The most important limitation of this widely used isolation technique is that the complete removal of the surrounding conjunctive tissue—including fibroblasts—is not possible under a stereomicroscope leading to a mixed culture of epithelial and mesenchymal cells [10]. Thus, for example evaluation of changes in gene expression of epithelial cells could be confounded by alterations in the surrounding fibroblasts. Moreover, due to the limited amount of the isolated tissue, studies of protein expression is limited to immunofluorescent labeling, whereas, the applicability of other techniques to study protein expressions are limited and difficult.

Organoid cultures (OCs) derived from tissue specific Leucine-rich repeat-containing G-protein coupled receptor 5 positive (Lgr5+) adult stem cells emerged recently as novel models of organ development and disease [11, 12]. By maintaining the activity of Wnt/β-Catenin signal transduction cascade—a key driver of most types of tissue stem cells [13]—OCs can be grown in vitro long-term in 3D extracellular matrix-based hydrogels; whereas, epithelial cells in the culture maintain the original cellular diversity and organization of the organ of origin [14]. The technique was originally developed to culture small intestinal Lgr5+ adult stem cells that generated crypt–villus like structures [15]. Since then OCs have been established from a wide range of organs in the gastrointestinal tract, including large intestine and esophagus [11], stomach [16], liver and pancreas [17]. Clear advantages of OCs over conventional 2D cell cultures are that in OCs more relevant cell-to-cell contact is maintained, whereas in 2D cultures the cells are attached to the plastic surface and cell-to-cell contacts are limited to the edges [18]. In pancreatic research currently OCs are studied as relevant human models of tissue development [19] and carcinogenesis [20]. The above described potential limitations of isolated ductal fragments might be overcome by the application of pancreatic OCs for both physiological and pathological studies. However, the physiological relevance of pancreatic OCs is currently not known.

In this manuscript we provide a side-by-side comparison of morphology and function of isolated primary mouse pancreatic ductal fragments and pancreatic OCs. Using end-point PCR analysis to compare mRNA expressions of 12 functional genes (encoding ion channels and transporters), we demonstrated that both primary ductal fragments and OCs express these genes. Moreover, our data confirmed that epithelial cells in pancreatic OCs maintain apical-basal polarity as demonstrated by electron microscopy and immunolabeling of the apical CFTR Cl^- channel, the basolateral Na^+/H^+ exchanger 1 (NHE1), and electrogenic Na^+/HCO_3^- cotransporter 1 (NBCe1). Functional comparison of ion secretion using fluorescent indicators of intracellular pH and Cl^- levels revealed no significant difference in the activities of Na^+ dependent basolateral HCO_3^- uptake, or in the apical HCO_3^- extrusion. We also showed that the intracellular Ca^{2+} signaling—a crucial intracellular signaling pathway in non-excitable epithelial cells—is highly comparable in primary ductal epithelial cells and OCs cells. Taken together, our data suggest that pancreatic ductal OCs are excellent models to study exocrine pancreatic ductal physiology and pathophysiology.

Materials and methods

Animals

Ten- to twelve-week-old FVB/N mice were used with adherence to the NIH guidelines and the EU directive 2010/63/EU for the protection of animals used for scientific purposes. The study was approved by the National Scientific Ethical Committee on Animal Experimentation under license number XXI./2522/2018.

Isolation of pancreatic ductal fragments

Pancreatic ductal fragments were isolated as described earlier [6]. Briefly, after terminal anesthesia the pancreas was surgically removed and digested for 30 min with 100 U/ml purified collagenase (Worthington, Cat. No.: LS005273), 0.1 mg/ml trypsin inhibitor (ThermoFisher Scientific, Cat. No.: 17075029) and 1 mg/ml bovine serum albumin (VWR, Cat. No.: 9048-46-8) in DMEM Nutirent Mixture F-12 Ham (Sigma, Cat. No.: D6421) at 37 °C in a shaking water bath. Small intra-/interlobular ducts were isolated by microdissection under stereomicroscope. Isolated ductal fragments were used for experimental analysis, or were cultured as described below.

Mouse ductal pancreatic organoid culture

For the establishment of OCs we used the previously published protocol by Boj et al. [20]. Briefly, isolated mouse ducts were resuspended in Corning® Matrigel (VWR, Cat. No.: 734-1100) and 10 µl Matrigel domes were plated into 24-well pates. The plates were placed on 37 °C until the Matrigel domes solidified. After that prewarmed Mouse Feeding Media was added to each well (for composition of

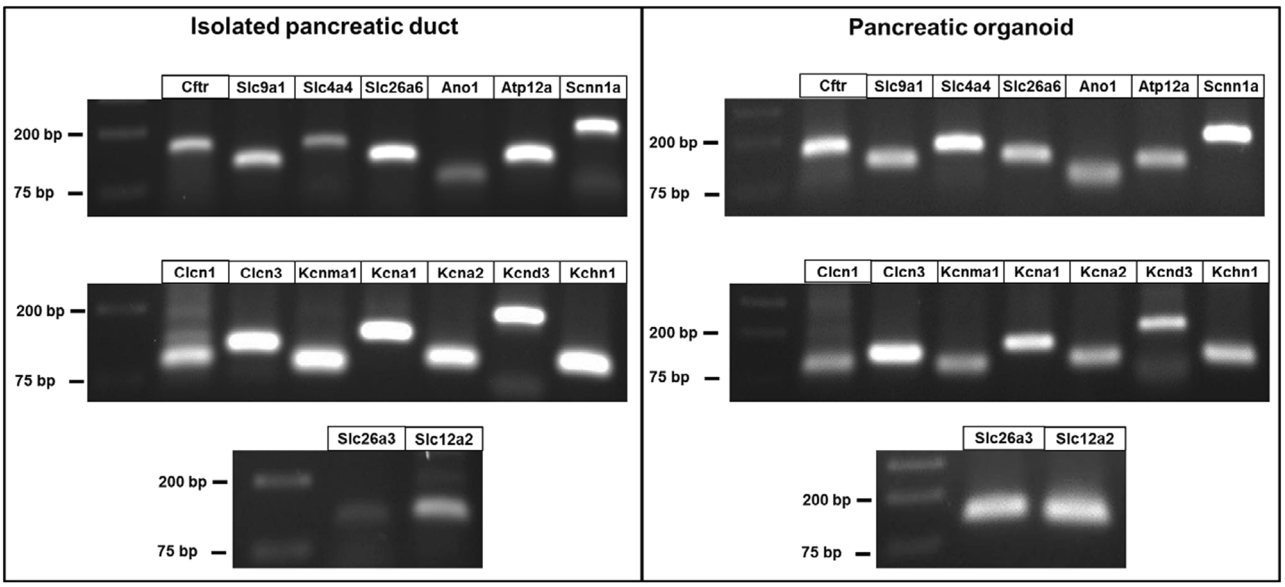

Fig. 1 Comparison of gene expression of isolated pancreatic ducts and pancreatic organoids. Left and right panels show the agarose gel images of cDNA samples derived from isolated mouse pancreatic ductal fragments and pancreatic organoids, respectively. The gene expression of the two samples showed a marked overlap. Images were captured after 35 cycles. List of investigated genes can be found in Supplementary Figure 1

feeding and digestion media please see Supplementary Table 1). Feeding media was replaced every other day and organoids were passaged weekly by gentle physical disruption and centrifugation. For the experiments organoids were used until passage no. 5. to avoid any changes in gene expression.

Gene expression analysis

The expression analysis of investigated genes was assessed by combining reverse-transcription (RT-PCR) and conventional polymerase chain reactions (PCR). Total mRNA was isolated from three independent biological replicates of mouse whole brain tissue, mouse ductal fragments, or OCs by NucleoSpin RNA XS kit (Macherey-Nagel, Ref.:740902.50) according to the manufacturer's instructions. The mRNA concentrations were measured by NanoDrop™ 2000 spectrophotometer (ThermoFisher Scientific). 1 µg purified mRNA was used for each cDNA synthesis step. RT-PCRs were carried out by using iScript™ cDNA Synthesis kit (Bio-Rad; Cat. No.: 1708890). For the conventional PCR amplification DreamTaq Hot Start DNA Polymerase (ThermoFisher Scientific, Cat. No.: EP1702) and cDNA specific primers were applied as indicated in Supplementary Table 2. All the primers were validated on template cDNA deriving from mouse brain tissue (Supplementary Fig. 1). To compare gene expression levels derived from the same experiments (which are represented by individual agarose gel images in Fig. 1), we used plot lanes analysis quantification by ImageJ software.

Immunofluorescent labeling

Isolated pancreatic ductal fragments or organoids were frozen after the first passage in Shandon Cryomatrix (ThermoFisher Scientific, Cat. No.: 6769006) and stored at −20 °C until sectioning. 7 µm thick sections were cut with cryostat (Leica CM 1860 UV) at −20 °C. Sections were fixed in 4% PFA-PBS for 15 min then washed in 1× Tris buffered saline (TBS) for 3 × 5 min. Antigen retrieval was performed in Sodium Citrate - Tween20 buffer (0.001 M Sodium Citrate Buffer, pH 6.0 and 0.05% Tween20) at 94 °C for 30 min. Sections were blocked with 0.1% goat serum and 10% bovine serum albumin (BSA)-TBS for 1 h. Incubation with primary antibodies were performed overnight at 4 °C. For the list and dilution of antibodies, please see Supplementary Table 3. Sections were incubated with secondary antibody for 2 h at room temperature. Nuclear staining was performed with 1 µg/ml Hoechst33342 (ThermoFisher Scientific; Cat. No.: 62249) for 15 min and sections were placed in Fluoromount mounting medium (Sigma-Aldrich; Cat. No.: F4680) then left to dry. Images were captured with a Zeiss LSM880 confocal microscope using a 40× oil immersion objective (Zeiss, NA: 1.4).

Electron microscopy

Sample preparation

Isolated pancreatic ductal fragments or organoids after the first passage were fixed for 24 h in 3% glutaraldehyde (Electron Microscopy Sciences, Cat. No: 16220) at room

temperature and washed for 3 × 15 min in 0.3 M cacodylate buffer (pH 7.4) (EMS, Cat. No: 12310). For contrasting samples were incubated in 3% potassium ferrocyanide (Sigma-Aldrich, Cat. No: 60279) and 2% osmium tetroxide (EMS, Cat. No: 19110) in 300 mM cacodylate buffer for 1 h at 4 °C. This was followed by 20 min incubation in 1% thiocarbohydrazide (Sigma-Aldrich, Cat. No.: 223220), then the samples were placed in 2% osmium tetroxide for 30 min at room temperature and finally samples were incubated overnight in 1% uranyl acetate at 4 °C. Sample dehydration was performed with 20%, 50%, 70%, 96% and absolute ethanol, respectively for 15 min in each dilution and 1,2-propylene oxide (Merck, Cat. No.: 8.07027.1001) was used as intermedier 2 × 5 min. All solutions were prepared with AccuGENE molecular biology water (Lonza, Cat. No.: 51223) and filtered through a 0.22 µm syringe filter. For infiltration Epon 812 resin was used according to the manufacturer's instructions (Embed 812 Resin, EMS, Cat. No.: 14900; DDS, EMS, Cat. No.: 13710, NMA, EMS, Cat. No.: 19000, BDMA, Sigma-Aldrich, Cat. No.: 185582). Sample infiltration was performed in two steps (propylene oxide + resin 1:1 solution then pure resin). Resin polymerization was done at 60 °C for 24 h.

Sectioning and imaging

Before sectioning, indium tin oxide covered glasses were put into a Quorum carbon coater (Quorum Q150R ES Plus, Quorum Tech) for negative glow discharge. The blocks were trimmed and 100 nm ultrathin sections were cut by a 35° Ultra jumbo diamond knife type (DIATOME) on an RMC Powertome ultramicrotome with 0.8 mm/s cutting speed. Post contrasting was performed with 5% uranyl acetate and Reynolds solution. Sections were carbon-coated and placed into a Zeiss Sigma 300 scanning electron microscope (SEM). Images were captured by an in chamber secondary electron detector. Imaging parameters were as follows: 2.34 A filament current, 5 kV acceleration voltage. 30 nm pixel size was used for lower magnification and 10 nm for higher magnification images.

Fluorescent microscopy

Pancreatic ductal fragments or organoids were attached to a poly-l-lysine coated coverglass and were incubated in standard HEPES solution with BCECF-AM (1.5 µmol/L), Fura2-AM (5 µmol/L), or MQAE (2 µmol/L) for 30 min at 37 °C. Cover glasses were then transferred to a perfusion chamber mounted on an Olympus IX71 inverted microscope. Dye loaded samples were excited with an Olympus MT-20 illumination system equipped with a 150 W xenon arc light source. For BCECF the filter combination was as follows: 434/17 nm and 497/16 nm single-band bandpass filters for excitation (Semrock; P/N: FF01-434/17-25 and FF01-497/16-25, respectively), 511 nm edge single-edge standard epi-fluorescence dichroic beamsplitter (Semrock; P/N: FF511-Di01-25 × 36) and 537/26 nm single-band bandpass filters for emission (Semrock; P/N: FF01-537/26-25). For Fura2: 340/26 nm and 387/11 nm single-band bandpass filters for excitation (Semrock; P/N: FF01-340/26-25 and FF01-387/11-25, respectively), 409 nm edge single-edge standard epi-fluorescence dichroic beamsplitter (Semrock; P/N: FF409-Di03-25 × 36) and 510/84 nm single-band bandpass filters for emission (Semrock; P/N: FF01-510/84-25). For MQAE: 340/26 nm single-band bandpass filters for excitation (Semrock; P/N: FF01-340/26-25), 409 nm edge single-edge standard epi-fluorescence dichroic beamsplitter (Semrock; P/N: FF409-Di03-25 × 36) and 510/84 nm single-band bandpass filters for emission (Semrock; P/N: FF01-510/84-25). The fluorescent signal was captured by a Hamamatsu ORCA-ER CCD camera trough a ×20 oil immersion objective (Olympus; NA: 0.8) with a temporal resolution of 1 s. Ratiometric image analysis was performed by Olympus excellence software.

For pH measurement with SNARF-1 (ThermoFisher Scientific; Cat. No.: C1272), or SNARF-1 dextran (ThermoFisher Scientific; Cat. No.: D3304) organoids were attached to a poly-l-lysine coated coverglass and were incubated in standard HEPES solution with SNARF-1 (10 µmol/L) for 30 min at 37 °C. SNARF-1 dextran was injected into the lumen of the organoids using a glass injection pipette. Images were captured by a Zeiss LSM880 confocal microscope was used with a ×40 water immersion objective (Zeiss, NA: 1.2). Samples were excited with 514 nm Argon laser and emitted fluorescent signal was captured by a GaASP detector between 550–580 nm and 610–650 nm respectively with a temporal resolution of 5 s. The ratio of the two emission wavelengths (640/580 ratio) was calculated by Zeiss Zen Black software.

Statistics

All data are expressed as means ± SEM. Significant differences between groups were determined by analysis of variance. $p < 0.05$ was considered statistically significant.

Results

mRNA expression of ion channels and transporters in isolated pancreatic ducts and organoids

To confirm that OCs are suitable to study pancreatic ductal secretion, first we wanted to check whether gene expression patterns of ion channels and transporter proteins (listed in Supplementary Fig. 1A) are comparable in isolated ducts and

organoids (cycle number: 35 in Fig. 1; cycle number: 30 in Supplementary Fig. 3). The relative band densities showing the gene expressions compared with each other within one gel are presented in Supplementary Fig. 4. Our results confirmed the expression of *Slc26a6*, *Cftr*, *Nhe1*, and *Nbce1* in both isolated ductal fragments and in pancreatic OCs. In addition, we demonstrated the expression of nongastric H^+/K^+ ATPase; Ca^{2+}-activated K^+ channel (BK channel); *Slc26a3* Cl^-/anion exchanger and the basolateral $Na^+/K^+/Cl^-$ symporter (*Nkcc*). The expression of K^+ channels in the pancreatic ductal epithelia is controversial and species dependent [21], therefore, we selected four members of the voltage-gated subfamily *Kcna1, Kcna2, Kcnd3,* and *Kcnh1*, which were not yet described in the pancreatic ductal epithelia to further confirm the uniformity of gene expression in primary ducts and OCs. We found that these four members of the subfamily are expressed in both samples strengthening their potential similarity. Very interestingly, we also detected the expression of genes coding the two members of the voltage-gated Cl^- channels (*Clcn1* and *Clcn3*), epithelial sodium channel (*Enac*) and the Ca^{2+}-activated Cl^- channel Anoctamin1 (*Ano1*, or *Tmem16a*) in both isolated primary ductal fragments and pancreatic OCs.

Morphological and functional polarity of pancreatic OCs

Comparison of the ultrastructure of isolated ductal fragments and pancreatic OCs highlighted that OCs were formed by a single layer of epithelial cells (Supplementary Fig. 5) that show similar apical-basal polarity as primary ductal epithelia (Fig. 2a, b). On the apical membrane, we detected brush border in both samples (arrows), whereas the mitochondria showed similar intracellular distribution around the lumen forming a belt-like structure in the apical segment of the cells (arrowheads) both in OCs and isolated ducts as reported earlier [10]. To investigate the functional polarity immunofluorescent labeling of both the OCs and primary ducts was performed. As demonstrated on the confocal images, we were able to show that NHE1 and NBCe1 are expressed solely on the basolateral membrane whereas CFTR is expressed exclusively on the apical membrane of the epithelial cells (Fig. 2c). Similarly to isolated ducts, these results confirmed the morphological and functional polarity of OCs.

Apical Cl^- dependent HCO_3^- secretion in pancreatic organoids

As the primary function of the ductal epithelia is ion (especially HCO_3^-) and fluid secretion, we used standard intracellular pH (pH_i) measurement based on the fluorescent pH indicator BCECF-AM to estimate the HCO_3^- efflux across the apical membrane to further confirm the functional similarity of OCs and isolated ducts. Cells were exposed to 20 mM NH_4Cl in HCO_3^-/CO_2-buffered solution from the basolateral side which triggered an immediate increase in pH_i due to the rapid influx of NH_3 across the membrane (Fig. 3a and Supplementary Fig. 7A). This was followed by a slower recovery of the alkaline pH_i toward the basal value. The recovery depends on the HCO_3^- efflux (i.e., secretion) from the ductal epithelia via the SLC26 Cl^-/HCO_3^- exchangers and CFTR [6]. Once NH_4Cl is removed, the pH_i drops to the acidic range due to the overshoot of the compensatory mechanisms. Again, this is followed by a slow recovery to reach basal pH_i. This recovery phase depends on activities of the basolateral NHE1 and NBCe1 [6]. The initial rate of recovery from alkalosis and acidosis was measured ($\Delta pH/\Delta t$) over the first 30 s and the base flux [$J(B^-)$] was calculated as previously described [6]. Using this approach, we were not able to show significant differences between primary isolated ductal epithelia and pancreatic OCs, suggesting that apical Cl^-/HCO_3^- exchange activity and basolateral HCO_3^- uptake is similar (Fig. 3a, b). In addition, exposure of the cells to 10 µM CFTR(inh)-172 (a specific inhibitor of CFTR channel) significantly decreased the base flux in both samples, suggesting that the functional activity of CFTR contributes to the recovery in OCs under these conditions (Fig. 3a, c). We also preformed this experimental protocol in HEPES buffered extracellular solution (Supplementary Fig. 6). Under these conditions, only recovery from acid load can be interpreted. This reflects NHE activity, which was significantly higher in isolated ducts.

Indirect measurement of CFTR activity in pancreatic OCs using fluorescent Cl^- indicator

Forskolin-induced swelling (FIS) is currently the state-of-the-art technique to estimate CFTR activity in 3D OCs [22]. FIS has several advantages (e.g., it is relatively simple and robust allowing precision medicine treatment [22]), but it also has some potential limitations as well (such as the increased intraluminal pressure). In these series of experiments we used an intracellular Cl^- level ($[Cl^-]_i$) sensitive fluorescent indicator MQAE to track Cl^- movement to estimate CFTR activity. The fluorescent signal emitted by MQAE inversely correlates with the $[Cl^-]_i$, thus an increase reports Cl^- efflux. Removal of extracellular Cl^- from the HCO_3^-/CO_2-buffered solution resulted in a decrease of $[Cl^-]_i$, most likely due to the Cl^- efflux from the cytosol via CFTR, which was significantly enhanced by Forskolin administration (Fig. 4). In addition, 10 µM CFTR(inh)-172 completely abolished the Cl^- extrusion, whereas the protein kinase A (PKA) inhibitor H-89 significantly impaired it to the

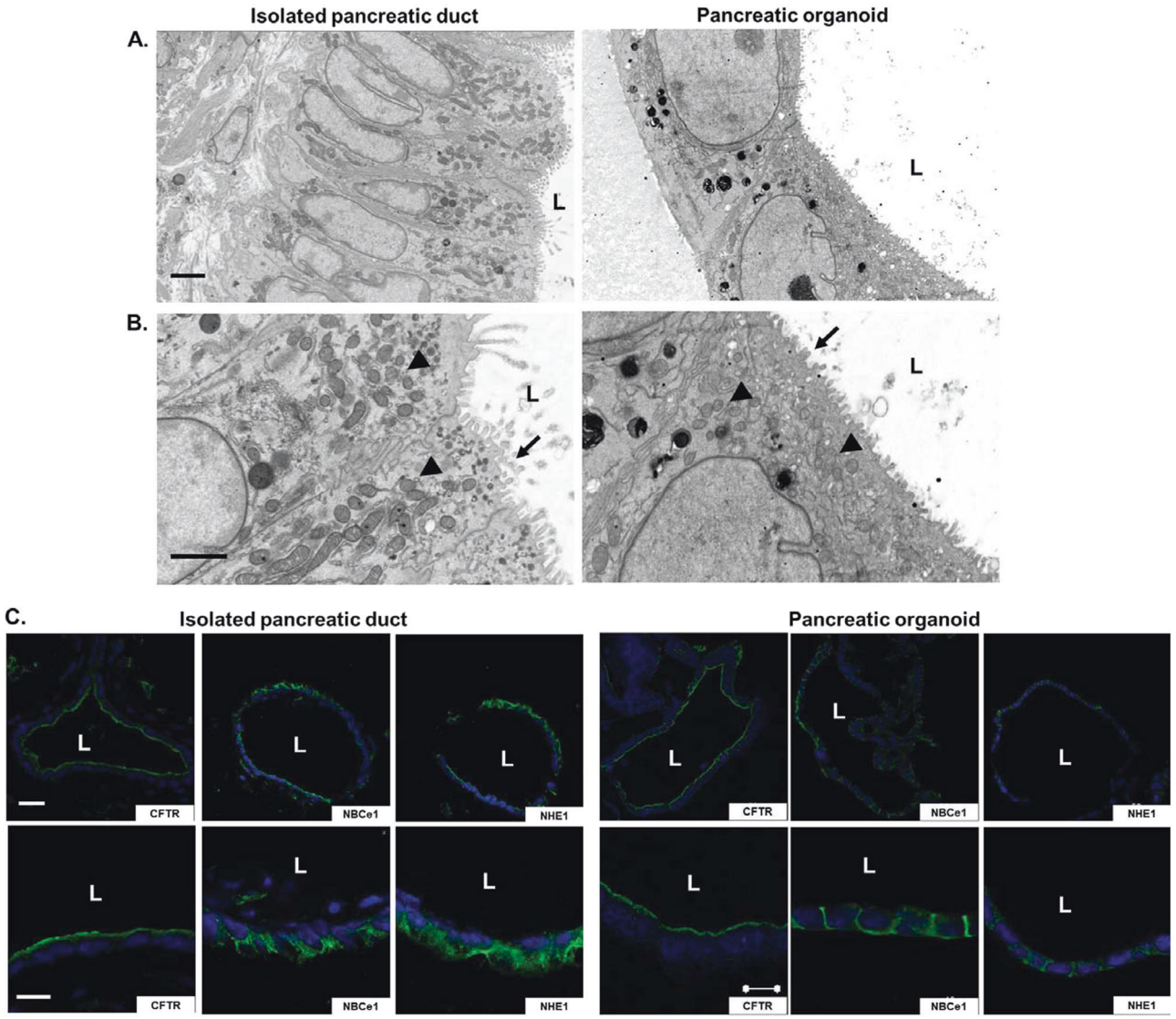

Fig. 2 Morphology and apical-basal polarity of isolated ducts and pancreatic organoids. Representative scanning electron microscope images show the ultrastructure of epithelial cells in isolated ducts and in pancreatic organoids. Brush border was observed on the apical membrane in both samples (arrows), whereas the majority of the mitochondria were located in the apical region of the cells (arrowheads) both in organoids and isolated ducts. L: lumen; scale bars: 2 µm in lower (**a**) 1 µm in higher magnification (**b**). **c** Representative confocal images demonstrate the polarized expression of proteins in epithelial cells. NHE1 and NBCe1 are expressed on the basolateral, whereas CFTR is expressed exclusively on the apical membrane. L: lumen; scale bars: 20 µm in lower (upper panel), 10 µm in higher magnification (lower panel)

nonstimulated control level further indicating that the measured Cl^- were due to the activity of CFTR. These results are consistent with our current knowledge of CFTR activity and regulation and thus this technique may be a powerful toolkit for researchers studying CFTR activity in 3D cultures.

We also utilized this technique to measure the activity of NKCC1 in isolated ducts and pancreatic organoids. As shown in Fig. 4c. the administration of 100 µM Bumetanide (an NKCC1 inhibitor) decreased the $[Cl^-]_i$ suggesting an NKCC1-dependent basolateral Cl^- uptake in ductal fragments and pancreatic organoids.

Basolateral Na^+ dependent HCO_3^- uptake in pancreatic organoids

To compare the activity of basolateral Na^+-dependent HCO_3^- uptake in primary pancreatic ductal fragments and pancreatic OCs, we applied the above described NH_4Cl administration in Na^+-free HCO_3^-/CO_2-buffered solution. Under these conditions the recovery from acidosis was almost completely abolished confirming that this process strongly depends on the extracellular Na^+ and suggesting the potential role of NHE1 and NBCe1 in the process (Fig. 5a). To characterize the contribution of each

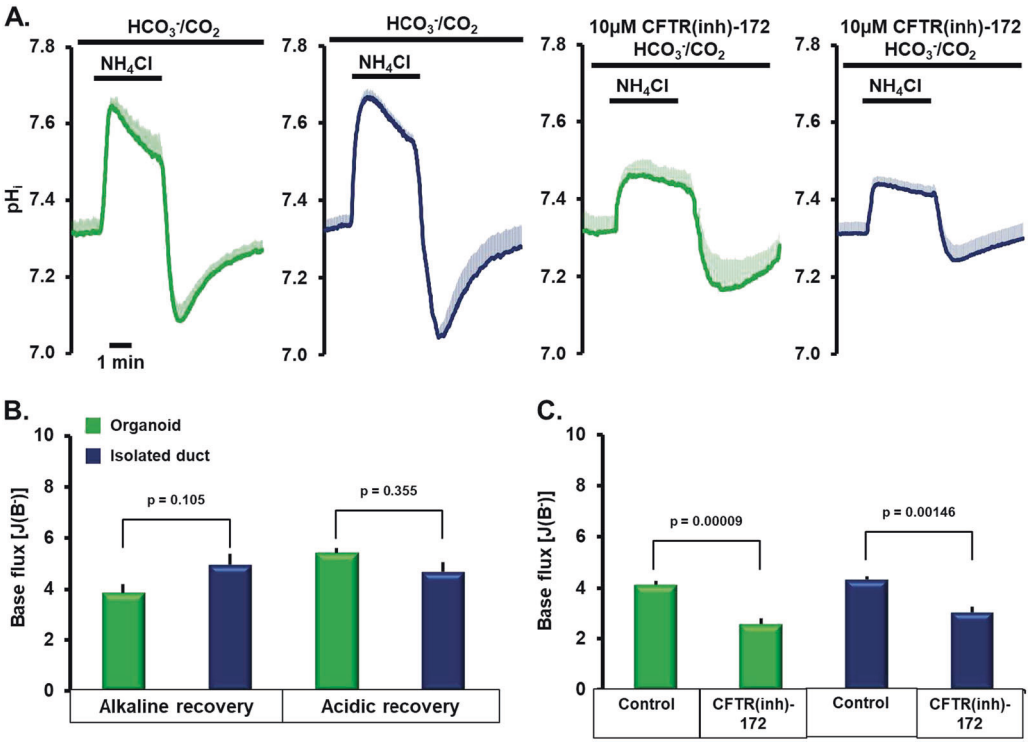

Fig. 3 Comparison of HCO_3^- secretion in isolated ducts and pancreatic organoids. **a** Average pH_i traces of 4–6 experiments for each conditions. Pancreatic ducts or organoids were perfused with HCO_3^-/CO_2-buffered extracellular solution and intracellular alkalization was achieved by 20 mM NH_4Cl administration in the absence or presence of CFTR(inh)-172. Bar charts of the calculated base fluxes of HCO_3^-. Comparison of alkaline and acidic recovery, as representation of the apical and basolateral transport activities, showed no difference in primary ducts vs pancreatic organoids (**b**). CFTR inhibition markedly decreased alkaline recovery in each experiments (**c**)

transporter in more details, we applied another protocol and specific inhibitors of NHE1 and NBCe1 (Supplementary Fig. 7B). During these series of experiments the standard HEPES was switched to HCO_3^-/CO_2-buffered solution triggering a rapid drop in pH_i due to the influx and intracellular conversion of CO_2 to carbonic acid and its dissociation to HCO_3^- and H^+. In the presence of extracellular Na^+ the pH_i is restored to the resting level by NHE1 and NBCe1. As the average traces of individual experiments (Fig. 5b, c) and the calculated base flux and $\Delta(pH_i)_{max}$ (Fig. 5d, e) demonstrate, both primary ducts and pancreatic OCs showed similar responses to the specific inhibition of NHE1 (10 μM EIPA) and NBCe1 (10 μM S0859). In both cases the inhibition of NHE1 caused a higher decrease in the calculated base flux (79.01% in OC and 70.62% in ducts) compared with the inhibition of NBCe1 (60.82% in OC and 53.32% in ducts). The combined inhibition of NHE1 and NBCe1 did not decrease the basolateral Na^+ dependent HCO_3^- uptake further.

Intracellular Ca^{2+} signaling in pancreatic organoids

In nonexcitable secretory epithelial cells, intracellular Ca^{2+} signaling is one of the major signal transduction pathways. Moreover, we and others have shown that changes of intracellular Ca^{2+} concentration regulates ion secretion in physiology [23] and impairs transport functions via complex mechanisms in pathology [10]. Therefore, we also compared Ca^{2+} signaling in primary pancreatic ducts and in OCs. First, we used two Ca^{2+} mobilizing agonists (ATP and carbachol) that release Ca^{2+} from the endoplasmic reticulum (ER) Ca^{2+} stores. We detected that both agonists induced peak-plateau type Ca^{2+} elevation in the tested concentrations (Fig. 6a). These signals showed no significant differences in the maximal response (Fig. 6c). We also compared the store operated Ca^{2+} entry caused by the ER store depletion (Fig. 6b). Using this assay, we found that the ER Ca^{2+} release induced by 25 μM cyclopiazonic acid was significantly higher in isolated ducts, whereas the Ca^{2+} influx was significantly higher in OCs (Fig. 6d). These observations need further investigation to determine the biological relevance of this phenomena.

Measurement of intraluminal pH in pancreatic organoids

As intraluminal pH has a major physiological relevance we developed a new technique to follow its changes in response to various treatments. First, we used SNARF-1 as a control to monitor intracellular pH changes with confocal

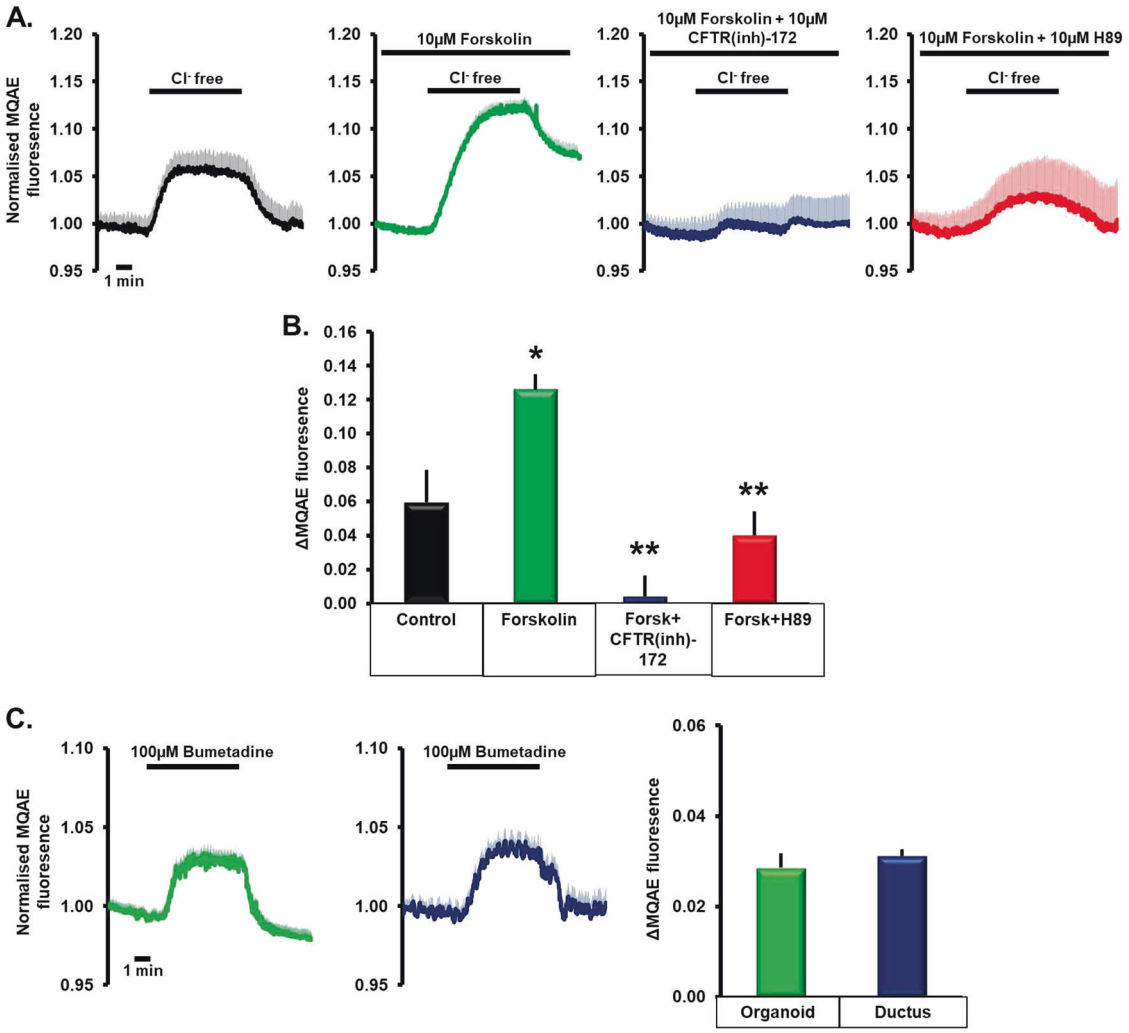

Fig. 4 Measurement of CFTR and NKCC1 activities in pancreatic organoids using Cl^- sensitive fluorescent dye. **a** Average traces of intracellular Cl^- levels of 4–6 experiments for each conditions. Pancreatic organoids were perfused with HCO_3^-/CO_2 buffered extracellular solution. Removal of extracellular Cl^- induced a decrease in intracellular Cl^- levels (reflected by an increase in fluorescent intensity) due to the activity of CFTR. **b** Bar charts of the maximal fluorescent intensity changes. 10 μM forskolin significantly increased, whereas 10 μM CFTR(inh)-172 and H-89 significantly impaired cAMP-stimulated CFTR activity in pancreatic organoids. $*p < 0.05$ vs Control, $**p < 0.05$ vs Forskolin. **c** Average traces of intracellular Cl^- levels and bar charts of NKCC1 activity. To measure NKCC1 activity, organoids and ductal fragments were treated with bumetanide in HCO_3^-/CO_2-buffered extracellular solution in organoids and ductal fragment

microscope (Fig. 7a and Supplementary Fig. 8). As demonstrated, this technique can be used to follow dynamic pH changes. In the next step a glass needle was used to inject dextran conjugated SNARF-1 into the lumen of the organoids (Fig. 7b). The injected dye was trapped in the lumen and was not taken up by the epithelial cells. Administration of NH_4Cl in HEPES-buffered solution caused a moderate increase in the intraluminal pH which could be attributed to the diffusion of NH_3 into the organoid lumen (Fig. 7c). In contrast, NH_4Cl in HCO_3^-/CO_2-buffered solution triggered a rapid and notable elevation of intraluminal pH due to the efflux of HCO_3^- to the lumen. This elevation was completely abolished by 10 μM CFTR (inh)-172 administration suggesting the major role of CFTR in this process.

Discussion

OCs have recently emerged as promising *ex vivo* models of tissue development, physiology and pathophysiology. Reports suggested that cells in OCs maintain tissue specific gene expression, cell morphology and function and may represent features of malignant diseases. Although organoids are used in an increasing number of studies, we only have limited experimental data about their physiological

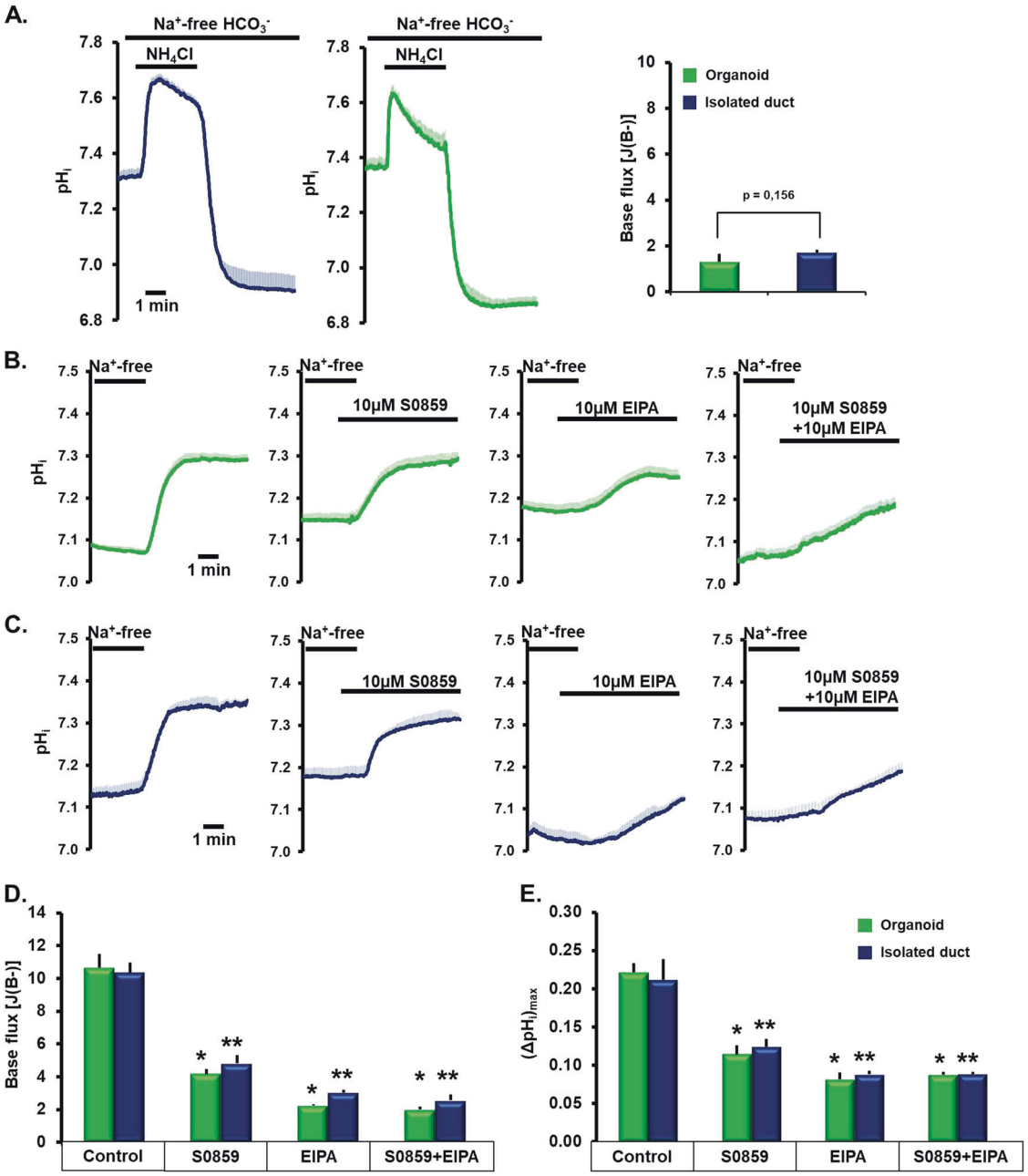

Fig. 5 Comparison of basolateral HCO_3^- uptake in isolated ducts and pancreatic organoids. **a** Average pH_i traces and bar charts from 4–6 experiments demonstrate that basolateral Na^+ removal almost completely abolished the recovery from intracellular acidosis. Average pH_i traces showing the effect of different inhibitors on the basolateral Na^+ dependent HCO_3^- uptake in HCO_3^-/CO_2 buffered extracellular solution in pancreatic organoids (**b**) and in isolated ducts (**c**) (4–6 experiments for each conditions). Bar charts of calculated base flux (**d**) and maximal pH changes (**e**) show that inhibition of NBCe1 (S0859) and/or NHE1 (EIPA) activity significantly decreased the recovery. No significant differences were detected between isolated ducts and organoids. $*p < 0.05$ vs Organoid Control; $**p < 0.05$ vs Isolated duct Control

relevance, especially in case of pancreatic OCs. Therefore, in this manuscript we provide side-by-side comparison of gene expression, cell morphology and function of pancreatic ductal epithelial cells derived from primary isolated ductal fragments and of pancreatic OCs.

Ion (especially HCO_3^-) and fluid secretion is the primary function of the pancreatic ductal epithelia, which is obtained by the interaction of the electrogenic SLC26A6 Cl^-/HCO_3^- exchanger and the CFTR Cl^- channel [1, 24]. Due to the molecular interaction between the two proteins the ductal cells are able to secrete and maintain 140 mM intraluminal HCO_3^- concentration (~5–6 fold higher than the intracellular) [25]. The current model suggests that in the proximal ducts CFTR provides the extracellular Cl^- for

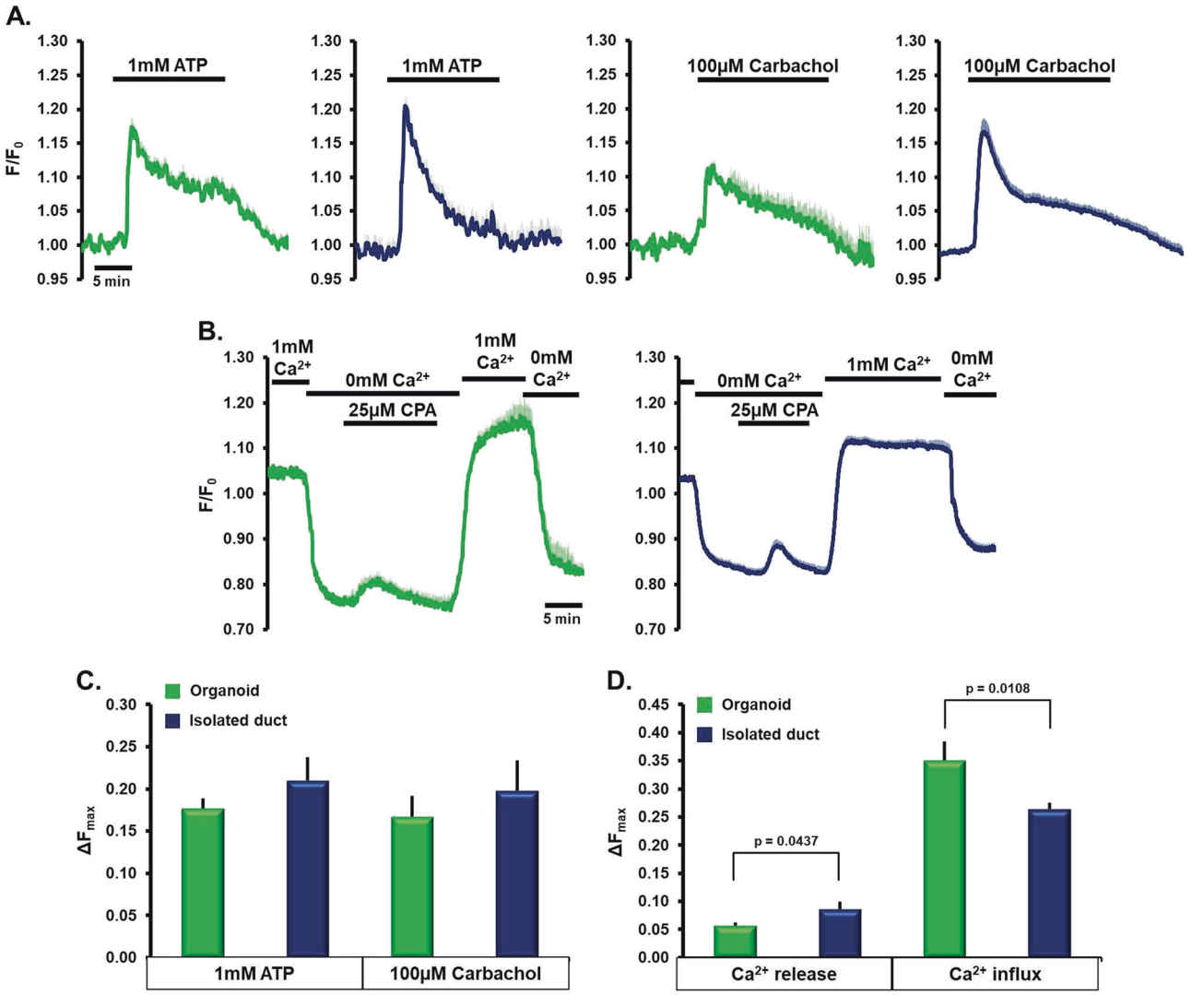

Fig. 6 Intracellular Ca^{2+} signaling in isolated pancreatic ducts and organoids. **a** Average traces of 4–6 experiments demonstrating the effect of 1 mM ATP, or 100 μM carbachol on pancreatic epithelial cells. Both agonists induced peak-plateau Ca^{2+} signals. **b** Ca^{2+} influx in pancreatic ducts and OCs (average traces of 4–6 experiments). ER Ca^{2+} release induced by 25 μM cyclopiazonic acid (CPA) and Ca^{2+} influx was measured by the maximal response to HCO_3^-/CO_2 buffered extracellular solution readdition of Ca^{2+}. Summary of the maximal Ca^{2+} responses to agonist stimulation (**c**) and ER Ca^{2+} release (first two columns) and Ca^{2+} influx (second two columns) (**d**)

the Cl^-/HCO_3^-exchange of SLC26A6. However, in the distal pancreatic ducts, the anion exchange of SLC26A6 is not possible to maintain due to the very low luminal and intracellular Cl^- concentration. Under these conditions CFTR permeability is switched by With-No-Lysine (WNK)/STE20/SPS1-related proline/alanine-rich kinase (SPAK) kinases in favor of HCO_3^- [26]. On the opposite site, the accumulation of the HCO_3^- across the basolateral membrane is mediated by the electrogenic NBCe1. Another factor in this process is the passive diffusion of CO_2 through the membrane followed by the carbonic anhydrase-mediated conversion of CO_2 to HCO_3^- and H^+ [27]. In addition to these, NHE1 maintains the pH_i by transporting excess H^+ from the cells. Therefore, first we analyzed the expression of genes encoding these ion channels and transporters in isolated ducts and OCs. Our results confirmed the expression of these genes in primary mouse ductal fragments and also in pancreatic OCs. Moreover, the expression of *Atp12a* (encoding nongastric H^+/K^+ ATPase); *Kcnma1* (encoding BK channel), *Slc26a3*, and *Nkcc1* overlapped in the two types of samples. We also found that four members of the voltage-gated potassium channel subfamily *Kcna1, Kcna2, Kcnd3*, and *Kcnh1* are expressed in pancreatic epithelial cells, which have not been described earlier. In addition, we showed the expression of two voltage-gated Cl^- channels: *Clcn1* and *Clcn3* that were not suggested earlier. Transcription of *Clcn3* has only been described in pancreatic β-cells, where it is localized on insulin granules and play a role in insulin processing and secretion through regulation of granular acidification [28].

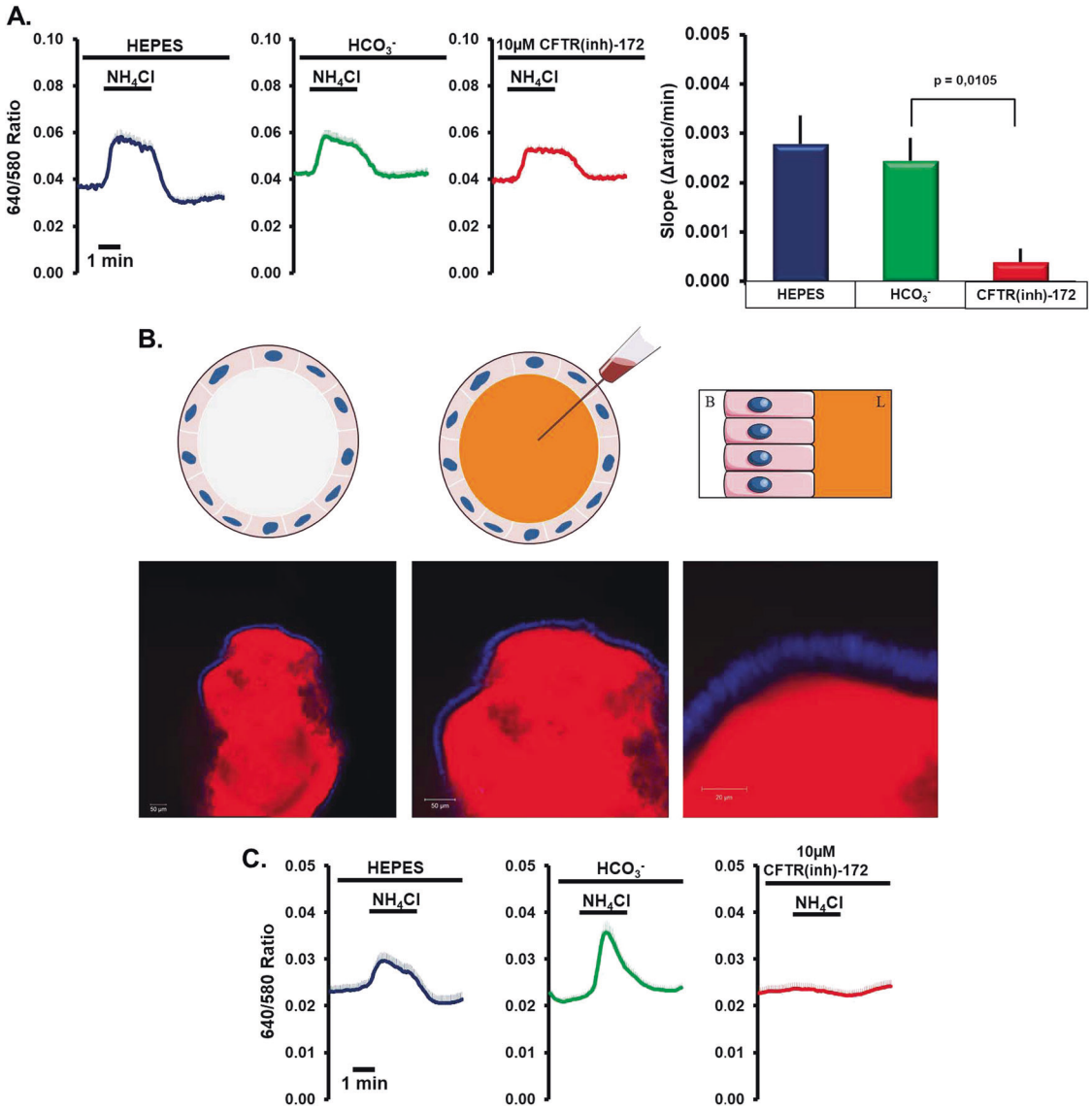

Fig. 7 Measurement of intracellular and intraluminal pH in pancreatic organoids. **a** Measurement of intracellular pH (pH_i) with SNARF-1. Average traces and bar charts of 4–6 experiments. Similarly to the earlier results NH_4Cl caused intracellular alkalosis followed by a slow regeneration, which was inhibited by CFTR(inh)-172. **b** Schematic representation of the administration of SNARF1-dextrane to the lumen of the organoids and confocal images of the SNARF1-dextrane loaded organoids. As demonstrated, SNARF1 was restricted to the intraluminal space and no intracellular dye uptake could be observed. **c** Average traces of intraluminal pH changes. Administration of NH_4Cl in HEPES-, or in HCO_3^-/CO_2-buffered solution triggered a rapid elevation of intraluminal pH due to the efflux of HCO_3^- to the lumen, which was completely abolished by 10 μM CFTR(inh)-172

Moreover, our results showed that *Enac* and *Ano1* are expressed in both isolated primary ductal fragments as well as pancreatic OC. The relatively strong expression of *Enac* in pancreatic epithelia is somewhat unexpected since earlier studies were not able to demonstrate functional activity of ENaC in rat pancreatic ducts [29] and according to the current hypothesis ENaC is not expressed and has no role in exocrine pancreatic epithelial cells [1]. In the next step, we compared the morphology of the isolated ducts and OCs with a special focus on apical-basal polarity. The ultrastructure of the epithelial cells in the two samples showed no major difference and the OCs epithelial cells represented the same features—increased apical density of mitochondria, brush border on the apical membrane—like primary ductal cells. Importantly, the distribution of proteins showed similar pattern in cross sections of organoids and isolated ducts. We confirmed that CFTR is expressed exclusively on the apical, whereas NHE1 and NBCe1 were found on the basolateral membrane, which is concordant to the current literature [1, 4]. Taken together, our results demonstrated a complete overlap of gene expression and morphology of isolated ductal fragments and pancreatic OCs and more

importantly the use of OCs can ensure that results are not derived from heterogeneous tissue fragments but from primary epithelial cell monolayers. Notably, these results also suggest that the exocrine pancreatic ductal secretion may be far more complicated than the currently used models suggest [30]. Further analysis will be needed to clarify the functional relevance of these results (especially the role of ENaC, CCls, and K^+ channels) and special attention should be paid to species dependent alterations in expression and eventually in protein function. However, if protein expression and function confirms these findings, our results might indicate the need of revision of the current model of pancreatic ductal secretion.

As mentioned earlier, only a limited number of studies have been published about the functional analysis of organoids. Recently Foulke-Abel et al. used human intestinal crypt-derived enteroids to investigate their functional relevance to ion transport physiology and pathophysiology [31]. Using undifferentiated and differentiated enteroids, they demonstrated that these organoids show similar apical-basal polarity to the human small intestine enterocytes and express functionally active NHE3, which is the most prominent transporter in this cell type. Organoid swelling was inhibited by inhibitors of CFTR, NKCC, and NHE3. Whereas intracellular acidification caused by forskolin administration in HCO_3/CO_2^- buffered solution was created by CFTR and electrogenic NBC1. In 2018, O'Malley et al. reported the establishment of a culture system of differentiated pancreatic ductal epithelial cells in a polarized monolayer [32]. In this 2D air-liquid interface culture system, cells were grown on semipermeable filters and were reported to develop epithelial cell morphology. Short circuit current and extracellular pH measurements revealed that these cells respond to increase of intracellular cAMP and express functionally active CFTR channels. Although, the culture system could overcome some limitations of isolated ductal fragments (such as the presence of contaminating fibroblasts) and it can be used for short circuit current measurements, it still possesses the drawbacks of the 2D culture systems [33], whereas maintenance of this culture seems to be tedious and less efficient compared with 3D organoid cultures. Although functional data are limited, the described results highlighted that organoids might be a powerful ex vivo system to represent original tissue morphology and functions and could be used to model pancreatic ductal secretory functions in physiology and pathology. Therefore, in this study we performed functional analysis of pancreatic OCs and compared them with the well-studied isolated ductal fragments used as a reference point. Measurements of apical HCO_3^- secretion and basolateral HCO_3^- uptake were highly comparable in OCs and primary ducts. In addition, the activities of other ion transport processes mediated by NHE1, or NKCC1 were similar in the two systems. Finally, the Ca^{2+} signaling, which is one of the major signal transduction pathways in the pancreatic ductal epithelia [34], showed similar characteristics in OCs further supporting the functional equality of pancreatic organoids with the primary ductal system.

As mentioned in the introduction, the intraductal pH has a major importance in the exocrine pancreatic physiology. Earlier studies showed that protons are coreleased during exocytosis of digestive enzymes thus causing significant intraluminal acidosis, which has to be compensated by ductal cells to avoid intrapancreatic trypsinogen activation [35] and the development of AP [36]. This was further confirmed in patients, where intraductal pH in acute biliary pancreatitis was significantly decreased compared with the controls (6.97 ± 0.13 vs 7.79 ± 0.20) [37]. Therefore, we developed a technique that utilizes dextran conjugated pH sensitive fluorescent dye SNARF1 to monitor pH changes in the lumen of the organoids. Using this technique, we were able to follow the pH elevation induced by NH_4Cl administration, which was completely blocked by CFTR inhibition.

Patient-derived pancreatic tumor organoids have been successfully used for disease modeling and to predict response to anticancer therapy [17, 30, 31]. In another study human pluripotent stem cells were used to generate acinar/ductal organoids to model cystic fibrosis [38]. In experimental setup that was more focused on organoid function Dekkers et al. used patient-derived rectal organoids to measure CFTR activity and predict response to CFTR corrector and/or potentiator therapy [39]. They used FIS which is currently the state-of-the-art technique to measure CFTR-dependent ion and fluid secretion [22]. Whereas FIS is relatively simple and robust method that correlates well with the individual response to cystic fibrosis treatment, it also might have some potential limitations. During forskolin stimulation the secreted fluid expands the lumen and the increasing intraluminal pressure prevents water efflux that might therefore not follow the ion current linearly. In addition, the increased tension might activate the mechanoreceptors (such as Piezo1) in the apical membrane of epithelial cells [40]. This shall not be a problem in samples with CFTR expression defects, where the initial fluid secretion is marginal [41]. However in wild type pancreatic organoids FIS leads to a relatively rapid rupture of the organoids (data not shown). Therefore instead of measuring the relative luminal volume of the organoids, we utilized a $[Cl^-]_i$ sensitive fluorescent indicator to follow Cl^- movements in pancreatic OCs [42]. Our results with this technique are consistent with the literature data since forskolin significantly enhanced, whereas CFTR, or PKA inhibition markedly decreased the increase of fluorescent signal. Therefore this technique could be potentially capitalized in pancreatic physiology research and in drug screening studies to identify compounds that improve exocrine pancreatic ductal secretion.

Taken together, after thorough analysis, we have demonstrated that epithelial cells in OCs remarkably correspond with the primary ductal epithelia. Our results confirmed that pancreatic OCs could be a relevant, highly reproducible ex vivo model system with increased throughput to study pancreatic secretory physiology and pathology and thus could be a potential solution for an unmet need in pancreatic research.

Acknowledgements The research was supported by funding from the Hungarian National Research, Development and Innovation Office (PD115974 and GINOP-2.3.2-15-2016-00048 to JM, PD116553 to PP, K119938 to RZ), the Ministry of Human Capacities (EFOP 3.6.2-16-2017-00006 to JM), Bolyai Research Fellowship (BO/00440/16/5 to JM, BO/00569/17 to PP), the Hungarian Academy of Sciences (LP2017–18/2017 to JM), by the National Excellence Program (20391-3/2018/FEKUSTRAT to JM), by the New National Excellence Program of the Ministry of Human Capacities (UNKP-18-4-SZTE-85 to PP, UNKP-18-3-I-SZTE-66 to MT) and EFOP 3.6.3-VEKOP-16-2017-00009 to MT. The authors are grateful to David Tuveson for providing the protocol of pancreatic organoid generation and to Hans Clevers for generously sharing the Noggin-expressing cell line with us.

Compliance with ethical standards

Conflict of interest The authors declare that they have no conflict of interest.

References

1. Lee MG, Ohana E, Park HW, Yang D, Muallem S. Molecular mechanism of pancreatic and salivary gland fluid and HCO_3 secretion. Physiol Rev. 2012;92:39–74.
2. Hegyi P, Pandol S, Venglovecz V, Rakonczay Z Jr. The acinar-ductal tango in the pathogenesis of acute pancreatitis. Gut. 2011;60:544–52.
3. Pallagi P, Venglovecz V, Rakonczay Z Jr., Borka K, Korompay A, et al. Trypsin reduces pancreatic ductal bicarbonate secretion by inhibiting CFTR Cl(-) channels and luminal anion exchangers. Gastroenterology. 2011;141:2228–39 e6.
4. Zeng M, Szymczak M, Ahuja M, Zheng C, Yin H, Swaim W, et al. Restoration of CFTR activity in ducts rescues acinar cell function and reduces inflammation in pancreatic and salivary glands of mice. Gastroenterology. 2017;153:1148–59.
5. Pallagi P, Balla Z, Singh AK, Dosa S, Ivanyi B, Kukor Z, et al. The role of pancreatic ductal secretion in protection against acute pancreatitis in mice*. Crit Care Med. 2014;42:e177–88.
6. Maleth J, Balazs A, Pallagi P, Balla Z, Kui B, Katona M, et al. Alcohol disrupts levels and function of the cystic fibrosis transmembrane conductance regulator to promote development of pancreatitis. Gastroenterology. 2015;148:427–39 e16.
7. Hegyi P, Wilschanski M, Muallem S, Lukacs GL, Sahin-Toth M, Uc A, et al. CFTR: a new horizon in the pathomechanism and treatment of pancreatitis. Rev Physiol, Biochem Pharmacol. 2016;170:37–66.
8. Argent BE, Arkle S, Cullen MJ, Green R. Morphological, biochemical and secretory studies on rat pancreatic ducts maintained in tissue culture. Q J Exp Physiol. 1986;71:633–48.
9. Hegyi P, Gray MA, Argent BE. Substance P inhibits bicarbonate secretion from guinea pig pancreatic ducts by modulating an anion exchanger. Am J Physiol Cell Physiol. 2003;285:C268–76.
10. Maleth J, Venglovecz V, Razga Z, Tiszlavicz L, Rakonczay Z Jr., Hegyi P. Non-conjugated chenodeoxycholate induces severe mitochondrial damage and inhibits bicarbonate transport in pancreatic duct cells. Gut. 2011;60:136–8.
11. Sato T, Stange DE, Ferrante M, Vries RG, Van Es JH, Van den Brink S, et al. Long-term expansion of epithelial organoids from human colon, adenoma, adenocarcinoma, and Barrett's epithelium. Gastroenterology. 2011;141:1762–72.
12. Clevers H. Modeling development and disease with organoids. Cell. 2016;165:1586–97.
13. Nusse R, Clevers H. Wnt/beta-catenin signaling, disease, and emerging therapeutic modalities. Cell. 2017;169:985–99.
14. Kretzschmar K, Clevers H. Organoids: modeling development and the stem cell niche in a dish. Dev Cell. 2016;38:590–600.
15. Sato T, Vries RG, Snippert HJ, van de Wetering M, Barker N, Stange DE, et al. Single Lgr5 stem cells build crypt-villus structures in vitro without a mesenchymal niche. Nature. 2009;459:262–5.
16. Barker N, Huch M, Kujala P, van de Wetering M, Snippert HJ, van Es JH, et al. Lgr5(+ve) stem cells drive self-renewal in the stomach and build long-lived gastric units in vitro. Cell Stem Cell. 2010;6:25–36.
17. Huch M, Bonfanti P, Boj SF, Sato T, Loomans CJ, van de Wetering M, et al. Unlimited in vitro expansion of adult bi-potent pancreas progenitors through the Lgr5/R-spondin axis. EMBO J. 2013;32:2708–21.
18. Simian M, Bissell MJ. Organoids: a historical perspective of thinking in three dimensions. J Cell Biol. 2017;216:31–40.
19. Dahl-Jensen SB, Yennek S, Flasse L, Larsen HL, Sever D, Karremore G, et al. Deconstructing the principles of ductal network formation in the pancreas. PLoS Biol. 2018;16:e2002842.
20. Boj SF, Hwang CI, Baker LA, Chio II, Engle DD, Corbo V, et al. Organoid models of human and mouse ductal pancreatic cancer. Cell. 2015;160:324–38.
21. Venglovecz V, Rakonczay Z Jr., Gray MA, Hegyi P. Potassium channels in pancreatic duct epithelial cells: their role, function and pathophysiological relevance. Pflugers Arch. 2015;467:625–40.
22. Dekkers JF, Berkers G, Kruisselbrink E, Vonk A, de Jonge HR, Janssens HM, et al. Characterizing responses to CFTR-modulating drugs using rectal organoids derived from subjects with cystic fibrosis. Sci Transl Med. 2016;8:344ra84.
23. Yang D, Li Q, So I, Huang CL, Ando H, Mizutani A, et al. IRBIT governs epithelial secretion in mice by antagonizing the WNK/SPAK kinase pathway. J Clin Invest. 2011;121:956–65.
24. Maleth J, Hegyi P. Calcium signaling in pancreatic ductal epithelial cells: An old friend and a nasty enemy. Cell Calcium 2014;55:337–45.
25. Hong JH, Park S, Shcheynikov N, Muallem S. Mechanism and synergism in epithelial fluid and electrolyte secretion. Pflugers Arch. 2014;466:1487–99.
26. Park HW, Nam JH, Kim JY, Namkung W, Yoon JS, Lee JS, et al. Dynamic regulation of CFTR bicarbonate permeability by [Cl-]i and its role in pancreatic bicarbonate secretion. Gastroenterology. 2010;139:620–31.
27. Dyck WP, Hightower NC, Janowitz HD. Effect of acetazolamide on human pancreatic secretion. Gastroenterology. 1972;62:547–52.
28. Deriy LV, Gomez EA, Jacobson DA, Wang X, Hopson JA, Liu XY, et al. The granular chloride channel ClC-3 is permissive for insulin secretion. Cell Metab. 2009;10:316–23.
29. Novak I, Hansen MR. Where have all the Na+ channels gone? In search of functional ENaC in exocrine pancreas. Biochim Biophys Acta. 2002;1566:162–8.

30. Yamaguchi M, Steward MC, Smallbone K, Sohma Y, Yamamoto A, Ko SB, et al. Bicarbonate-rich fluid secretion predicted by a computational model of guinea-pig pancreatic duct epithelium. J Physiol. 2017;595:1947–72.
31. Foulke-Abel J, In J, Yin J, Zachos NC, Kovbasnjuk O, Estes MK, et al. Human enteroids as a model of upper small intestinal ion transport physiology and pathophysiology. Gastroenterology. 2016;150:638–49 e8.
32. O'Malley Y, Rotti PG, Thornell IM, Vanegas Calderon OG, Febres-Aldana C, Durham K, et al. Development of a polarized pancreatic ductular cell epithelium for physiological studies. J Appl Physiol. 2018;125:97–106.
33. Horvath P, Aulner N, Bickle M, Davies AM, Nery ED, Ebner D, et al. Screening out irrelevant cell-based models of disease. Nat Rev Drug Discov. 2016;15:751–69.
34. Maleth J, Hegyi P. Calcium signaling in pancreatic ductal epithelial cells: an old friend and a nasty enemy. Cell Calcium. 2014;55:337–45.
35. Behrendorff N, Floetenmeyer M, Schwiening C, Thorn P. Protons released during pancreatic acinar cell secretion acidify the lumen and contribute to pancreatitis in mice. Gastroenterology. 2010;139:1711–20. 20 e1–5
36. Geisz A, Sahin-Toth M. A preclinical model of chronic pancreatitis driven by trypsinogen autoactivation. Nat Commun. 2018;9:5033.
37. Takacs T, Rosztoczy A, Maleth J, Rakonczay Z Jr., Hegyi P. Intraductal acidosis in acute biliary pancreatitis. Pancreatology. 2013;13:333–5.
38. Hohwieler M, Illing A, Hermann PC, Mayer T, Stockmann M, Perkhofer L, et al. Human pluripotent stem cell-derived acinar/ductal organoids generate human pancreas upon orthotopic transplantation and allow disease modelling. Gut. 2017;66:473–86.
39. Dekkers JF, Wiegerinck CL, de Jonge HR, Bronsveld I, Janssens HM, de Winter-de Groot KM, et al. A functional CFTR assay using primary cystic fibrosis intestinal organoids. Nat Med. 2013;19:939–45.
40. Romac JM, Shahid RA, Swain SM, Vigna SR, Liddle RA. Piezo1 is a mechanically activated ion channel and mediates pressure induced pancreatitis. Nat Commun. 2018;9:1715.
41. Boj SF, Vonk AM, Statia M, Su J, Vries RR, Beekman JM, et al. Forskolin-induced swelling in intestinal organoids: an in vitro assay for assessing drug response in cystic fibrosis patients. J Vis Exp. 2017.
42. Ko SB, Shcheynikov N, Choi JY, Luo X, Ishibashi K, Thomas PJ, et al. A molecular mechanism for aberrant CFTR-dependent HCO(3)(-) transport in cystic fibrosis. EMBO J. 2002;21:5662–72.